USING LIPID BILAYERS IN AN ARTIFICIAL AXON SYSTEM

Zachary Thomas VanDerwerker

Thesis submitted to the faculty of the Virginia Polytechnic Institute and State University in partial fulfillment of the requirements for the degree of

Master of Science
In
Mechanical Engineering

Mary E. Kasarda, Co-Chair
Donald J. Leo, Co-Chair
Stephen A. Sarles

September 23, 2013
Blacksburg, Virginia

Keywords: Lipid bilayer, droplet interface bilayer, droplet on hydrogel bilayer (DHB), alamethicin, artificial axon system

USING LIPID BILAYERS IN AN ARTIFICIAL AXON SYSTEM

Zachary Thomas VanDerwerker

ABSTRACT

Since the rise of multicellular organisms, nature has created a wide range of solutions for life on Earth. This diverse set of solutions presents a broad design space for a number of bio-inspired technologies in many different fields. Of particular interest for this work is the computational and processing power of neurons in the brain. Neuronal networks for transmitting and processing signals have advantages to their electronic counterparts in terms of power efficiency and the ability to handle component failure. In this thesis, an artificial axon system using droplet on hydrogel bilayers (DHBs) in conjunction with alamethicin channels was developed to show properties of action potential signal propagation that occur in myelinated nerve cells. The research demonstrates that the artificial axon system is capable of modifying signals that travel perpendicular to a lipid bilayer interface due to the voltage-gating properties of alamethicin within the connected bilayer. The system was used to show a signal boosting behavior similar to what occurs in the nodes of Ranvier of a myelinated axon. In addition, the artificial axon system was used to show that alamethicin channels within a lipid bilayer behave similarly to slow-acting potassium channels in a real axon in that they follow a sigmoid activation curve in response to a step potential change.

Acknowledgements

I would like to sincerely thank Dr. Mary E. Kasarda, Dr. Donald J. Leo, and Dr. Stephen A. Sarles for their guidance and support throughout this project. Without their help, the work presented in this thesis would not have been possible.

I would also like to thank my colleagues at both the Biomolecular Materials and Systems Lab (BMSL) and Center for Intelligent Material Systems and Structures (CIMMS) for their help and advice. I am very glad to have worked with such an intelligent team.

To my parents, thank you for supporting me throughout this process. Two down, three to go.

Table of Contents

List of Figures

List of Tables

Chapter 1: Introduction and Background

1.1 Introduction and Motivation

Since the rise of multicellular organisms, nature has created a wide range of solutions for life on Earth. This diverse set of solutions presents a broad design space for a number of bio-inspired technologies in many different fields. For example, Sharklet sheet-plastic (Sharklet Technologies), used in hospitals and restaurants to greatly reduce the growth of bacterial colonies, was inspired by the unique microscopic texture of shark skin. Road signs take advantage of fluorescent materials, originally inspired by fireflies, to help drivers cope with driving in poor weather conditions. Velcro hook and loop fasteners were inspired by the burrs of burdock attaching to fur and clothing. Even many of the pumping mechanisms used today are based on nature's diaphragm pumps such as the heart and lungs [1].

One particular system in nature that has been a point for bio-inspiration is the neuronal network that transmits and processes signals all over the body. This network is made up of individual neuron cells, each typically only a few micrometers in length [2]. Neurons share multiple connection points with other neurons, which leads to a complex, but powerful system. The work in this thesis seeks to expand neuron bio-inspiration work by utilizing artificial lipid bilayers.

The motivation for this work is towards developing a system that functions similarly to a neuron by taking advantage of lipid bilayers. Neurons form complex biological systems that are capable of signal transmission and processing. The brain, composed of billions of neurons, is much more power-efficient than electronics and better able to handle component failure [3]. If the solder in a motherboard cracks such that the electrical connection is destroyed, the entire motherboard could easily be rendered useless. However, an individual that loses 40% of all neurons in the brain could still have good cerebral activity and be capable of functioning at a high level [4]. The 40% loss is rare, but imagine missing 40% of the components in a computer motherboard. Neuronal networks for transmitting and processing signals clearly have advantages to their electronic counterparts.

In this thesis, an artificial axon system was developed using droplet on hydrogel bilayers (DHBs) in conjunction with alamethicin channels in order to recreate properties of action potential signal propagation that occur in myelinated nerve cells. The research demonstrates that the artificial axon

system is capable of modifying signals that travel perpendicular to a lipid bilayer interface due to the voltage-gating properties of alamethicin within the connected bilayer. The system was used to show a signal boosting behavior similar to what occurs in the nodes of Ranvier of a myelinated axon. In addition, the artificial axon system was used to show that alamethicin channels within a lipid bilayer behave similarly to slow-acting potassium channels in a real axon in that they follow a sigmoid activation curve in response to a step potential change.

1.2 Background Information on Relevant Biology

1.2.1 Cell Biology

All living things are made up of cells. Cells can be classified as either prokaryotic or eukaryotic. Prokaryotic cells are characterized by their small size, typically ranging between $1 - 10\ \mu m$ in length, the absence of a nucleus, and single cellular [5]. The most common prokaryotes are bacteria such as the photosynthetic cyanobacteria (blue-green bacteria) [6]. Eukaryotic cells are more evolved, are typically larger ($10 - 100\ \mu m$ in length), have a nucleus, and make up multicellular organisms such as humans [5].

1.2.2 Cell Membrane

All living things are made up of small building blocks called cells. In multicellular organisms, such as animals, cells work together in order to carry out vital functions such as energy conversion and movement. All cells are surrounded by a membrane, composed primarily of a lipid bilayer with embedded proteins (Figure 1-1), which acts as a barrier between the cell interior and the extracellular environment [7]. The cell membrane is a selective barrier in that it allows only certain materials to enter and exit the cell. It also allows ions to travel through special protein channels, which is critical for the function of nerve cells in terms of transmitting signals. Unique proteins can also be found embedded within the cellular membrane, which can act as sensors for the cell. These proteins can change shapes depending on the sensing mechanism which allows ions and small molecules to enter or exit a cell. Some of the most common sensing mechanisms are the potential across a membrane (voltage-gated), presence of certain molecules (ligand-gated), change in membrane tension (mechano-sensitive), and the presence or absence of light (light-sensitive) [8]. For a specific example, ligand-gated proteins change shape in the presence of certain molecules. By changing shape, ligand-gated proteins could open (gate) allowing molecules to enter/exit the cell [5].

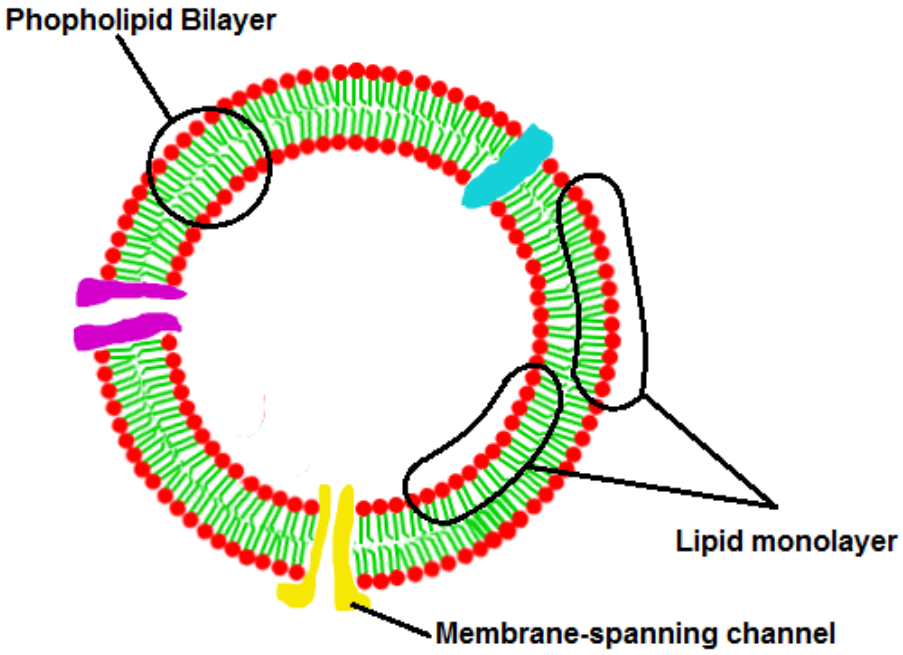

Figure 1-1: **Major components of cell membrane**.

The current model of cell membranes is known as the fluid mosaic model, which was introduced by Singer and Nicolson in the early 1970s [9]. The model suggests that lipid molecules do not often "flip-flop" between monolayers, but that they move laterally very easily. This lateral movement is dependent on the lipid bilayer's fluidity [9], which is dependent on the bilayer composition [10].

1.2.3 Lipids

Cell membranes are primarily composed of phospholipids, which are amphiphillic molecules consisting of a phosphate head group connected to an organic molecule tail. Close to half of the mass of most animal cells are comprised of phospholipids and the remainder of the mass consists of cholesterol and glycolipids as well as membrane proteins [10]. Phospholipids are amphipathic in that they have both polar (head) and non-polar (tail) parts. This is a key property because it allows lipids to form the bilayer membrane that surrounds cells [5]. Figure 1-2 is a diagram showing the hydrophilic (likes water) polar head and hydrophobic (fears water) non-polar tail of a phospholipid.

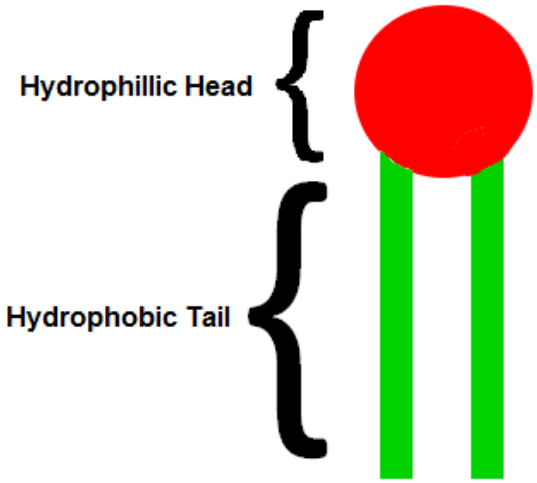

Figure 1-2: **Diagram of phospholipid.**

Lipids will naturally self-assemble with one another in order to reach thermodynamic equilibrium, which means the system is balanced (no net flow of energy). The hydrophilic heads will orient toward a polar environment (water) whereas the hydrophilic tails will be oriented away from the polar environment (towards the non polar oil). For example, lipids in a water solution would form micelle, planar lipid bilayers, or vesicles (liposomes) where the hydrophilic heads would shield the hydrophobic tails from the water [11]. Since lipids will self-assemble, lipid bilayers have a self-healing ability that allows the bilayer to recover, for example from a hole, by rearranging the lipids [10]. Simple artificial cell membranes can therefore be formed by taking advantage of this lipid self-assembly characteristic.

1.2.4 A Brief History of the Cell Membrane Lipid Bilayer

Robert Hooke is most commonly known for his observation of and coining of the term “cell” when he observed cork slices under a microscope in 1665. A lesser known fact is that Hooke also studied soap bubbles, which have similar properties as lipids, and noticed black areas on some of the bubbles in 1672. Nearly 30 years later, Sir Isaac Newton estimated the thickness of the black areas on soap films to be about 9.5 nm thick, which is actually a very realistic value [12]. The black areas that both Hooke and Newton observed were due to bilayers. The black color was due to the interference of the reflected light from the water/surfactant interface and the phase-shifted light from the surfactant/water interface, which occurred when light tried to pass through the lipid bilayer [13].

In the late 1890s, Charles Ernest Overton determined that membranes must consist of lipids based on permeability studies of membranes to non-electrolytes and their corresponding lipid solubility [14]. Later, in 1917 I. Langumir developed the "Langmuir trough" for studying monolayers of amphiphilic molecules. Eight years later, though based on incorrect experimental methods, Gorter and Grendel proposed that the cell membrane was characterized by a lipid bilayer structure. This structure consisted of two lipid monolayers where the hydrophobic tails of opposite monolayers were in contact with one another and the hydrophilic heads were exposed to the aqueous environment [15]. In 1935, Danielli and Davson included proteins into the bilayer lipid membrane model [16]. The currently accepted model of the cell membrane structure was presented in 1972 by Singer and Nicolson as the fluid-mosaic model [7, 9], which was shown previously in Figure 1-1.

1.2.5 Short Review of Methods for Forming Artificial Lipid Bilayers

There are a variety of ways to form lipid bilayers[1] dating back to the Montal-Mueller (MM/lipid folding) technique developed in early 1970s [17]. While each method has its advantages and disadvantages, this thesis will only discuss the droplet interface bilayers (DIBs) and the droplet on hydrogel bilayers (DHBs) techniques of forming artificial bilayers [18].

1.2.5.1 Droplet Interface Bilayers (DIBs)

By utilizing the lipid-in technique where the lipids are contained in an aqueous solution, a lipid monolayer can be formed at a water-oil interface [19]. Since oil is insoluble in water, the hexadecane (oil) and aqueous solution will not mix. The density of hexadecane is approximately $0.77\ g/cm^3$ at $25\ ^\circ C$, which is less than water. Aqueous droplets will therefore be submerged in a hexadecane bath. The hydrophobic tails of the individual lipid molecules want to get away from the water, so they become oriented towards the hexadecane solution. The hydrophilic heads, however, remain pointed towards the aqueous solution. Figure 1-3 shows a 2-D diagram of a single aqueous droplet that contains the lipid solution. Note how the lipids orient themselves around the water/oil interface. The water/oil interface can only support a certain number of lipids so, although it is not shown in the diagram, there are excess lipids in the aqueous droplet. It should also be noted that the droplets 3D, so the lipid monolayer covers the entirety of the droplet shape.

[1] Sarles describes common methods for forming lipid bilayers in his doctoral dissertation. Refer to Section 1.3.2 "Methods of Lipid Bilayer Formation" [11. Sarles, S.A., *Physical Encapsulation of Interface Bilayers*, 2010, Virginia Polytechnic Institute and State University.]

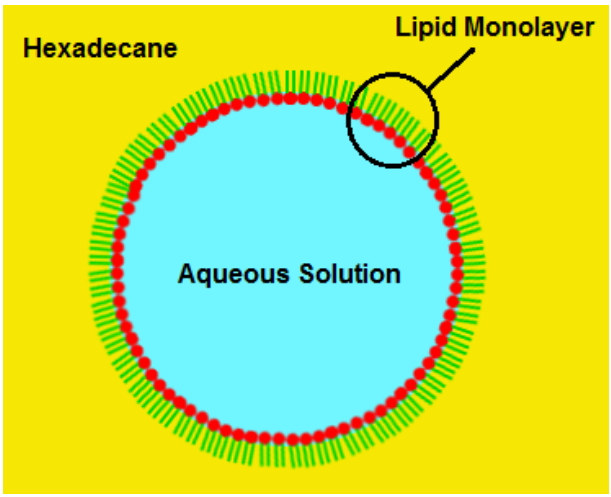

Figure 1-3: **Diagram of a single aqueous droplet containing the lipid solution in an oil (hexadecane) bath. The lipid monolayer forms at the water-oil (hexadecane) interface.**

Figure 1-4 shows that by bringing two "droplets" together, a lipid bilayer can be formed where the two lipid monolayers come in contact with one another. This occurs because the lipid tails "zip" together, which purges the oil from between the monolayers. This phenomenon will be discussed in more detail later in Chapter 2.

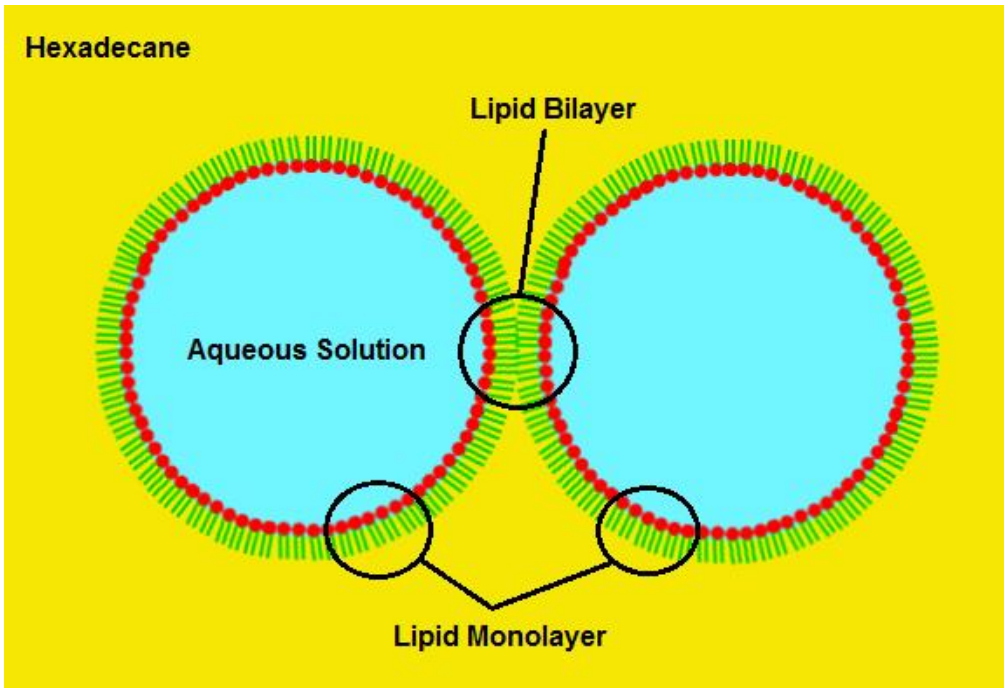

Figure 1-4: **Diagram of two droplets, each surrounded by a lipid monolayer, coming into contact to form a lipid bilayer at the interface.**

1.2.5.2 Droplet on Hydrogel Bilayers

Hydrogels are highly absorbent hydrophilic polymer chain networks [20], which can be used to anchor aqueous droplets in order to form lipid bilayers [18, 21, 22]. The general concepts involved in forming a lipid bilayer using DHB techniques are very similar to that of using DIB techniques. The difference is that DHB techniques involve anchoring a droplet to a hydrogel substrate. By attaching a droplet to a hydrogel, the experimenter has greater control over the position of the droplet, which can allow the experimenter to regulate the size of the bilayer area to some extent [23, 24].

Figure 1-5 shows a diagram of two aqueous droplets anchored to a hydrogel base. The hydrogels can be attached to a rigid (or flexible) support material that could be manually manipulated. Note that the hydrogels are porous (like a sponge) such that the aqueous solution can easily diffuse into them. The major advantage to using hydrogels to support aqueous droplets is the ability to anchor the droplets to a particular area on a substrate and the ability to manipulate the anchored droplets with a support material. By manipulating the anchored droplets, the size of the bilayer can be controlled to a degree. This technique is called the regulated attachment method (RAM) [25].

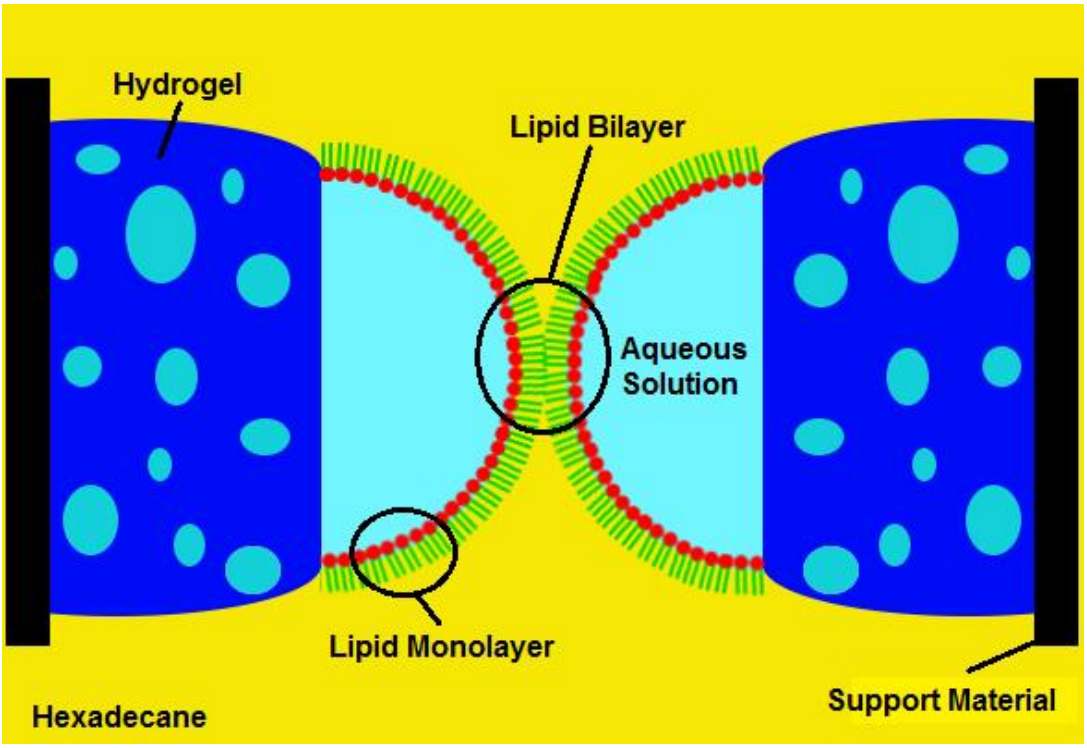

Figure 1-5: **Diagram of two aqueous droplets supported by hydrogels connected to support material.**

Figure 1-6 shows pictures of aqueous droplets supported by hydrogels. Figure 1-6A shows the aqueous droplets (each surrounded by a lipid monolayer) separated from one another. The two droplets are then brought into contact with one another (Figure 1-6B) in order to form a lipid bilayer. Note that the left aqueous droplet is supported by a hydrogel connected to a micropipette. To bring the droplets into contact, a micromanipulator is used to control the position of the micropipette. Sometimes, the lipid bilayer fails by rupturing as shown in Figure 1-6C. When the bilayer has ruptured, the two droplets are said to have coalesced. Bilayers can rupture for a number of reasons including large potentials and excessive mechanical vibration [11].

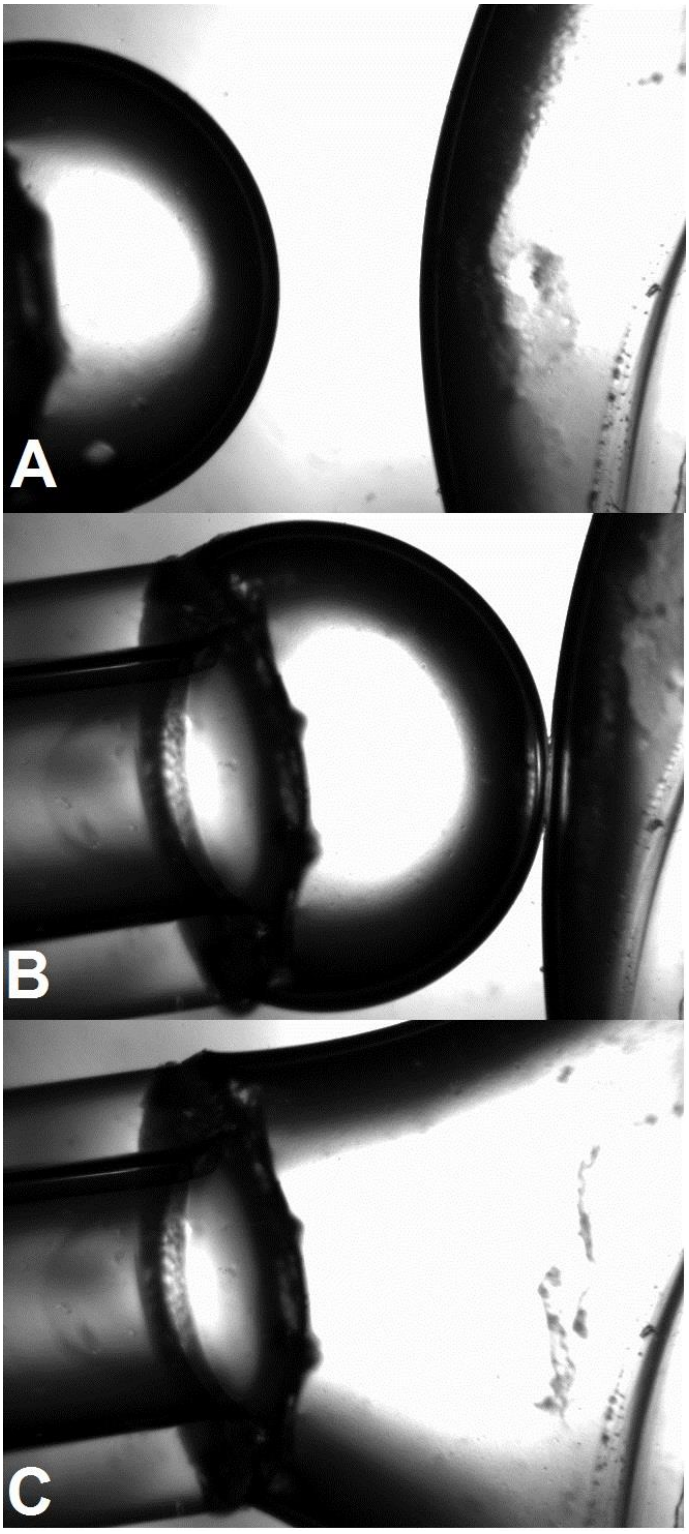

Figure 1-6: **Pictures of two lipid monolayers. A) Two lipid monolayers (each anchored to a separate hydrogel as shown in the diagram in Figure 1-5) separated from one another. B) Two lipid monolayers are brought together using a micromanipulator controlled micropipette to form a lipid bilayer. C) The lipid bilayer has ruptured at the two monolayers are said to have "coalesced."**

1.3 Alamethicin, a Channel-Forming Peptide

Alamethicin is a channel-forming peptide that is produced by the fungus *Trichoderma viride* [26, 27]. When *Trichoderma viride* is attacked by a microorganism, the alamethicin peptides form pores in the microorganism's cell membrane, causing the membrane to rupture, which often kills (or severely impairs) the microorganism [28, 29]. When incorporated in the formation of both planar lipid bilayers and droplet interface bilayers (DIBs), alamethicin induces a voltage-dependent conductance behavior [11, 30, 31]. In other words, the current flowing through a bilayer that contains alamethicin channels is highly dependent on the voltage across the bilayer. The work presented in this thesis shows that signals traveling through an electrolyte pipeline connected perpendicularly to a lipid bilayer can be altered by taking advantage of the unique properties of alamethicin channels.

1.4 Neurons and Signal Transmission

One of the goals of this work is to use artificial lipid bilayer systems to mimic parts of the signal transmission process in a neuron. This section will discuss the basic concepts involved in neuron signal transmission.

1.4.1 The Neuron

The human nervous system is made up of billions of neurons [32]. These neurons help transmit signals around the body. It is important to note that neurons vary considerably in structure and complexity. This section will describe the major components of a typical neuron.

Figure 1-7 shows a diagram of a neuron, a single cell (excluding the myelin sheath), which is surrounded by a lipid bilayer membrane. The dendrites are connected to axon terminals of other neurons. The soma contains the majority of the neuron's organelles (including the nucleus). When an action potential (signal) is generated, it travels down the axon towards the axon terminals. The myelin sheath wraps around the neuron's axon (produced by other cells called Schwann cells), which helps insulate the axon in order to increase the action potential conduction velocity [2, 32]. Neuron cell body diameter can range from approximately 5-100 μm. Axon lengths vary considerably ranging from less than a millimeter to longer than a meter [32]. Neurons are typically connected to one another by an axon terminal to dendrite connection called a synapse. In a human cortex, a single neuron can contain over 50,000 synapses [33].

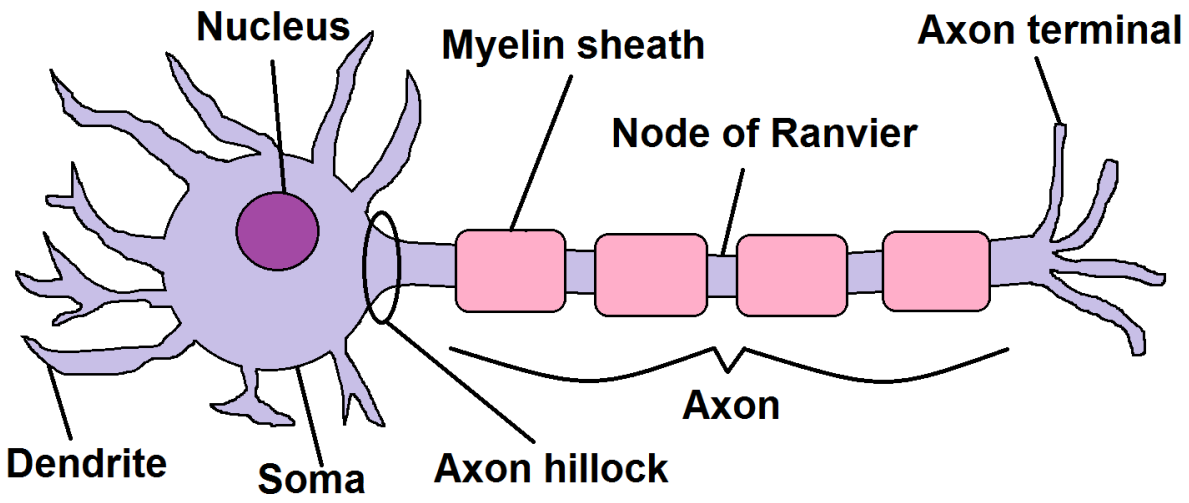

Figure 1-7: **Labeled diagram of neuron.**

In mammalian cells, a neuron's axon is typically covered with a myelin sheath that is created from separate cells called Schwann cells. The myelin sheath wraps around the axon like a roll of tape insulating the axon [2, 32]. Nodes of Ranvier are uninsulated points along the axon that exist between separate myelin sheaths, which occur about every 200-2000 µm along the length of the axon. Each Node of Ranvier is only about 1-2 µm in length [32, 34]. The myelin sheaths and Nodes of Ranvier play important roles in efficient signal transmission in mammalian cells which will be discussed later.

1.4.2 Neuron Signal Propagation Basics

When a synapse fires, an electrical signal is sent through a dendrite towards the soma (refer to Figure 1-7). The signal is then combined with signals from other dendrites (due to the firing of other synapses). If the combined signal reaches a particular threshold, an action potential is generated at the point where the soma is connected to the axon (axon hillock). The action potential is an all-or-nothing event, which means the action potential cannot vary in amplitude. In other words, if the combined signal does not reach the threshold potential, then no signal is sent down the axon. If, however, the combined signal reaches the threshold potential, then an action potential is generated and the signal is transmitted down the length of the axon (carried via ions) to the axon terminals [2, 10, 32, 35, 36].

Electrical signals travel through neurons via ions. Ion concentration gradients as well has ion pumps help drive the ion (signal) flow. The major ionic concentrations in typical mammalian neurons can be found in Table 1-1. Note that the extracellular (outside of the neuron) concentration consists mainly of

sodium (Na^+) and chloride (Cl^-) ions while the intracellular (inside neuron) concentration consists mainly of potassium (K^+) ions. There are ionic concentration gradients across the cell membrane and these gradients lead to a potential (voltage) across the membrane. The resting potential, measured relative to the extracellular fluid, across a neuron membrane is about -70 to -60 mV [2, 10, 32, 35]. In other words, the interior of the cell is less positive compared to the exterior. Cells use energy to drive ion pumps which help maintain this non-zero potential [37].

Table 1-1: **Extracellular and Intracellular Ionic Concentrations of Typical Mammalian Neurons [10, 32, 36, 38]**

Ion	Extracellular Concentration (mM)	Intracellular Concentration (mM)
Sodium, Na^+	140-145	5-15
Potassium, K^+	4-5	130-140
Calcium, Ca^{2+}	1-2.5	0.0001*
Chloride, Cl^-	110-120	5-15

*Note that the total intracellular Ca2+ concentration is between 1-2.5 mM, but most of it is bound or sequestered, so the concentration in the cytoplasm is much lower.

The cell membrane is about 50 times more permeable to potassium (K^+) ions than sodium (Na^+) ions, so it's much easier for potassium (K^+) ions inside the cell to exit than it is for sodium (Na^+) ions to enter. Due to the large difference in potassium (K^+) ion concentrations across the cell membrane, potassium (K^+) ions leave the cell, creating a less positive interior. This potassium (K^+) ion leakage is limited because an electrical potential is created across the cell membrane as the potassium (K^+) ions exit, so eventually the force due to the potassium (K^+) ion concentration gradient is balanced with the opposing force due to the created potential (electrical gradient). When the balancing effects of the sodium (Na^+) ion concentrations as well as other charged particles are considered as well[2], the result leads to the -70 to -60 mV resting potential [2, 39].

Neurons use the resting potential to help drive a signal down the length of their axons. As mentioned previously, channels in the lipid bilayer allow ions to pass through them when open. These ion channels

[2] The potential across a membrane that considers the effects of multiple charged ions is typically approximated using the Goldman-Hodgkin-Katz (GHK) equation 39. Goldman, D.E., *Potential, impedance, and rectification in membranes.* The Journal of General Physiology, 1943. **27**(1): p. 37-60..

are opened and closed in a variety of different ways including voltage-gated and ligand[3]-gated. Voltage-gated ion channels open based on the difference in voltage across a lipid bilayer. For example, assume that the voltage-gated ion channel shown in Figure 1-8 is closed when the potential across the cell membrane is -70 mV. The potential may fluctuate near -70 mV for a period of time, but at some point, the potential across the membrane could increase to the voltage-gated ion channel's threshold potential (-25 mV in Figure 1-8). Once the potential across the membrane reaches the threshold potential of the voltage-gated ion channel, then the channel opens.

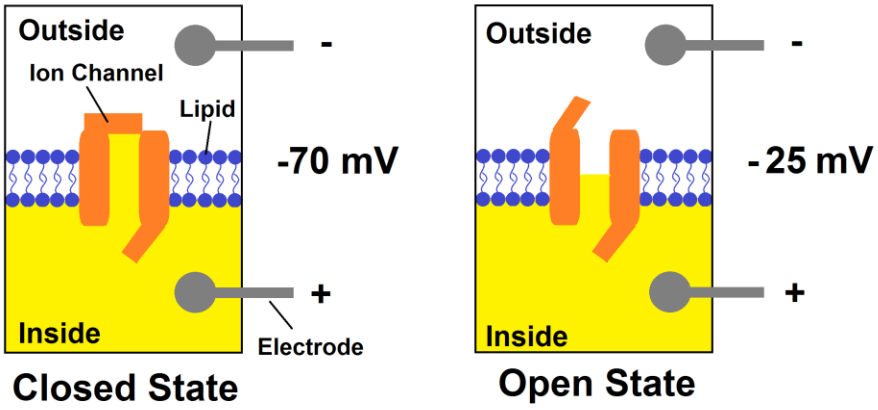

Figure 1-8: **Diagram of voltage-gated ion channel.**

Ligand-gated ion channels are regulated by specific ions or molecules as shown in Figure 1-9. When a particular ion or molecule attaches to the ligand-gated ion channel, it will change states. Once the ion or molecule is removed from the channel, the channel closes again.

[3] A ligand is an atom or molecule. A ligand-gated channel is operated by the attachment and detachment of a specific ligand. For example, a ligand-gated channel might open when a specific ligand attaches to it and might close when the ligand is removed.

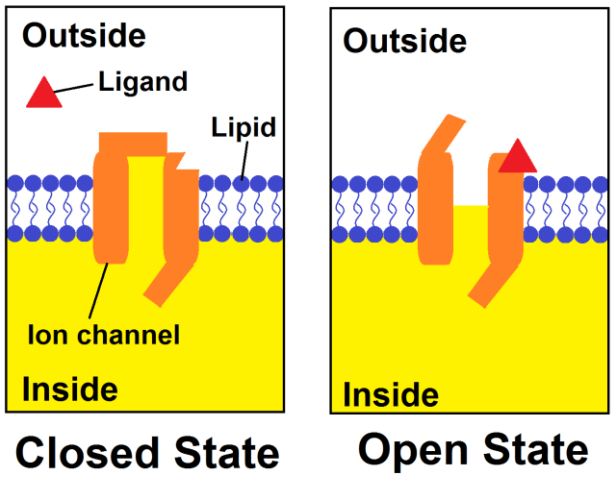

Figure 1-9: **Diagram of ligand-gated ion channel.**

Ion channels are often very selective as to what ions they let pass [2]. For example, a sodium channel may be well suited for sodium (Na^+) ions to travel through, but the larger potassium (K^+) ions may not be able to fit [32].

The two major means of signal propagation are electrotonic (ion diffusion) and through an action potential. Figure 1-10 shows that when a voltage-gated ion channel is opened, sodium (Na^+) ions start to flood into the cell. The Na^+ ions flow into the cell due to the concentration difference and the potential across the membrane. Due to the lower concentration of Na^+ ions inside the cell, when the ion channel opens, the ions immediately diffuse into the cell. The greater the difference in concentration, the greater the number of ions that enter/exit the cell when an ion channel opens. The cell interior is less positive than the exterior, so the positively charged Na^+ ions also flood inside due to the charge difference [2]. Since the channels are selective, the potassium ions much less likely to flow out of the cell via the same channels that the sodium ions are traveling through into cell.

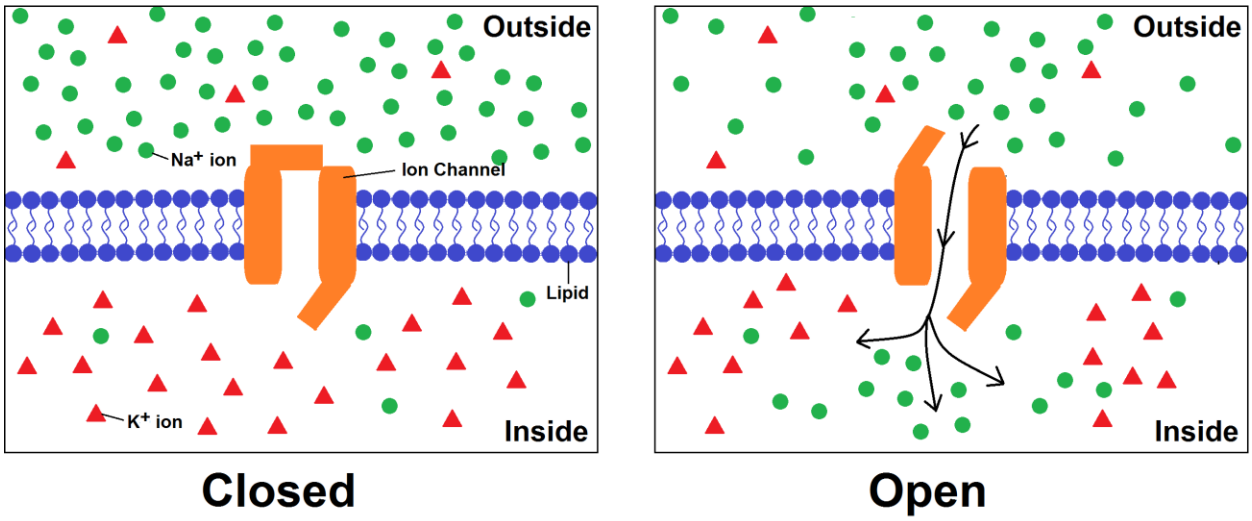

Figure 1-10: **Electronic signal propagation via electrotonic transmission.**

Electrotonic transmission is very fast, but the signal weakens with distance due to a current leaking effect and the fact that the ion influx will slow down due to the smaller concentration and potential gradients across the membrane [32]. The length constant refers to the distance the signal travels before the current (and voltage change) reduces to 1/e (~37%) of the site of entry value. For neurons, the length constants are usually on the order of 100 µm [32]. As the axon diameter increases, the length constant increases as well, so signals transmitted electrotonically can travel longer distances in larger diameter axons [2, 32]. Some species, such as squids, take advantage of this fast means of signal transmission by having large diameter axons.

Action potentials allow electrical signals to be conducted over very long distances without the signal-decay-over-distance effect of electrotonic transmission by taking advantage of the voltage-gated properties of various ion channels in conjunction with the ion concentration gradients across the membrane. Action potentials can be used with much smaller diameter axons, which is important when considering how neurons are packed in an organism. For example, typical mammalian axons range in diameter from about 1-20 µm [40], whereas squid axons range from about 300-800 µm in diameter [41]. Based on these values, a mammal would need a neck that could accommodate over 225 times more axon cross-sectional area in order have the same number of axons.

The axon hillock is the region of a neuron where the soma is connected to the axon. As discussed previously, signals from the multiple dendrites are summed in this region. If the resulting summed

signal reaches a threshold potential value, then voltage-gated sodium channels in the axon hillock become open. Sodium ions in the extracellular fluid around the axon hillock flood into the cell via the voltage-gated sodium channels due to the concentration difference (refer to Table 1-1). As the sodium ions rush into the axon hillock region, they start to diffuse down the axon towards the first myelinated region of the axon (refer to Figure 1-11).

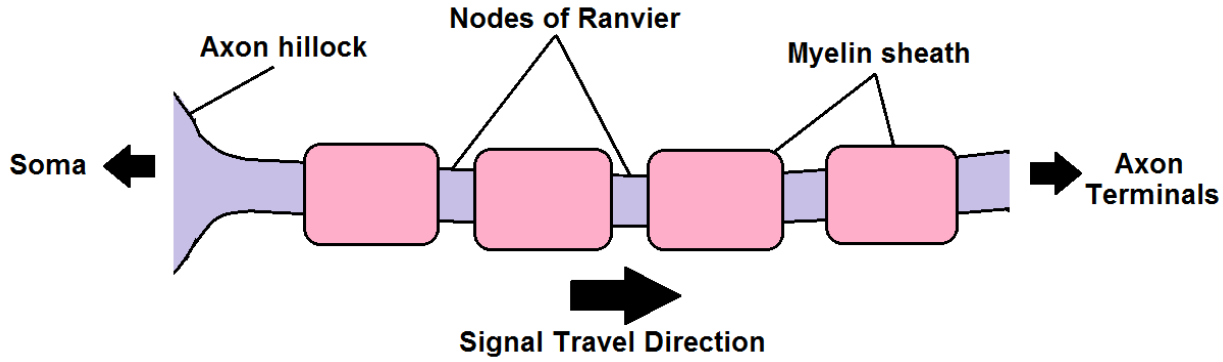

Figure 1-11: **Diagram of neuron axon. Refer to Figure 1-7 for complete diagram of neuron.**

The purpose of the myelin sheath is to insulate the axon, which reduces the amount of current leakage out of the neuron as the signal travels down the axon. However, even with the myelin, current can leak out of the neuron, causing the signal to diminish over distance. The Nodes of Ranvier help alleviate this problem by boosting the signal.

Recall that the nodes of Ranvier are the short uninsulated spaces between the myelinated regions. In these spaces, the neuron's membrane is directly exposed to the extracellular fluid. As the sodium ions flow through the first myelinated region of the axon and into the first node of Ranvier, the potential across the membrane (in the node of Ranvier) increases (moves closer to 0). This increase in potential causes voltage-gated sodium ion channels, which are highly concentrated in the nodes of Ranvier, to open and allow more sodium ions from the extracellular fluid to flood into the axon effectively boosting the signal back to its original magnitude[4]. The sodium ions then flow down through the second myelinated region towards the second node of Ranvier repeating the process. In this way, a signal that originated in the axon hillock is propagated down the length of the axon to the axon terminals [32]. In other words, while the signal amplitude does decay in the myelinated regions, the decayed amplitude is still large enough one it reaches the nodes of Ranvier to open the sodium channels.

[4] Recall that due to leakage, the amplitude of the action potential decays in the myelinated region of the axon.

Up to this point, it has only been explained how a neuron sends a single signal down its axon. Neurons are capable of operating at a speed of approximately 1 kHz. In other words, a single neuron could send 1000 signals down its axon in 1 second. Most neurons, however, operate at much lower frequencies (1 - ~300-400 Hz) [42]. In preparation to send a second signal after the first, a neuron must restore the resting potential that was eliminated when the sodium ions flooded into the cell. To restore the resting potential, the neuron must move the sodium ions back out of the cell to the extracellular fluid and a neuron does this by using pumps. A key pump is the sodium-potassium (Na^+/K^+) ion pump that uses ATP to transport 3 sodium ions from inside the cell to the extracellular fluid and bring 2 potassium ions from the extracellular fluid back into the cell [37]. After the resting potential is restored, the neuron is capable of sending another signal down its axon.

Figure 1-12 is a diagram of the action potential. This plot shows the voltage across the axonal membrane (at a specific point along the axon) as a function of time. The action potential is an "all-or-nothing" event. In other words, an action potential is either generated or it is not. Once the potential across the membrane reaches the threshold potential ($-50\ mV$ in Figure 1-12), an action potential is generated. Both the sodium (Na^+) and potassium (K^+) ion channels open in the membrane at this point, but the Na^+ channels open much more quickly than the K^+ channels. Due to the concentration gradient (Table 1-1), Na^+ ions rush into the cell via the Na^+ channels. At the peak of the action potential ($30\ mV$ in Figure 1-12), the K^+ channels are fully open and the Na^+ channels close. Due the concentration gradient, K^+ ions leave the cell, which repolarizes the cell[5]. The K^+ channels actually remain open after the membrane potential has reached the resting potential ($-70\ mV$ in Figure 1-12), which hyperpolarizes the cell. At this point, the K^+ channels close, allowing the Na/K pumps to restore the cell to the resting potential [10, 36, 43].

[5] Note that the sodium ion channels do not open during the repolarization because there is a refractory period where the sodium ion channels are unable to open. This mechanism helps prevents overstimulation and puts a limit on the frequency at which signals can be generated.

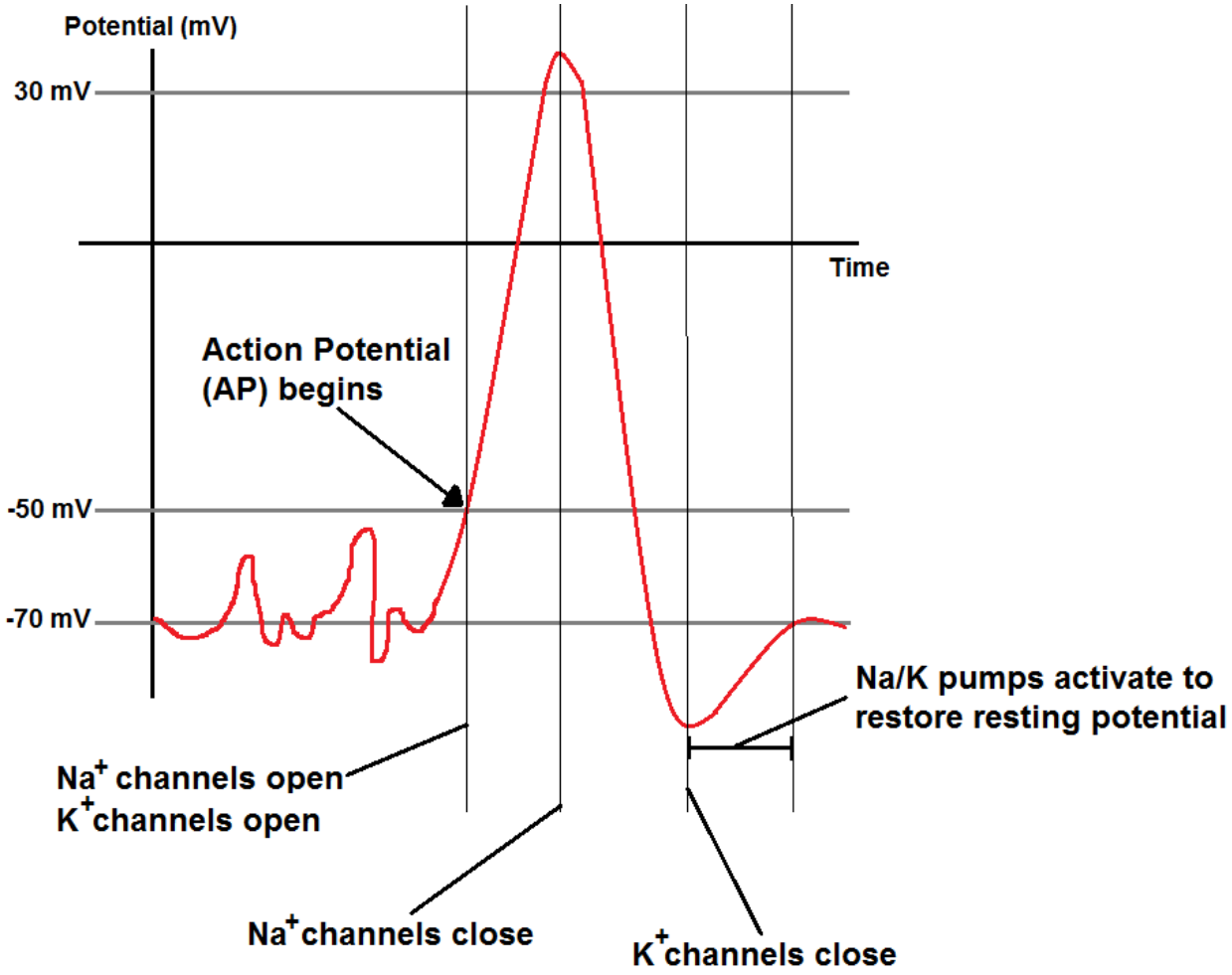

Figure 1-12: **Diagram of action potential.**

1.4.3 Neuron to Neuron Signal Transmission

Signal transmission through a neuron is an ionic process, however, signal transmission from neuron to neuron is a chemical process [2]. Most neurons are connected with an axon terminal to dendrite connection as shown in Figure 6, which is called a synapse. Recall that a single neuron is connected to many other neuron and a single neuron can share many synapses with another neuron as shown in Figure 1-13 [2].

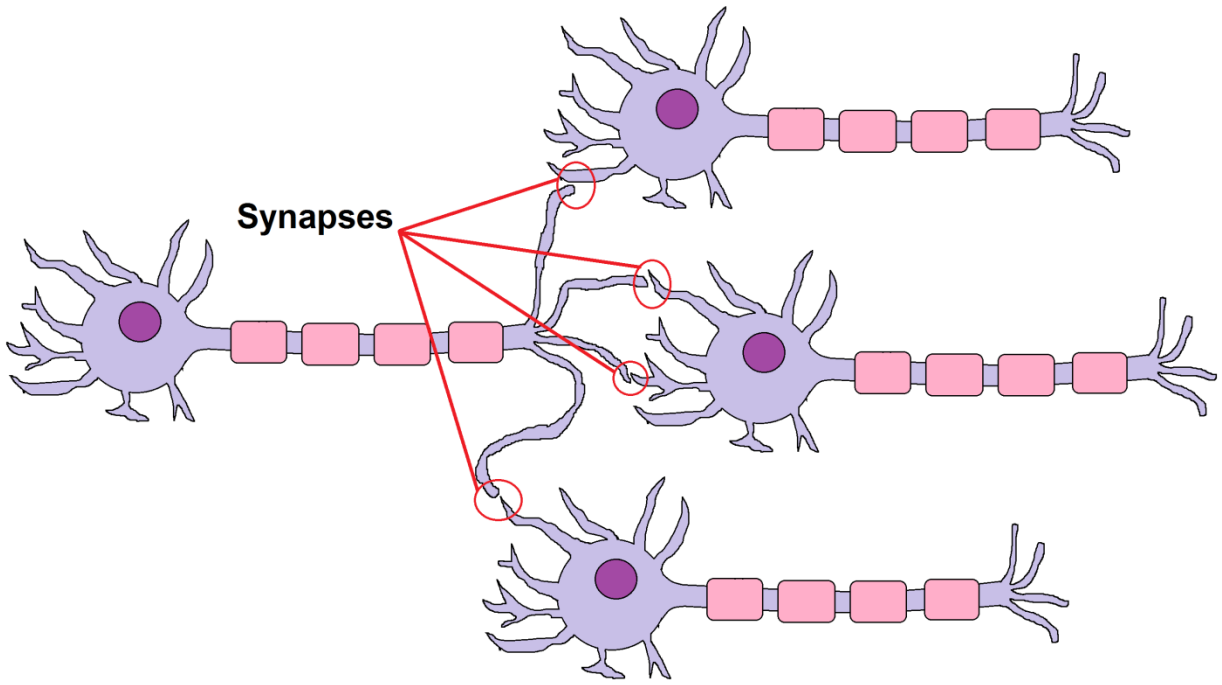

Figure 1-13: **Diagram showing how neurons are typically connected to one another.**

Figure 1-14 shows a diagram of close-up view of a synapse. Note that there is a small gap between the two neurons called the synaptic cleft, which is shown in Figure 1-15. This gap is about 10 – 20 nm in length [2, 32], which means that the neurons are not directly touching one another[6], so an electrical signal could not simply continue using electrotonic transmission or action potentials.

[6] This is typically the case, but there are cases where a "gap junction" exists in that the two neurons are directly connected with a series of proteins 32. Nolte, J., *The Human Brain: An Introduction to its Functional Anatomy, 6th Edition.* 2008..

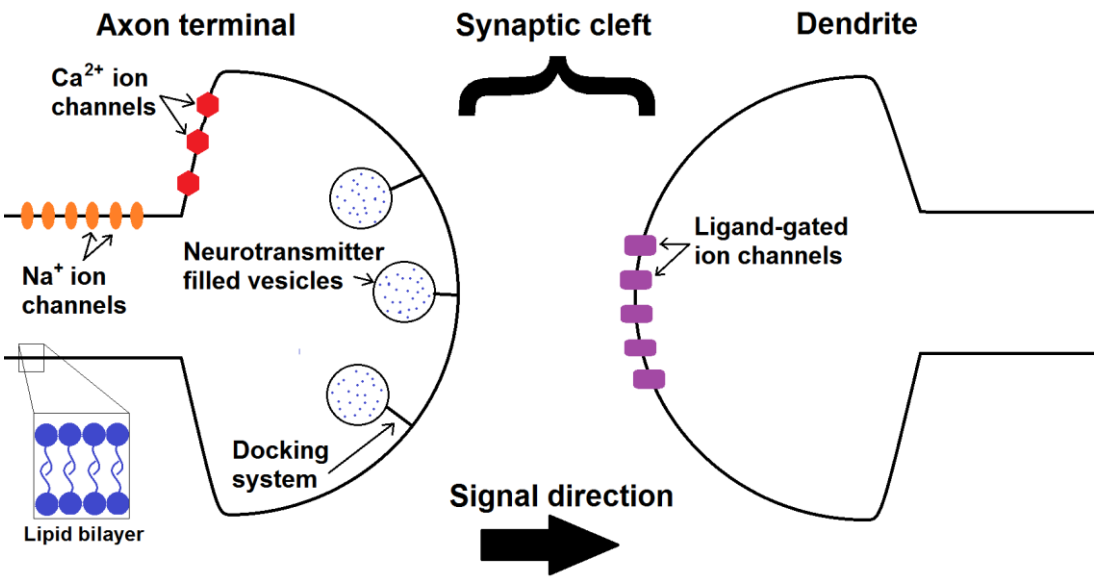

Figure 1-14: **Close-up view diagram of the synapse.**

The axon terminal, also referred to as the presynaptic ending, contains multiple vesicles that are filled with a high concentration of neurotransmitters. Each vesicle is surrounded by a spherical lipid bilayer which encloses the neurotransmitters. Most of these vesicles are about 40 nm in diameter, but larger vesicles with diameters greater than 100 nm exist in small quantities [32].

As the signal travels through the axon towards an axon terminal, the sodium ion channels open in succession as described previously. Once the signal reaches the presynaptic ending, the calcium (Ca^{2+}) ion channels open. The Ca^{2+} ions flood into the cell and attach to the docking system that holds the neurotransmitter vesicles in place. The Ca^{2+} ions alter the proteins that make up the docking system allowing the vesicles to move towards the lipid bilayer separating the presynaptic ending from the synaptic cleft (refer to Figure 8). Once the vesicles reach the axon terminal lipid bilayer, exocytosis occurs and the neurotransmitters are released into the synaptic cleft. This process, from the action potential reaching the calcium ion channels to the release of neurotransmitters is less than 1 ms [2]. This process of releasing the neurotransmitters is shown in Figure 1-15.

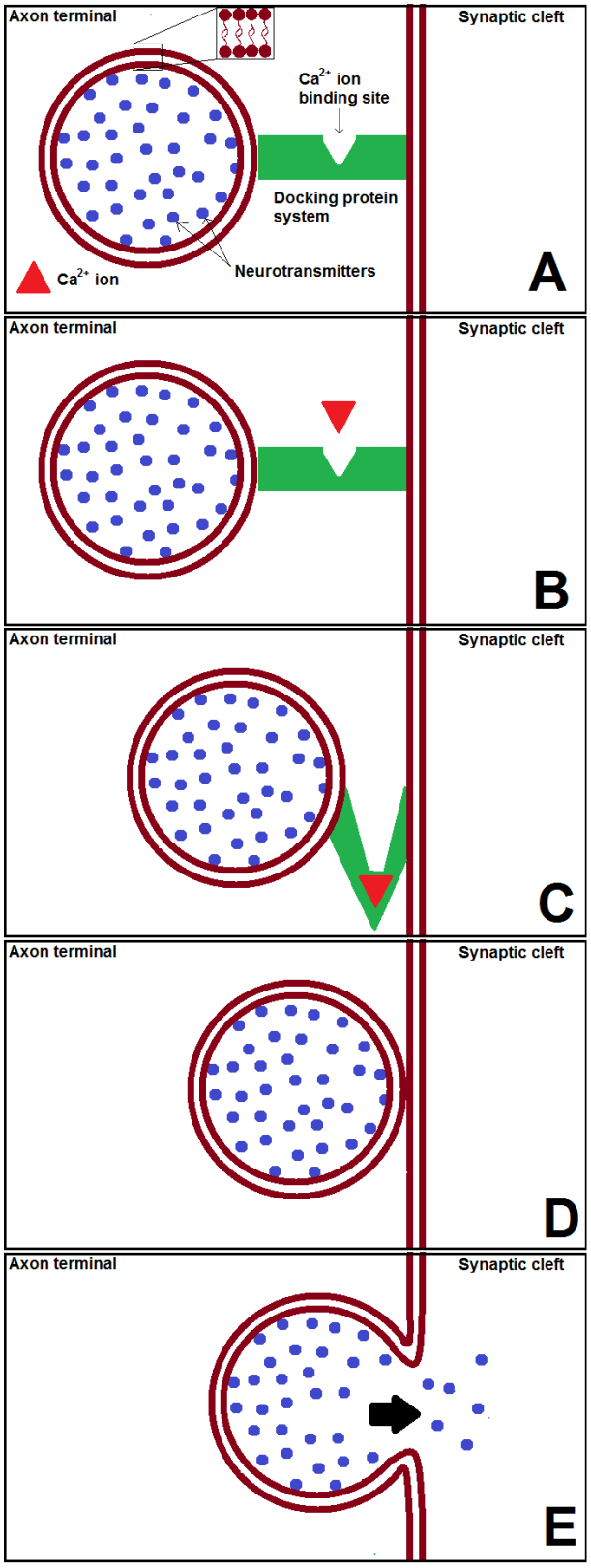

Figure 1-15: **Diagram of a vesicle releasing neurotransmitters into synaptic cleft.**

The released neurotransmitters travel towards the dendrite (postsynaptic ending) of the next neuron. The neurotransmitters attach to the ligand-gated ion channels (refer to Figure 1-9), causing sodium ions to flood into the dendrite allowing the signal to travel through the next neuron [32]. This entire process starting with the activation of the calcium ion channels in the presynaptic ending to the activation of the ligand-gated ion channels of the postsynaptic ending can occur in less than 200 μs [32].

1.5 Research Goals

This thesis has two major research goals. The first is to create an artificial axon system using droplet on hydrogel bilayers (DHBs) in conjunction with alamethicin channels that is capable of showing properties of action potential signal propagation that occurs in myelinated nerve cells. The focus is to use the artificial axon system to recreate biological signal conduction velocities, the action potential amplitude boosting behavior that occurs in the nodes of Ranvier of myelinated nerve cells, and the role of slow-acting potassium channels that help restore the axonal membrane to the resting potential. The second research goal is to investigate how the artificial axon system could be used in other applications such as signal processing that do not necessarily mimic its biological equivalent.

Chapter 2: Experimental Methodology

This chapter presents several topics related to the verifying the existence of a lipid bilayer, techniques used to measure bilayer properties, preparing solutions used to form bilayers, and a discussion of the basic operating principles of a patch-clamp amplifier. The chapter begins by introducing the equivalent circuit model for a droplet interface bilayer (DIB), which is equivalent to that of a droplet on hydrogel bilayer (DHB). Measurement techniques including real-time capacitance recording, electrical impedance spectrometry (EIS), and cyclic voltammetry (CV) are then presented. The procedures for preparing the lipid solution, alamethicin peptides, UV-curable hydrogel, and silver-silver chloride electrodes are also included. The chapter ends with a discussion on the basic operating principles of an Axon Instruments Axopatch 200B (Molecular Devices, Sunnyvale CA), which was used to take the majority of the measurements presented in this thesis.

2.1 Equivalent Circuit Model for a DIB/DHB Lipid Bilayer

Figure 2-1 shows a diagram of two aqueous droplets containing an electrolyte and lipids that are brought into contact with one another to form a lipid bilayer at the interface. An electrode (gray) has been placed inside each of the two droplets in order to electrically stimulate and measure the bilayer properties. The equivalent circuit diagram for the two droplet system is shown. The lipid bilayer is modeled as a resistor and capacitor connected in parallel [11, 44, 45]. There is also a small resistance (relative to the bilayer resistance) associated with the electrolyte solution.

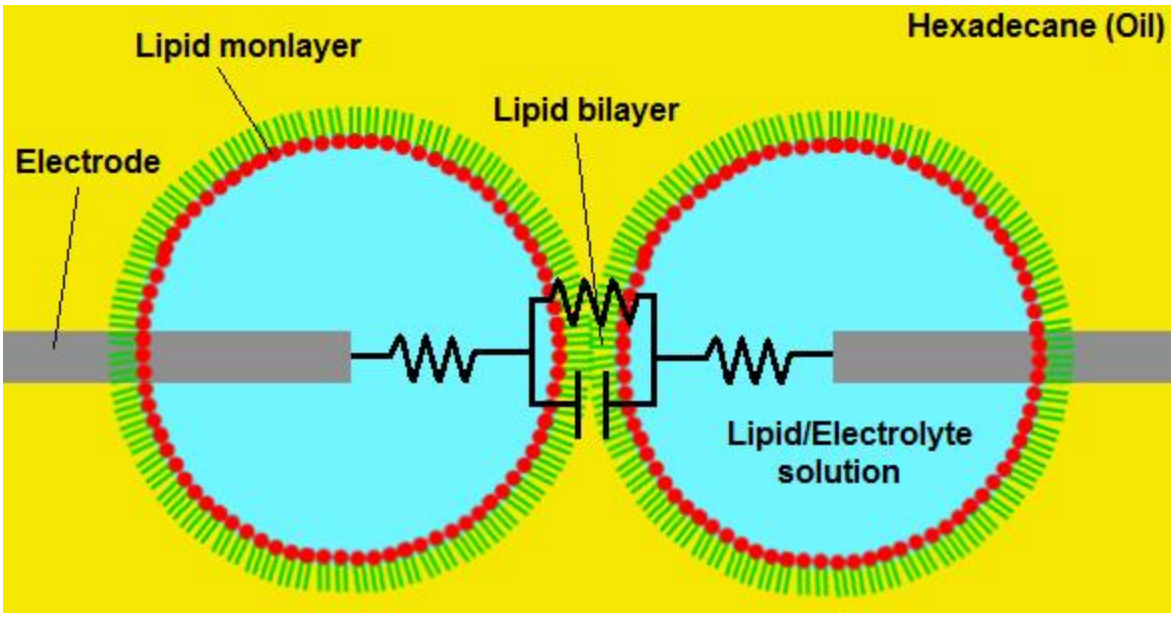

Figure 2-1: **Diagram of two aqueous droplets containing an electrolyte and lipids brought into contact with one another to form a bilayer at the interface. The equivalent circuit model for the system is overlaid on the diagram.**

The two electrolyte resistances can be lumped into a single resistor, R_E, as shown in Figure 2-2. R_M and C_M represent the lipid bilayer's resistance and capacitance, respectively.

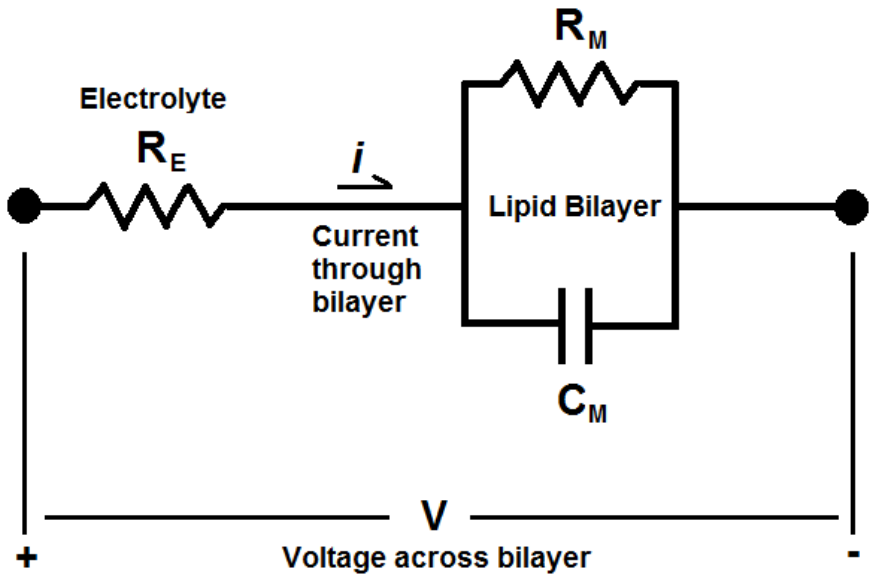

Figure 2-2: **Equivalent electrical circuit for a single lipid bilayer**

2.2 Verifying the Existence of a Bilayer

Due to the small size of the system, it is difficult to verify the existence of a lipid bilayer based on a visual inspection alone. In order to ensure that a bilayer has been formed, the system (Figure 2-1) is electrically stimulated with a trianglular voltage wave and the current response is recorded. The existence of a bilayer can be determined based on the characteristics of the current response.

Based on the bilayer circuit model shown in Figure 2-2, the total current, i, is split once it reaches the bilayer. Part of the current flows through the bilayer resistor, R_M, and the remaining amount flows through the bilayer capacitor, C_M. Assuming that the impedance (complex resistance) of R_M is much greater than that of C_M, then the current flowing through R_M is negligible compared to that through C_M. In other words, nearly all of i flows through C_M and a negligible amount flows through R_M. Based on this assumption, R_M can be removed from the circuit model. This occurs when a bilayer has formed.

Current through a capacitor can be calculated as:

$$i = C\frac{dV}{dt} \tag{2-1}$$

Where i is the current, C is the capacitance, and $\frac{dV}{dt}$ is the time derivative of the voltage. For simplicity, assume that the voltage drop across the electrolyte resistor, R_E, is negligible. R_E is typically on the order of $k\Omega$, whereas R_M is on the order of $G\Omega$. Therefore, the current that travels through the system can be calculated by using Equation (2-1):

$$i = C_M\frac{dV}{dt} \tag{2-2}$$

Based on Equation (2-2), if a triangular voltage signal operating at $10\ Hz$[7], V, is applied across a bilayer, then the current through the bilayer should be square as shown in Figure 2-3 because $\frac{dV}{dt}$ is constant while the triangle wave is either increasing or decreasing. Note that Figure 2-3 was generated using the bilayer circuit model shown in Figure 2-2. Based on the plot, for expected values of the bilayer

[7] Note that the frequency of the triangle wave is important because the current can only be assumed to be capacitive above a certain frequency (typically ~$10\ Hz$). Refer to the phase plot of a resistor and capacitor connected in parallel.

resistance ($\sim 10\ G\Omega$), it is a reasonable to assume that the current through the bilayer resistor, R_M, is negligible based on the square current response. If the current through R_M was not negligible, the current through the bilayer would have a noticeable positive slope at the peak of the square wave and a negative slope at the trough.

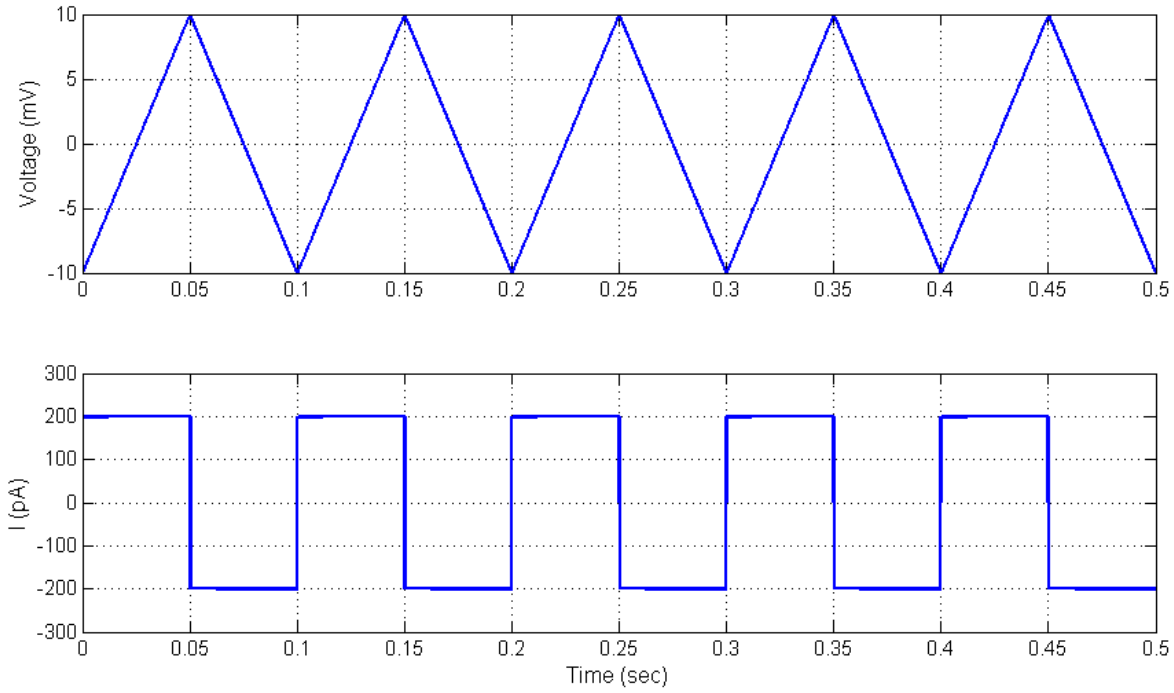

Figure 2-3: **Simulated current response through a lipid bilayer in response to a triangular input voltage signal. (Top) The input voltage signal is a 20 mV_{pp} sawtooth signal operating at $10\ Hz$. (Bottom) Ideal current response through a single bilayer to a triangular voltage input signal. Circuit parameters: $R_E = 10\ k\Omega, R_M = 10\ G\Omega, C_M = 500\ pF$. The MATLAB code used to generate this plot can be found in Section A.5 in Appendix A.**

Figure 2-4 shows the experimental current response through a real lipid bilayer to a $20\ mV_{pp}$ triangular signal operating at $10\ Hz$. As expected, the current through the lipid bilayer is square since the current is predominately capacitive. The spikes observed in the current plot are due to noise in the system such electrical noise, mechanical vibrations, etc.

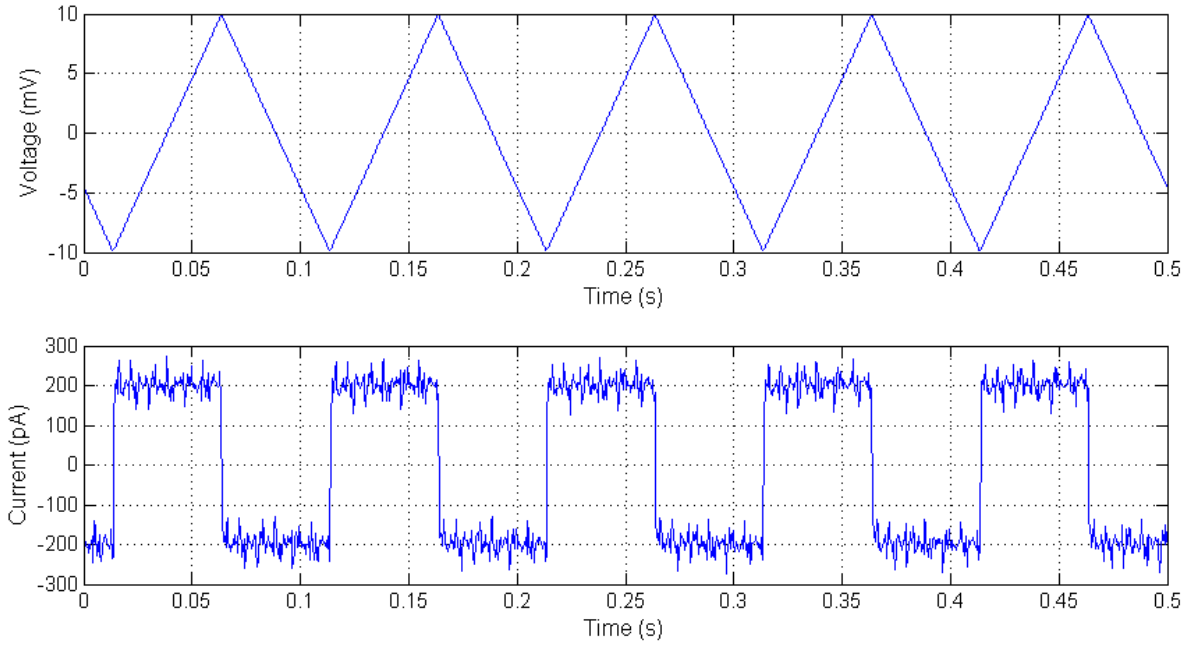

Figure 2-4: **(Top)** $20\ mV_{pp}$ **triangular signal operating at** $10\ Hz$ **applied across a lipid bilayer. (Bottom) Current through a lipid bilayer in response to the input voltage signal.**

Based on the data in Figure 2-4, a lipid bilayer exists because the response shows a capacitive behavior. If a bilayer had not formed, the current response would either be a flat line at $i = 0$ (oil has not been purged from between the monolayers) or triangular if there were significant leaks in the bilayer. Assuming the response looked like that in Figure 2-4, the experimenter would know that he/she has formed a lipid bilayer.

For many types of experiments, it is important to use a bilayer of similar size in an effort to control as many variables as possible across all tests. In order to do this, the area of the bilayer can be calculated using the measured capacitance. Using Equation (2-2), the capacitance of the bilayer shown in Figure 2-4 can be approximated as:

$$C_M = i\frac{dt}{dV} = (200\ pA)\frac{0.05\ s}{20\ mV}\cdot\frac{1000\ mV}{1\ V} = 500\ pF$$

The specific capacitance of lipid bilayers has been measured as approximately $0.4 - 0.6\ \frac{\mu F}{cm^2}$ [46-49], although a value of $0.6\ \frac{\mu F}{cm^2}$ seems to be the accepted value for DPhPC lipid bilayers. Assuming the bilayer area is circular, then the area of the bilayer can be calculated as:

$$A = \pi \frac{D^2}{4}$$

Where A is the area of the bilayer and D is the diameter of the bilayer.

In order to determine diameter of the bilayer, the area of the bilayer must be known. The specific capacitance can be used in conjunction with the capacitance of the bilayer to approximate the area as follows:

$$A = \sigma C_M$$

Where C_M is the bilayer capacitance and σ is the specific capacitance.

By solving for D using the previous two equations, the the diameter of the bilayer shown in Figure 2-4 can be calculated as:

$$D = \sqrt{\frac{4}{\pi}\frac{C_M}{\sigma}} = \sqrt{\frac{4}{\pi} \cdot \frac{500\ pF}{0.6\ \frac{\mu F}{cm^2}} \cdot \frac{1\ \mu F}{(10^6\ pF)} \cdot \frac{(10^8\ \mu m^2)}{1\ cm^2}} = 326\ \mu m$$

Figure 2-5 is a theoretical plot of both the bilayer capacitance and diameter as a function of the measured peak square wave current for DPhPC lipids. For the data shown in Figure 2-4, the peak current is approximately $200\ pA$, the expected capacitance (based on the plot) is $500\ pF$ and the corresponding diameter is about $325\ \mu m$. These values match the previous calculations.

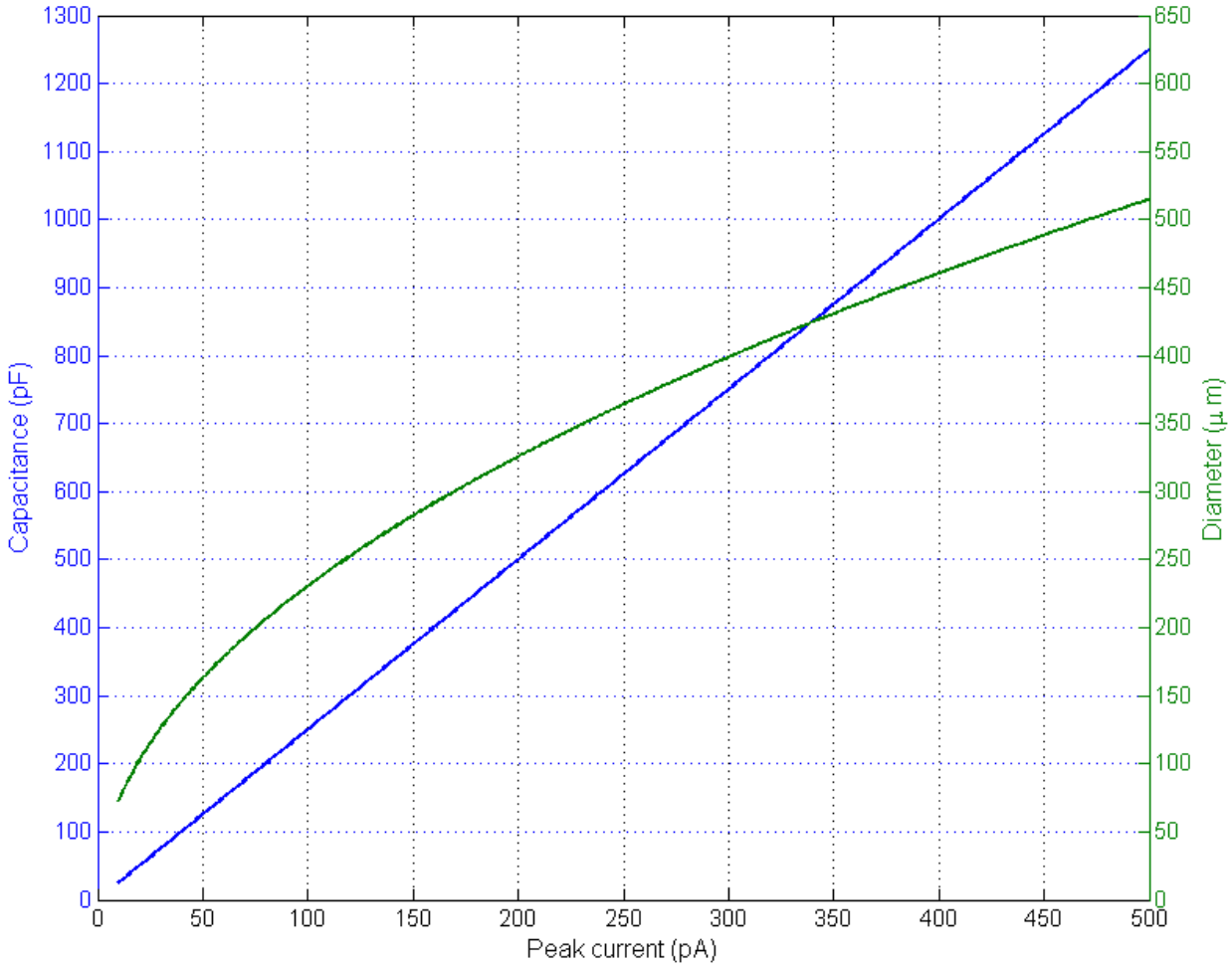

Figure 2-5: **Bilayer capacitance and diameter as a function of the peak square wave current for a $20\ mV_{pp}$ $(10\ Hz)$ potential applied across the bilayer. Note that this plot assumes that the bilayer resistive current is negligible. Note that this theoretical plot is only for DPhPC lipids assuming the specific capacitance is $0.6\ \mu F/cm^2$.**

2.3 Zipping/Growing Behavior of Bilayers

When two aqueous droplets consisting of lipids and an electrolyte are brought together, a bilayer will not necessarily immediately form. The reasoning is that when the two droplets are brought together, there is a small amount of hexadecane (oil) that is trapped in the interface. In order for a bilayer to form, this excess hexadecane must be purged from the interface which occurs due to van der Waal forces acting on the two lipid monolayers [11].

During the transition time where the oil is being removed and the two lipid monolayers are "zipping" together [11], there is a rise in the measured current because the capacitance (C_M) in the system is increasing. However, for experiments presented in this thesis, the "zipping" event where the bilayer is

formed could range between $1-5\ min$ after the droplets are brought into contact. In other words, the droplets could be in contact for $5\ min$ before the current started to increase due to the "zipping" event. During an experiment, the droplets would be brought into contact and a $20\ mV_{pp}\ (10\ Hz)$ triangle wave would be applied across the interface. The experimenter would then wait until he/she saw a sudden increase in the current amplitude, which would indicate the formation of a lipid bilayer as the oil was removed from between the monolayers (Figure 2-6). It should be noted that by applying a small DC potential $(20-50\ mV)$ along with the $20\ mV_{pp}\ (10\ Hz)$ triangle wave, that the oil can be expelled more quickly. The DC potential creates an additional force that helps purge the oil from the interface.

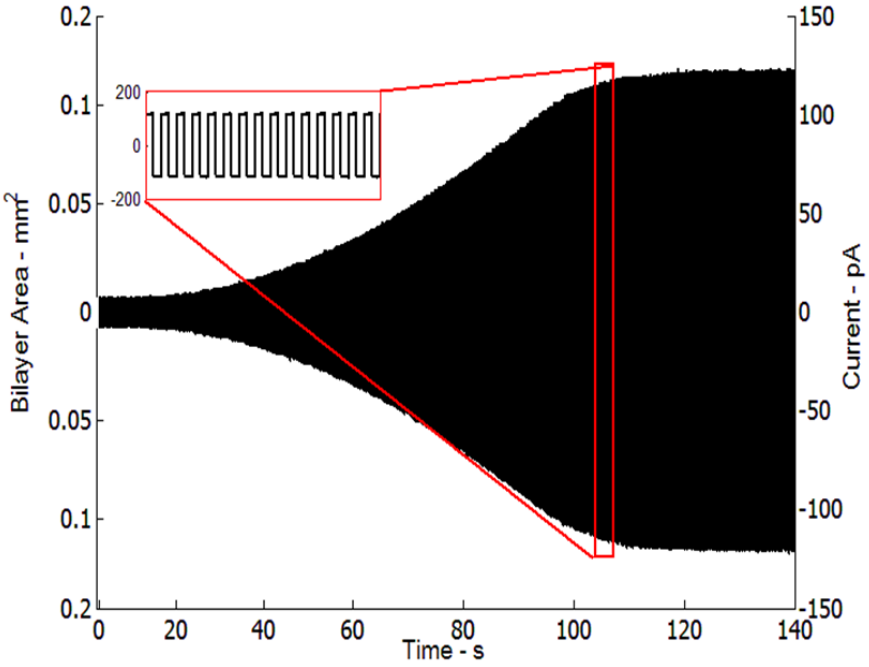

Figure 2-6: **Plot showing bilayer formation. The right axis shows the current increasing as the two monolayers zip together and the left axis shows the corresponding increase in bilayer area as the zipping occurs. This plot is reprinted with permission from Taylor Young [23].**

2.4 Electrical Impedance Spectroscopy (EIS)

Electrical Impedance Spectroscopy (EIS) is the measure of the impedance (resistivity to current flow) of a system as a function of frequency. Impedance, $Z(\omega)$, is defined as:

$$Z(\omega) = \frac{V(\omega)}{I(\omega)} \tag{2-3}$$

where ω is the excitation frequency (rad/s), V is the voltage (Volts), and I is the current (Amps). The complex impedance varies for different electrical components. Equation (2-4) shows the complex impedance of a resistor and a capacitor. Note that the impedance of a resistor is independent of the excitation frequency. A capacitor's impedance, however, is inversely related to the excitation frequency. As the excitation frequency and capacitance is increased, the impedance decreases.

$$Z_{Resistor} = R, \;\; Z_{Capacitor} = \frac{1}{j\omega C} \tag{2-4}$$

where R is the resistance, C is the capacitance, ω is the excitation frequency (rad/s), and j is a complex number.

By using complex impedances, all of the circuit elements can be combined similarly to combining multiple resistors connected in a circuit. For example, the equivalent resistance of multiple resistors in series is simply the sum of all of the resistances, whereas the equivalent resistance of multiple resistors in parallel is the inverse of the sum of all the inverses of the resistances. This same method of combining resistors can be used with complex impedances, which allows you to combine the impedances of resistors and capacitors into a single equivalent impedance.

The equivalent impedance for the circuit shown in Figure 2-2, is:

$$Z_{eq} = Z_{R_E} + \frac{Z_{R_M} Z_{C_M}}{Z_{R_M} + Z_{C_M}} \tag{2-5}$$

Substituting Equation (2-4) into Equation (2-5) yields:

$$Z_{eq} = R_E + \frac{R_M}{j\omega R_M C_M + 1} \tag{2-6}$$

Using the complex form of Ohm's Law (Equation (2-3)), the transfer function can be written as:

$$\frac{I(\omega)}{V(\omega)} = \left[R_E + \frac{R_M}{j\omega R_M C_M + 1} \right]^{-1} \tag{2-7}$$

Where $V(\omega)$ is the voltage applied to the system (input) and $I(\omega)$ is the measured current (output).

By varying the excitation frequency, ω, of the input voltage, $V(\omega)$, and recording the corresponding current, $I(\omega)$, the results can be fitted to Equation (2-7) in order to determine the system parameters (R_E, R_M, C_M). For example, Figure 2-7 shows the EIS data for a test circuit consisting of a $5\ G\Omega\ (\pm 0.5\ G\Omega)$ resistor in parallel with $500\ pF\ (\pm 50\ pF)$ capacitor all in series with a $1\ M\Omega\ (\pm 0.1\ M\Omega)$ resistor (same as the bilayer model in Figure 2-2). Using a MATLAB code[8], a best-fit transfer function (labeled "Model" in Figure 2-7) can be used to estimate the values of the circuit components. The estimated values of the circuit components for the experimental data shown in Figure 2-7 can be found in Table 2-1.

.

.

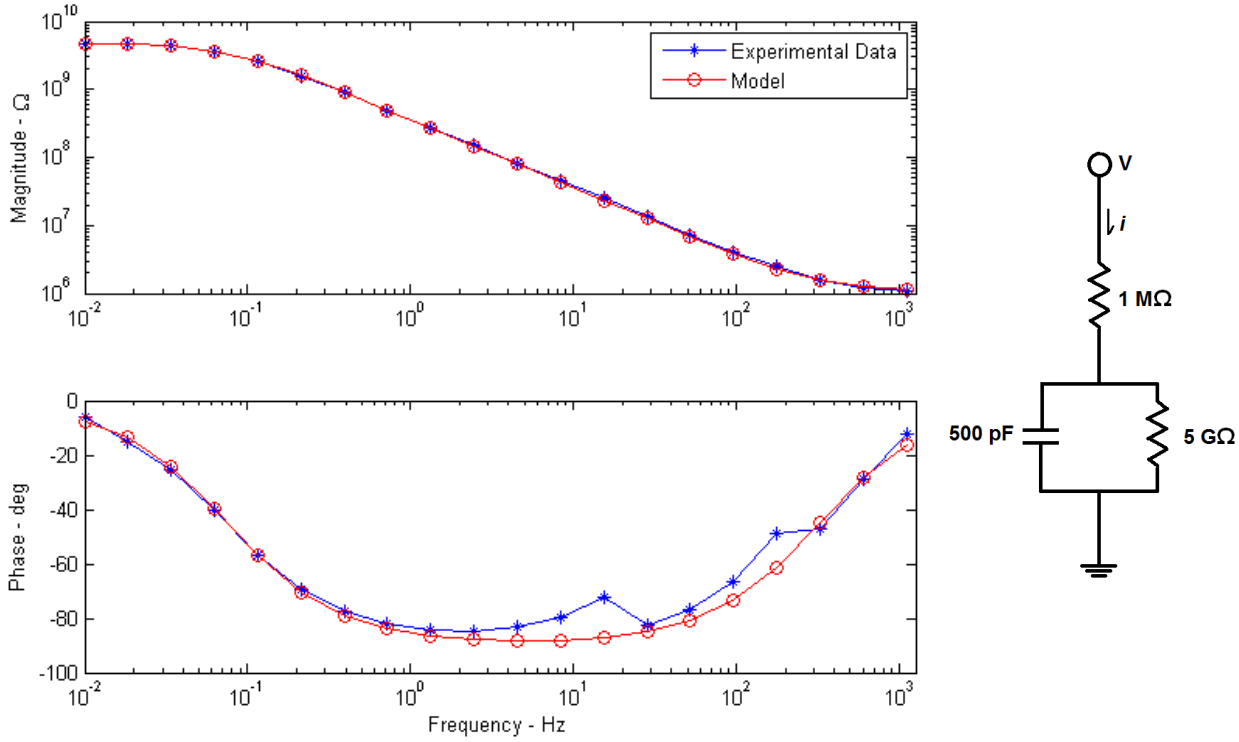

Figure 2-7: **Left) Electrical impedance spectroscopy data for the electrical circuit shown. Right) Electrical circuit diagram.**

[8] The MATLAB code used to fit a specific transfer function to experimental EIS data was originally developed by Dr. Andy Sarles (refer to Appendix A: EIS Data Fitting).

Table 2-1: **MATLAB code results for the EIS data shown in Figure 2-7. The "Listed Value" refers to the value of the individual electrical circuit components. For example, a $1\ M\Omega$ resistor with a tolerance of $\pm 10\%$ was used as the "Electrolyte Resistance." Refer to Appendix A: Supporting MATLAB Codes for a copy of the script.**

Circuit Component	Listed Value	Code Results
Electrolyte Resistance	$1\ M\Omega\ (\pm 0.1\ M\Omega)$	$1.1\ M\Omega$
Bilayer Resistance	$5\ G\Omega\ (\pm 0.5\ G\Omega)$	$4.8\ G\Omega$
Bilayer Capacitance	$500\ pF\ (\pm 50\ pF)$	$440\ pF$

2.5 Cyclic Voltammetry (CV)

Cyclic voltammetry (CV) measurements consist of stepping through applied potentials and measuring the current through the system. For example, Figure 2-8 shows the CV data for a $1\ M\Omega$ resistor. As expected, the current through the resistor is linearly related to the applied voltage across it according to Ohm's Law.

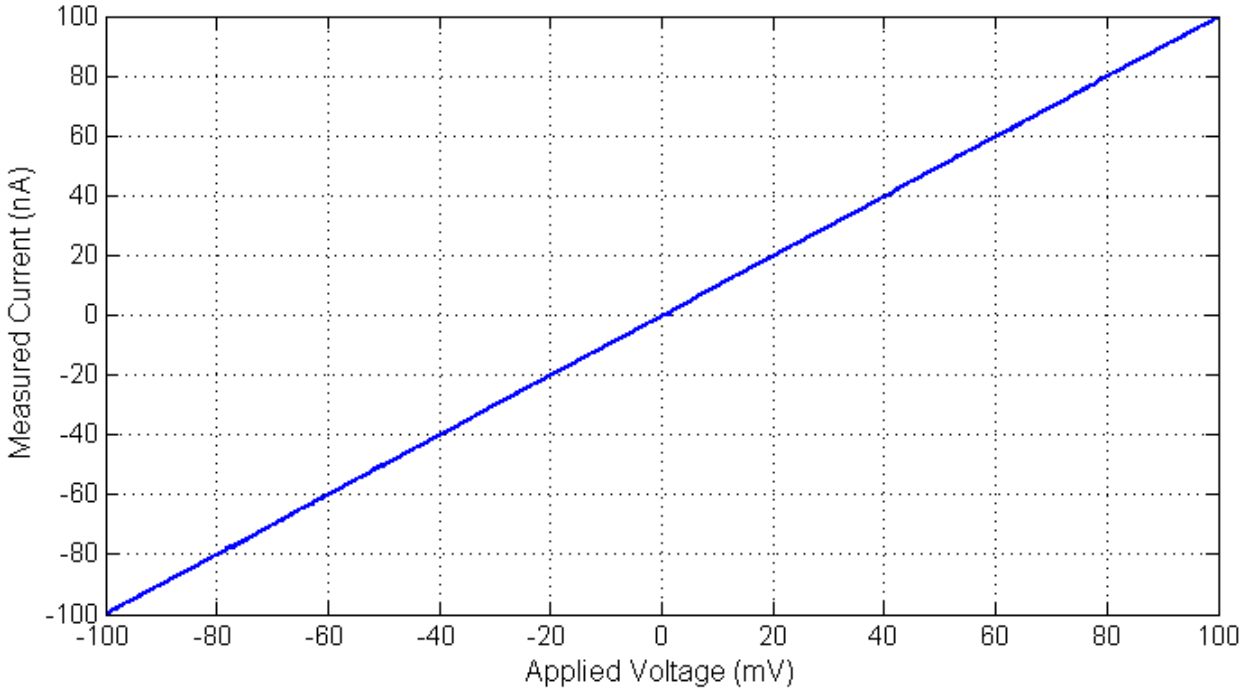

Figure 2-8: **Cyclic voltammetry data for a $1\ M\Omega$ resistor.**

When alamethicin peptides are mixed in the lipid/electrolyte solution, pores will form in the bilayer in response to an applied voltage across the bilayer. When the pores are formed, more current can flow through the bilayer as a result of the reduced bilayer resistance. Figure 2-9 shows the cyclic voltammetry data for a bilayer that contains alamethicin peptides (blue) and a bilayer that does not

contain alamethicin peptides (red). Based on the plot, once the potential across the bilayer (x-axis) reaches approximately $60\ mV$ in magnitude, the alamethicin peptides begin to form pores which increases the total current flowing through the bilayer (y-axis).

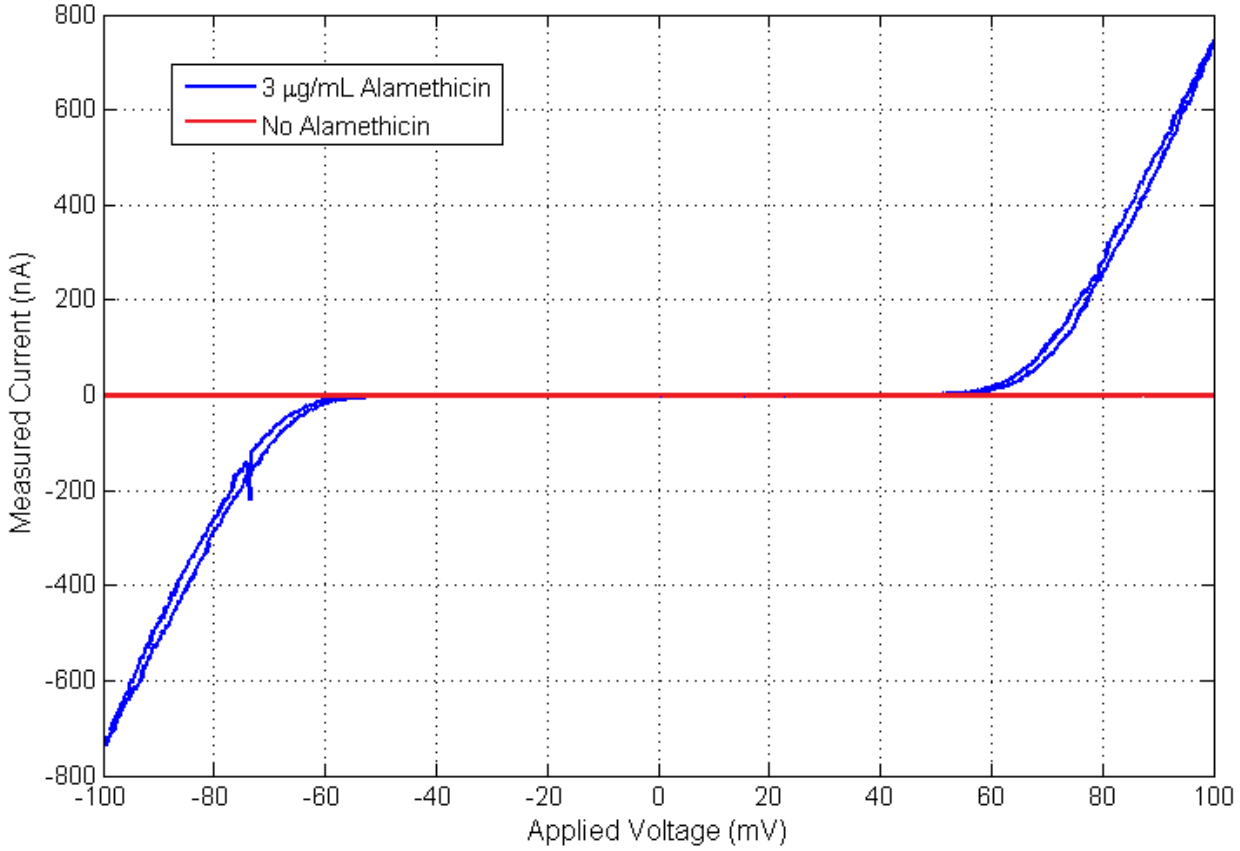

Figure 2-9: **Cyclic voltammetry data for two different bilayers: one with $3\ \mu g/mL$ alamethicin (blue) and one without alamethicin (red). Blue) $3\ \mu g/mL$ case: $1100\ pF$ $(\sim 480\ \mu m)$ Red) No alamethicin case: $360\ pF$ $(\sim 280\ \mu m)$. $500\ mM$ KCl electrolyte concentration.**

2.6 Silver-Silver Chloride Electrodes

In traditional electrical circuits, current travels as electrons through conductive materials such as copper wire [50]. In biological cells, as discussed previously, current is conducted as charged particles known as ions through an electrolyte solution[9]. In order to electrically stimulate an experimental lipid bilayer and record the current response, there must be a conversion point between the stimulating/measurement system (traditional wires/electrons) and the biological system (electrolyte/ions). Silver electrodes with a silver-chloride coating are used as this conversion point.

[9] The electrolyte solution used in this thesis is potassium chloride (KCl). When mixed with water, KCl dissociates to form K^+ and Cl^- ions.

250 µm diameter silver wire (Goodfellow, Huntingdon, England) electrodes were placed in a 50/50 (% vol) bleach (Clorox) and water solution for a 30 minute period in order to apply the silver-chloride coating. The chlorided electrodes were then rinsed in DI water for 2-3 minutes and then dried under a nitrogen stream. Note that after the chloriding period, the electrode has two ends. Once end has the chloride coating and the other does not. This is important because the chloride coating acts as an insulator between two metal contacts, so the chlorided end should be inserted in the droplet whereas the non-coated end is attached to the measurement system. The chlorided portions of the electrode can be distinguished from the unchlorided parts by its characteristic brownish purple color.

In order to convert the current from electrons to ions, a chemical reaction occurs at the electrode/electrolyte interface. The silver chloride electrode reaction is shown below:

$$AgCl(s) + e^- \leftrightharpoons Ag(s) + Cl^- \quad \textbf{(2-8)}$$

Where $AgCl(s)$ is the solid silver-chloride (coating), e^- is an electron, $Ag(s)$ is the solid pure silver, and Cl^- is a chloride ion. If a Cl^- ion reacts with one of an electrodes' silver atoms $\left(Ag(s)\right)$, then it will produce a $\left(AgCl(s)\right)$ molecule and an electron (e^-). In this way, a signal in the electrolyte (transmitted via Cl^- ions) is converted to a signal in metal wires (transmitted via electrons e^-). The $\leftrightharpoons$ sign indicates that the reaction can happen both ways, so signals can be converted from electrons to ions as well.

2.7 Chemical Preparation

This section describes the process for preparing the aqueous lipid solution and the UV-curable hydrogel solution. It also describes how alamethicin, which is stored in ethanol, can be incorporated into the lipid solution.

2.7.1 Aqueous Lipid/Electrolyte Solution

The aqueous solution consists of a suspension of phospholipid vesicles, biological buffering agent, and potassium chloride all contained in deionized water. A powder form of 1,2-diphytanoyl-*sn*-glycero-3-phosphocholine (DPhPC) lipids (Avanti Polar Lipids, Inc., Alabaster, AL) is mixed with a potassium chloride (KCl, Sigma Aldrich, St. Louis, MO) solution and 10 mM 3-(N-Morpholino propanesulfonic acid (MOPS, Sigma Aldrich, St. Louis, MO) to get a final concentration of 2 $\frac{mg\ DPhPC\ \ lipids}{ml}$ solution. Please

note that the concentration of the potassium chloride solution is either $10\ mM$ KCl or $500\ mM$ KCl for the data presented in this thesis. The experimental data presented in Chapters 3 & 4, the electrolyte concentration is $10\ mM$ KCl. For the the data presented in Chapter 5, however, the KCl concentration is $500\ mM$ KCl.

After the solution is mixed (often by simply shaking the container by hand), the solution must be frozen and thawed for 6 cycles. After the cycles are complete, the solution is filtered 2-3 times using a polypropylene in-line holder (Sterlitech, Kent, WA) with a 0.4 µm polycarbonate membrane filter (Sterlitech). The solution is then filtered 2-3 times with a 0.1 µm Isopore membrane filter (Millipore, Billerica, MA). The aqueous solution is stable for up to 1 year if stored at -20°C.

The alamethicin peptide (produced by the fungus *Trichoderma viride*) comes in a powder form (A.G. Scientific, San Diego, CA) and is mixed with ethanol (Sigma Aldrich, ST. Lous, MO) at a 0.1% (wt./vol.) concentration for storage. The solution is stored at -20°C. Ethanol negatively affects the stability of lipid bilayers [51], so it is important that the ethanol be sufficiently diluted by mixing the alamethicin in ethanol solution with the aqueous solution. The alamethicin concentration is often diluted from a $100\ \frac{mg}{mL\ ethanol}$concentration down to a $10-100\ \frac{ng}{mL\ aqueous\ solution}$ concentration. It is assumed that the change in concentration of lipids ($2\frac{mg}{ml}$ in aqueous solution) is negligible for this dilution process.

2.7.2 Hydrogel Solution Preparation

The UV curable hydrogel solution was prepared by melting 15 grams of poly(ethylene-glycol) dimethacrylate 1000 MW (PEG-DMA 1000MW, Polysciences, Inc., Warrington, PA) in an $80\ ℃$ oven. A 10 mM KCl solution was added to the melted PEG-DMA until the total mixture measured 15 mL. The mixture was then shaken (by hand) for 1-2 minutes and placed back in the oven for a 10 minute period. The mixture container was wrapped in electrical tape to limit the amount of UV exposure and 0.075 g of Irgacure 2959 (BASF, The Chemical Company), the UV curing agent, was added. Note that once the UV curing agent is added, the hydrogel solution will begin solidify when exposed to UV light. The mixture was shaken again for a 1-2 minute period and placed back in the oven for a 10 minute period. The final solution composition was $40\%\ \frac{wt.}{vol.}$ PEG-DMA with $0.5\%\ \frac{wt.}{vol.}$ Irgacure 2959 mixed in a 10 mM KCl solution.

2.8 Axopatch Theory and Operation

As shown in the experimental result in Figure 2-4, the current through the bilayer was measured in picoAmps[10]. The smallest current that traditional digital multimeters (DMMs) can read is microAmps, which is 1 million times larger than a picoAmp. In order to measure currents in the picoAmp range, a patch-clamp amplifier circuit can be used. For the experiments presented in this thesis, an Axon Instruments Axopatch 200B (Molecular Devices, Sunnyvale CA) was used in conjunction with a Digidata 1440A (Molecular Devices) to make the electrical measurements.

In order to familiarize the reader with the measurement system configuration, Figure 2-10 shows how the Axopatch 200B is connected to a droplet interface bilayer (DIB) in order to electrically stimulate it and record measurements. The two aqueous droplets are connected to the headstage (CV 203BU), which is connected to the Axopatch 200B. The headstage is small unit that is connected directly to the aqueous droplets. It contains additional circuitry that helps reduce signal noise while operating the Axopatch 200B in certain modes. In order to apply a signal to the bilayer, an Agilent 33220A function generator (Agilent Technologies, Santa Clara, CA) is used. Note that the signal coming out of the function generator is divided by 50 (due to the Axopatch 200B's internal circuitry) before it is applied to the headstage [52]. For example, a $100\ mV_{pp}$ sine wave generated at the function generator would only apply a $2\ mV_{pp}$ sine wave at the two electrodes in the aqueous droplets.

[10] There are 1 trillion (10^{12}) picoAmps in an Amp.

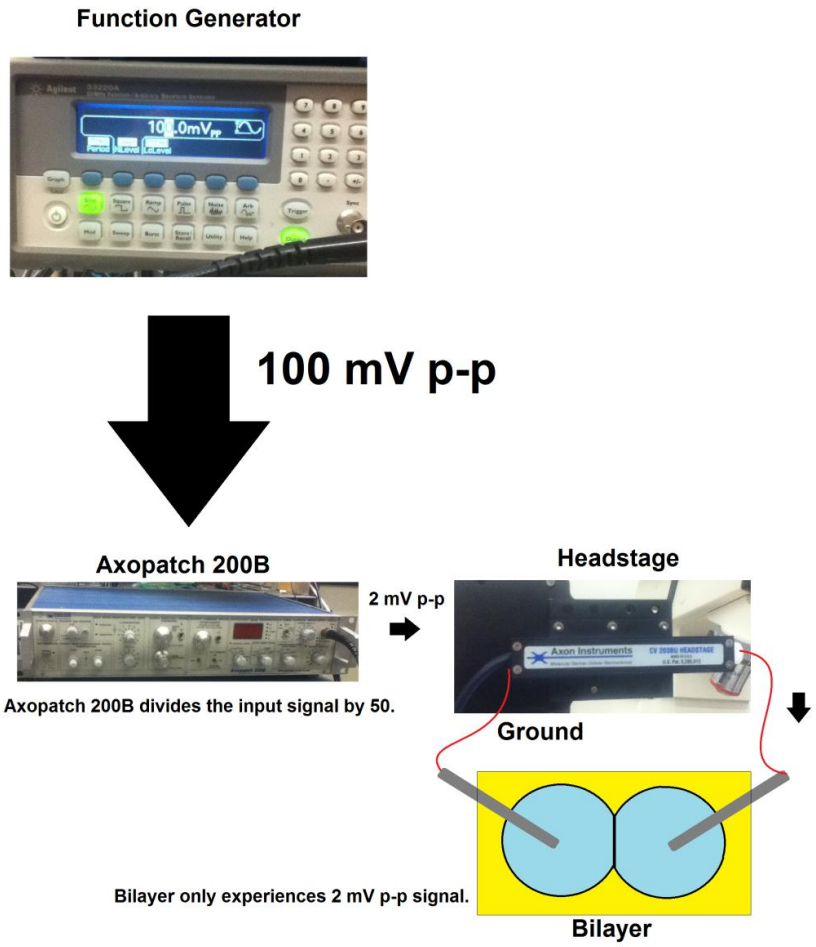

Figure 2-10: **Diagram of how signal travels from the function generator to the bilayer. Note that the Axopatch 200B will divide the input signal by 50 before outputting it to the headstage.**

The following subsections detail the basic patch clamp amplifier circuit used in the Axopatch 200B to measure currents and voltages at a cellular level. They discuss the operation of this circuit in both the voltage clamp and current clamp modes. Please note that this section draws largely from concepts discussed in Microelectrode Techniques: The Plymouth Workshop Handbook [53].

2.8.1 Brief Review of Operational Amplifiers

An operational amplifier (op-amp) is a large gain voltage amplifier. For the diagram shown in Figure 2-11, the relationship between the output voltage, V_o, and the input voltages, V_- and V_+, is:

$$V_o = A(V_+ - V_-) \tag{2-9}$$

Where A is the open loop gain, which is typically very large ($> 10^5$). Keep in mind, although it is not shown in the diagram, an op-amp requires a power source. The power source limits the peak output voltage.

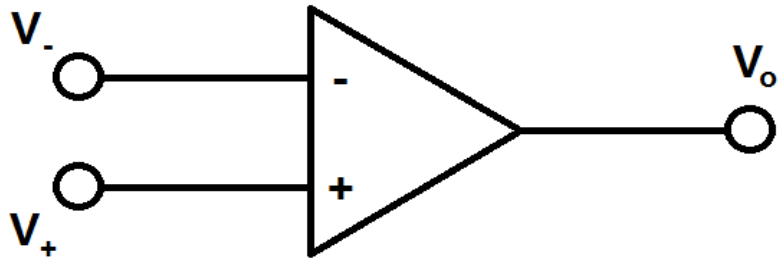

Figure 2-11: **Diagram of differential operational amplifier (op-amp).**

By connecting the output line of an op-amp to the (-) terminal (refer to Figure 2-12), a negative feedback system can be created. For this case, the op-amp will attempt to keep the input voltages, V_- and V_+, equal to one another. From Equation (2-9):

$$V_o = A(V_+ - V_-)$$

Because the output line is connected to the (-) terminal:

$$V_- = V_o$$

Substituting this back into Equation (2-1) yields:

$$V_o = \frac{A}{1+A} V_+$$

As long as A is very large, $V_o = V_- = V_+$. If some perturbation causes a voltage difference between the inputs, the system will correct itself to keep the magnitude of the input voltages equal to one another.

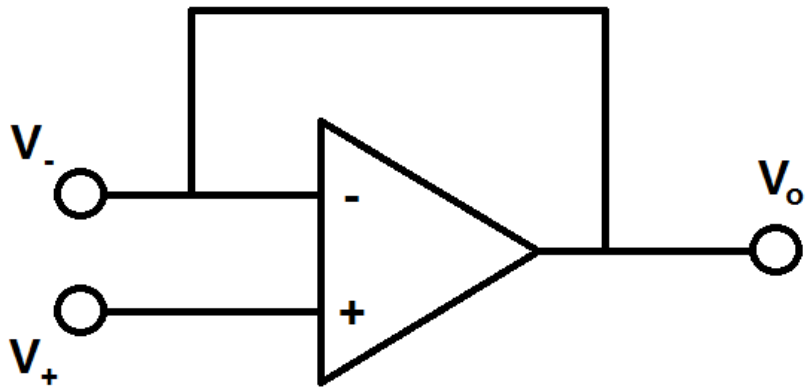

Figure 2-12: **Diagram of op-amp set up as a negative feedback system.**

Op-amps can also be used as inverting amplifiers. By placing a resistor, R_2, between the output line, V_0, and the (-) input terminal, V_-, and placing a resistor, R_1, between the input voltage, V_{in}, and the (-) input terminal. V_{in} can then be amplified by a large (but controllable) factor to V_o (refer to Figure 2-13).

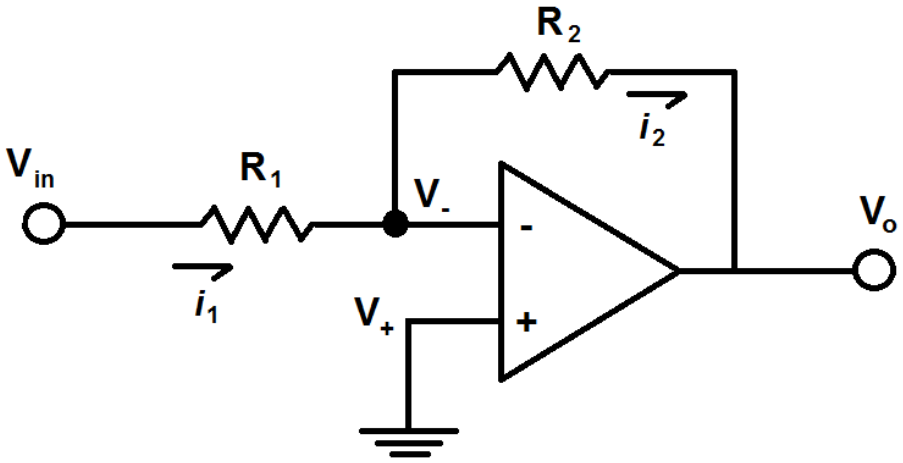

Figure 2-13: **Diagram of op-amp set up as an inverting amplifier.**

To find the relationship of the output voltage to the input voltage, start by summing the currents into the node shown in Figure 2-13 depicted by a solid black circle. Based on Kirchhoff's Current Law, the sum of the currents into the node must be equal to the sum of the currents out of the node. For ideal op-amps, there is no current flowing into the (-) or (+) terminals, so:

$$i_1 = i_2$$

Using Ohm's Law ($V = IR$), the previous equation can be rewritten as:

$$\frac{V_{in} - V_-}{R_1} = \frac{V_- - V_o}{R_2}$$

Recall that for ideal op-amps, the gain is very large (approaching infinity), which means the two input voltages are the same (one of the golden rules of op-amps), so:

$$V_- = V_+$$

Because the (+) side is connected to ground:

$$V_- = V_+ = 0$$

Substituting this into the above equations yields:

$$\frac{V_o}{V_{in}} = -\frac{R_2}{R_1} \qquad \text{(2-10)}$$

Equation (2-10) indicates that V_o is $-\frac{R_2}{R_1}$ times V_{in}. If the goal is to amplify V_{in}, then R_2 should be much larger than R_1. The Axopatch 200B functions based on the principles of the inverting amplifier op-amp circuit.

2.8.2 Voltage Clamp Mode

The Axopatch 200B uses an inverting amplifier[11] (in conjunction with other circuitry) to take small current measurements. Cell currents are on the order of picoAmps, so it would be difficult to measure these currents with traditional ammeters particularly due to signal-to-noise ratio issue. The idea behind the Axopatch 200B is to amplify the current signal so it can be measured using an inverting amplifier op-amp circuit.

[11] An inverting amplifier is used because a non-inverting amplifier has an input impedance that approaches infinity, which can lead to signal (current) reflections in the system.

Figure 2-14 shows a diagram of the resistive feedback system that the Axopatch 200B headstage (refer back to Figure 2-10) uses connected to an artificial bilayer. C_M and R_M are the capacitance and resistance of the bilayer, respectively. Note that R_E incorporates the resistance of the electrolytic solution in the two droplets as well as the resistance of the Ag/AgCl electrodes (refer back to Figure 2-1).

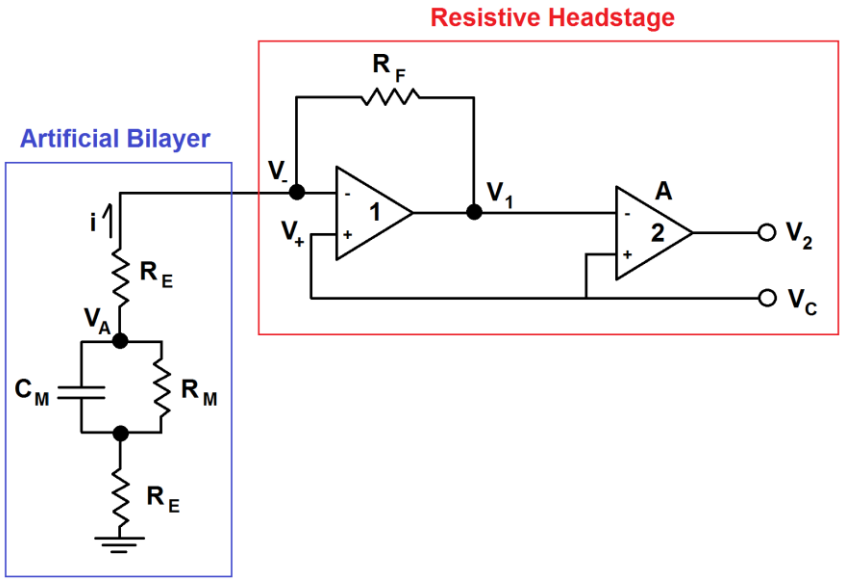

Figure 2-14: **Diagram of resistive headstage connected to an artificial bilayer.**

The Axopatch 200B operates in one of two modes: voltage clamp and current clamp. In voltage clamp mode ($V = 0$), the Axopatch 200B attempts to keep the voltage across the two electrodes connected to the headstage set to a particular value (V_C in Figure 2-14). For the case where the electrolyte resistances are ignored ($R_E = 0$), the Axopatch 200B would be attempted to keep V_A (the voltage across the bilayer) equal to the command potential, V_C. In this way, the user is able to control the voltage across the bilayer.

In order to get an understanding of how the Axopatch 200B is able to measure picoAmp currents, consider the circuit diagram shown in Figure 2-14. By applying Kirchhoff's Current Law in conjunction with Ohm's Law to the node beside the first op-amp's (-) terminal, the following equation can be developed:

$$\frac{V_A - V_-}{R_E} = \frac{V_- - V_1}{R_F}$$

Note that because $V_C = V_+ = 0$, V_- must also be equal to 0 assuming the op-amp has ideal characteristics. Therefore,

$$\frac{V_1}{V_A} = -\frac{R_F}{R_E} \tag{2-11}$$

Equation (2-11) shows the relationship between the potential across the membrane[12], V_A, and the voltage on the output side of the first op-amp, V_1, shown in Figure 2-14. For the CV203BU headstage that is used with the Axopatch 200B, the feedback resistor, R_F, varies depending on the β setting (refer to Table 2-2). Note that for the experiments presented in this thesis, $\beta = 1$, so the feedback resistance is $500\ M\Omega$.

Table 2-2: **Feedback resistor values for different configuration settings on the Axopatch 200B [52]. Used under fair use, 2013.**

Configuration Setting, β	**Feedback Resistance, R_F, MΩ**
0.1	50
1[13]	500

The Axopatch 200B is designed as a current to voltage (I-V) converter. In other words, the voltage output is proportional to the current input [52]. To measure the input current (membrane current), i, the Axopatch 200B measures the output voltage of the second op-amp, V_2 (Figure 2-14), and then uses the relationship between V_2 and i to determine i. V_2 is related to V_1 by Equation (2-12):

$$V_2 = A(V_C - V_1) \tag{2-12}$$

Recall that Kirchhoff's Current Law states that for a particular node, the sum of the currents into the node must be equal to the sum of the currents out of the node. Applying this to the node nearest to the

[12] Technically V_A is not the actual potential across the membrane because there is a small voltage drop due to the resistance between the membrane and the ground. However, if it is assumed that the voltage drop between the membrane and ground is negligible, $V_A$is the potential across the membrane.
[13] All experimental results in this thesis were with an Axopatch 200B Configuration Setting of Whole Cell β = 1.

$V\_$ terminal of the first op-amp in Figure 2-14 (represented by a black dot), the following relationship can be shown using Ohm's Law:

$$\frac{V_A - V\_}{R_E} = \frac{V\_ - V_1}{R_F}$$

Replacing the $\frac{V_A - V\_}{R_E}$ by i yields:

$$i = \frac{V\_ - V_1}{R_F}$$

Solving for V_1:

$$V_1 = V\_ - iR_F$$

Substituting this equation into Equation (2-12) yields:

$$V_2 = A(V_C - V\_ - iR_F) \tag{2-13}$$

In voltage clamp mode where $V_C = 0$, $V\_$ is also equal to 0 according to ideal op-amp assumptions. Therefore, the Axopatch 200B can approximate i using the following relationship in voltage clamp mode:

$$i = \frac{V_2}{AR_F} \tag{2-14}$$

In other words, the Axopatch 200B measures V_2 and then divides it by a factor of AR_F to determine the current i. Remember, i, is the current through the lipid bilayer. A is the gain of the second op-amp shown in Figure 2-14 and R_F is a known feedback resistance (refer to Table 2-2). Keep in mind, Equation (2-14) is only true for the case where the Axopatch 200B is operating in voltage-clamp mode where the command voltage, $V_C = 0$, although the principle applies to any command voltage.

Somewhat surprisingly, the gain of the second op-amp (Figure 2-14), A, is 1 for the CV203BU headstage [52]. The reason a second op-amp with a unity gain is used in the circuit is to isolate the input circuitry from the output circuitry. Recall that for an ideal op-amp, neither the (-) nor the (+) input terminals draw current. Therefore, the current, i, does not travel past the second op-amp. The second op amp copies the voltage, V_1, as V_2. This is an important part of the patch clamp amplifier because the circuitry past the second op-amp will not disturb the part of the circuitry that includes the lipid bilayer [52].

2.8.3 External Signal

One question that might arise is, "if the system is voltage clamped such that $V_C = 0$, then why would a current be measured?" When using droplet interface bilayers where the electrolyte concentration is the same on both sides of the bilayer, there would be no current flowing through the bilayer when the system was voltage clamped at $V_C = 0$, so the measured current, i, would indeed be zero. However, to verify the existence of a bilayer, the user often applies a triangular voltage signal across the bilayer (Section 2.3). If a bilayer has formed, then the output signal would be a square wave based on the current equation for a capacitor Equation (2-1). A function generator would generate the signal and then it can be input into the Axopatch 200B. The Axopatch 200B is sufficiently fast to continually adjust V_C to match the input signal from the function generator.

Note that the input signal from the function generator is scaled depending on how it is connected to the Axopatch 200B. If the function generator is connected to the BNC port labeled "EXTERNAL COMMAND INPUT (front panel switched)" located on the back of the Axopatch 200B, the signal from the function generator is divided by 50 before it is applied to the bilayer. For example, if the function generator is set to output a 500 mV peak-to-peak triangular wave at 10 Hz to the Axopatch 200B, the bilayer would experience a 10 mV peak-to-peak triangular wave at 10 Hz.

2.8.4 Current Clamp Mode

As mentioned previously, the Axopatch 200B is designed as a current to voltage (I-V) converter. It converts small currents to amplified voltage values (via op-amps) and then calculates the current based on the known circuit components. This is ideal for voltage clamping applications. The ideal current clamp circuit, however, would be a voltage follower where the system controlled the current directly (rather than through V_C) and measured the pipette voltage. To simulate current clamp mode, the CV203BU headstage takes advantage of an additional feedback loop that continually adjusts the

command voltage such that the measured current[14] is as close to the desired value as possible. For example, if the user wanted to clamp the current through the bilayer (i, Figure 2-14) at zero, then the headstage would continually adjust the voltage across the bilayer, V_A, via the command voltage, V_C, such that the measured current was 0.

When using droplet interface bilayer (DIBs), the electrodes are often directly embedded in the droplets. In traditional patch-clamp experiments, however, one electrode is placed inside a micropipette (typically made of glass) that is filled with an electrolyte solution. The micropipette has a tapered end that allows the experimenter to pierce biological cells. The tapered end of the micropipette results a resistance (a few $M\Omega$s) between the membrane and the actual electrode. This resistance is included in R_E (Figure 2-14) between V_A and $V\_$. In DIB experiments, however, R_E is much smaller because there is no tapered end micropipette to create additional resistance between the bilayer and the electrode.

One of the issues of using low resistance pipettes, as is the case with typical DIB experiments, is that the gain becomes very large, which leads to instability [52]. Recall from Equation (2-11) that the gain is related to the ratio of the feedback resistor, R_F, to the pipette resistance, R_E. For traditional experiments that use Ag/AgCl electrodes in a saturated saline solution inside a tapered end micropipette, R_E is typically on the order of several MΩ. The equivalent pipette resistance for two Ag/AgCl electrodes in an electrolyte (DIB case) is several orders of magnitude smaller[15], which would lead to a higher gain value and possible instability in the system while the Axopatch 200B was operating in current clamp mode.

Keep in mind that Equation (2-11) is not valid for the Axopatch 200B in current clamp mode because it assumes that the command potential, V_C, is equal to 0. As discussed previously, in current clamp mode, the system clamps the current at 0 by changing V_C. The gain equation in current clamp mode (as well as for the voltage clamp mode when $V_c \neq 0$) is as follows:

[14] Keep in mind that the Axopatch 200B is not measuring the current directly. Rather, it is measuring a voltage, then applying a known factor to calculate the current.

[15] Based on crude measurements, the resistance has a slight dependence on the saline concentration, but is typically less than 10 kΩ. Two Ag/AgCl electrodes were placed in a plastic dish filled with a particular concentration of KCl (10 mM/ 500 mM) and and a multimeter was used to measure the resistance between the two.

$$\frac{V_1}{V_A} = \frac{V_C}{V_A}\left(1 + \frac{R_F}{R_E}\right) - \frac{R_F}{R_E} \tag{2-15}$$

2.9 Chapter Summary and Conclusions

This chapter introduced the electrical model for a lipid bilayer system that consisted of a resistor (electrolyte) connected in series with a resistor (bilayer) and capacitor (bilayer) that were connected in parallel with one another (refer to Figure 2-2). The impedance of the bilayer capacitor is much lower than that of the bilayer resistor, so in order to verify the existence of a bilayer, a triangular voltage wave is applied across the two droplet interface and the corresponding current through the interface is measured. If the measured current has a square form, the system is displaying a capacitive behavior. In addition, the amplitude of the current square wave should increase as the two monolayers "zip" together to form a bilayer.

Two common measurement techniques that are used in lipid bilayer research are Electrical Impedance Spectroscopy (EIS) and Cyclic Voltammetry (CV). EIS is a measurement test where a sinusoidal voltage is applied to the system at varying frequencies. The corresponding current at each of the applied frequencies is measured. The best-fit transfer function corresponding to the bilayer circuit model can be fit to the data in order to determine the resistor and capacitor values. CV is a measurement test where the DC voltage is varied and the corresponding current is recorded. This is a particularly useful test when experimenting with voltage-gated channels in a bilayer.

Silver (Ag) electrodes with a silver-chloride (AgCl) coating are used to convert currents to and from electron flow in wires to ion flow in the electrolyte solution. This is important because currents in biological (lipid bilayer) systems are conducted via ions, whereas currents in traditional wires are conducted as electrons.

An Axon Instruments Axopatch 200B (Molecular Devices, Sunnyvale CA) was used to take the majority of electrical measurements presented in this thesis. It is capable of measuring picoAmp currents by utilizing an inverting amplifier circuit in conjunction with a second op-amp.

Chapter 3: Artificial Axon System and Preliminary Experiments

This chapter introduces the artificial axon system that was developed to show properties of action potential signal propagation that occurs in myelinated nerve cells. It also includes background information related to signal conduction velocity in biological nerve cells as well as experimental results related to measuring signal conduction velocity in the artificial axon system. The goal was to show that the signal conduction velocity in the artificial axon was similar to that in a real nerve cell. However, based on the experimental results, the conduction velocity in the artificial axon system is orders of magnitude faster than that its biological counterpart.

3.1 Artificial Axon System

There are three main components in a myelinated nerve cell axon [2, 32]. The intracellular fluid, which contains the sodium (Na^+) and potassium (K^+) ions that carry the signal through the axon similarly to the electrons that carry a signal through a copper wire. The myelinated regions of an axon are covered in an insulating material that separates the neuron membrane from the extracellular fluid that surrounds the cell. The nodes of Ranvier are small regions along the axon in between the myelinated regions where the axon membrane is directly exposed to the extracellular fluid.

Figure 3-1 shows a diagram of the artificial axon system. A hydrogel is formed in a well in the substrate used to contain the bilayer. Capillary tubing is filled with an electrolyte and is inserted into the substrate in order to electrically connected the hydrogel (and thus the bilayer) to the electrolyte line (refer to the CAD models in Figure 3-2). The bilayer is formed at the interface of the droplet anchored to the hydrogel in the substrate and the droplet anchored to the hydrogel within the micromanipulator-controlled micropipette. A signal can be input via the input electrode and the bilayer can be used to modify the signal as it travels towards the ground electrode.

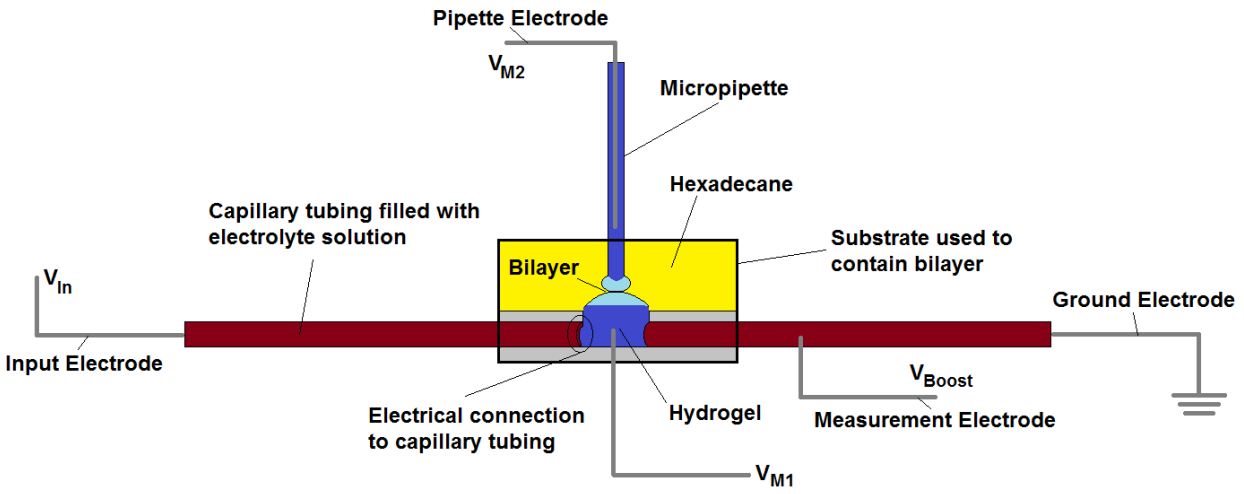

Figure 3-1: **Diagram of the artificial axon system where a bilayer is connected perpendicularly to an electrolyte line (capillary tubing filled with electrolyte solution).**

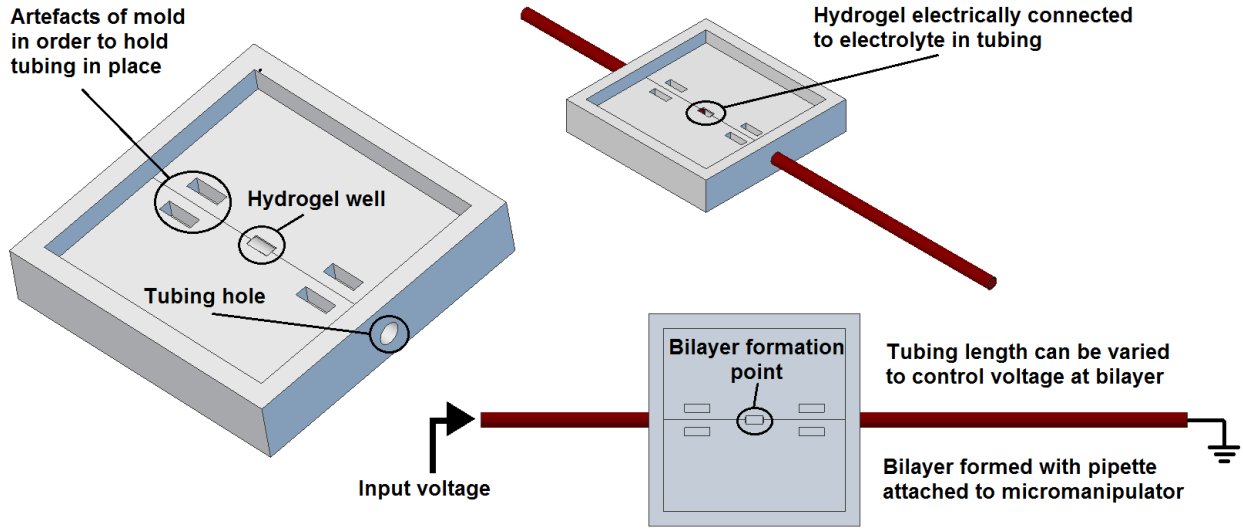

Figure 3-2: **CAD models of the polyurethane substrate used to electrically connect a bilayer to capillary tubing filled with an electrolyte. Note that one lipid monolayer is formed by attaching to the hydrogel in the hydrogel well and the second monolayer is attached to a micropipette that is brought into contact with the other monolayer using a micromanipulator. Refer to Appendix B for the dimensions.**

The potassium chloride (KCl) electrolyte that is within the capillary tubing as well as within the hydrogel (anchored to the substrate) is analogous to the axon's intracellular fluid. The capillary tubing is similar to the myelinated region where the axonal membrane is insulated from the extracellular fluid. The bilayer formed at the interface between the two droplets anchored by hydrogel within the micropipette and the hydrogel within the substrate is representative of a node of Ranvier where the axon membrane (lipid bilayer) is directly exposed to the extracellular fluid (KCl electrolyte contained within the

micropipette). Figure 3-3 shows the artificial axon system with corresponding axon component diagram (Figure 1-11) overlain.

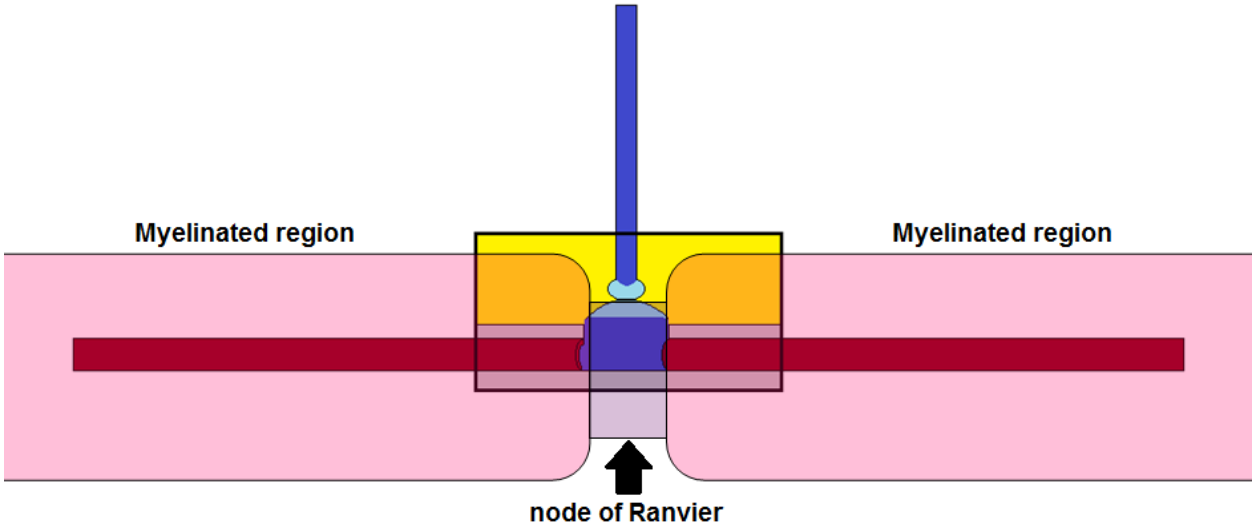

Figure 3-3: **Diagram of artificial axon system with myelinated axon diagram overlain (Figure 1-11).**

One can imagine a system consisting of multiple artificial axon systems connected in series. In this setup, there are multiple myelinated regions as well as nodes of Ranvier. If a signal is input to the system, the signal should move along the axon from left to right as in an axon.

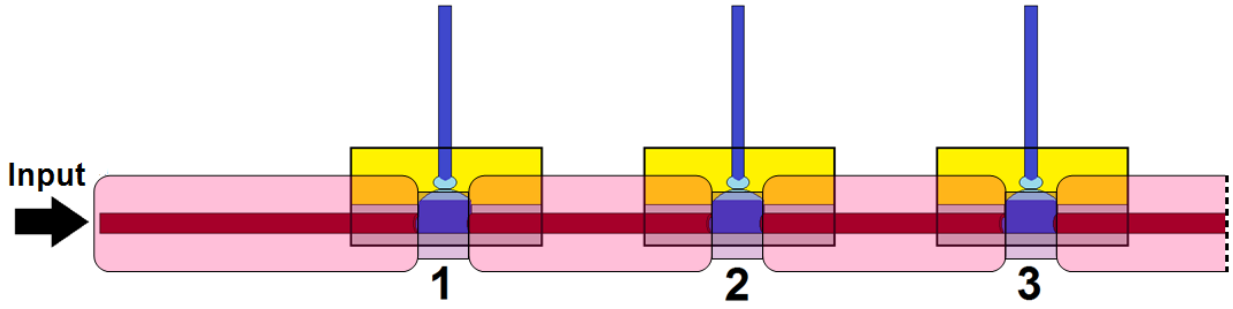

Figure 3-4: **Diagram of multiple artificial axon systems connected in series. The corresponding myelinated axon diagram is overlain (Figure 1-11).**

If the voltage across the membrane was simultaneously measured at points 1-3, the expected result would look similar to that shown in Figure 3-5. The signal reaches point 1, then point 2, and finally point 3 in succession. Note that there is a time delay (Δt) between the signal reaching each point in the

system. Assuming that the signal conduction velocity is constant, the time delay between successive points would be linearly related to the length of capillarity tubing between the points.

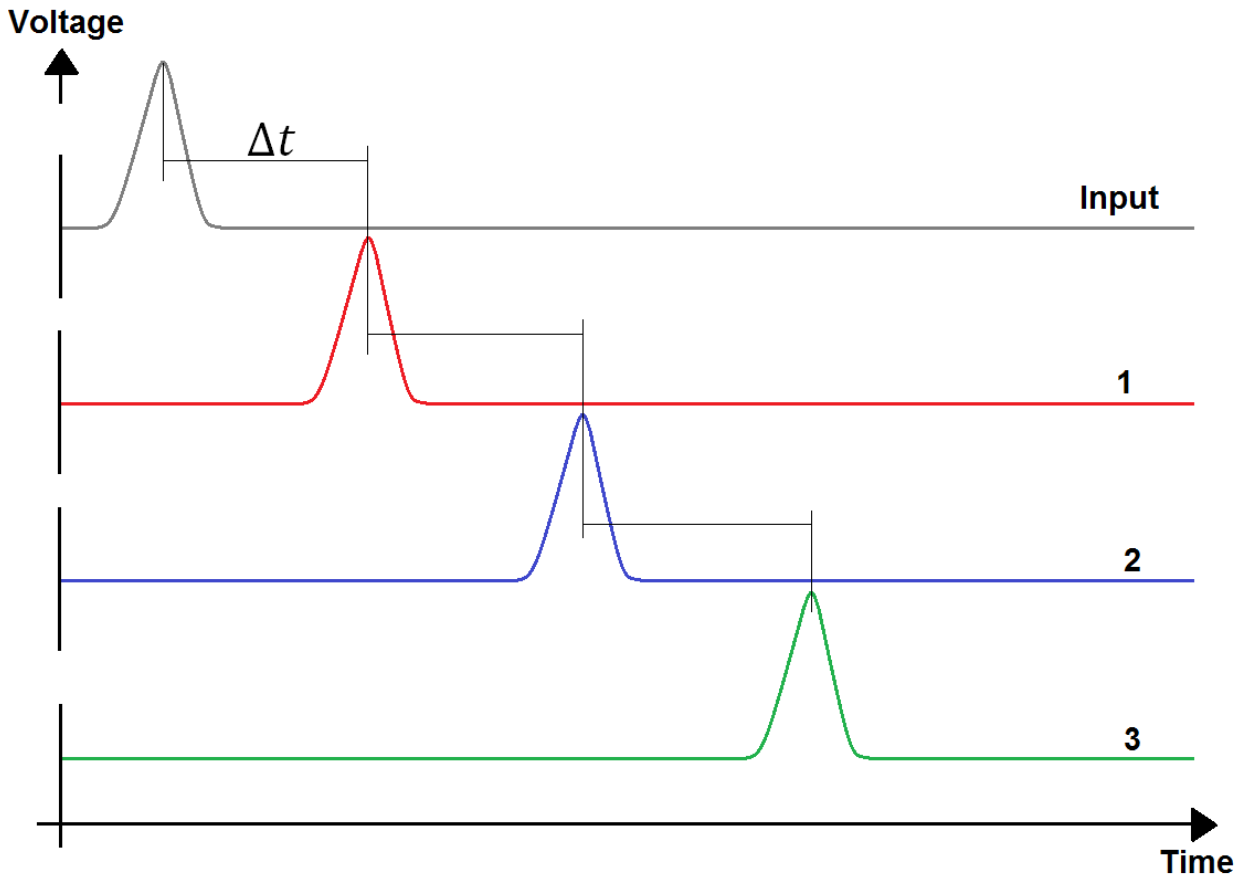

Figure 3-5: **Expected plot of voltage measured at points 1-3 as a function of time for the system shown in Figure 3-4.**

The goal was to use the system shown in Figure 3-4 in order to reproduce a plot similar to that of Figure 3-5. This would show that droplet on hydrogel bilayers could be connected in a way that functioned like a neuron's axon. In order to this, the measurement system (refer back to Figure 2-10) had to be capable of measuring the signal conduction velocity in the proposed system.

3.2 Signal Conduction Velocity in Neurons

In a neuron's axon (Figure 1-7, copied on the following page for convenience), there is a small delay between the signal at the beginning of the axon (axon hillock) and the signal received by the axon terminals. In other words, it takes the signal some amount of time to move from the beginning of the axon to the axon terminals. This delay is due to the propagation speed (conduction velocity) of the signal traveling down the length of the axon. Conduction velocities in mammalian axons have been measured

as high as $100 - 120\ m/s$ [2, 32], but are typically slower ($< 100\ m/s$) depending on the diameter of the axon [54].

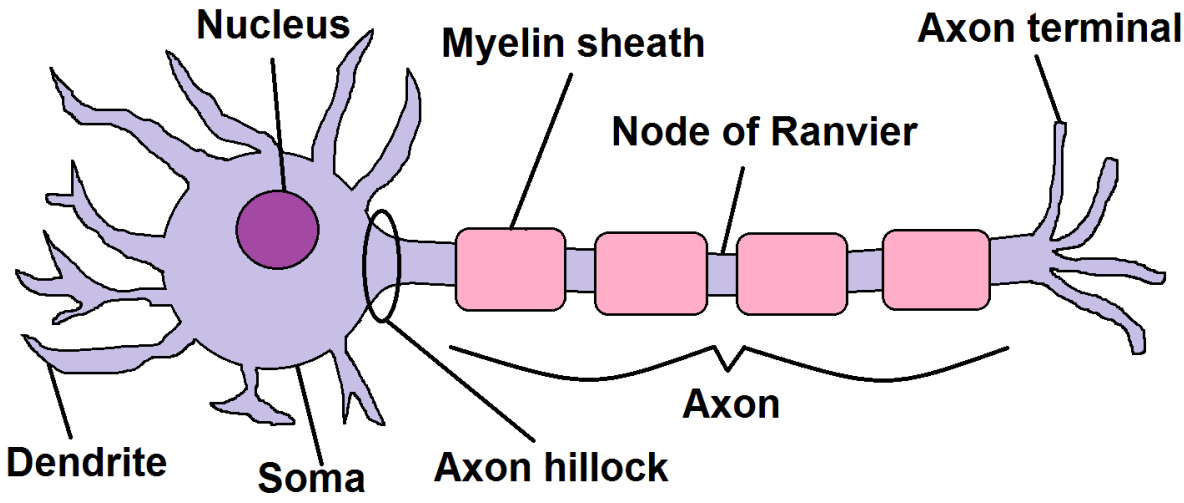

Figure 1-7: Labeled Diagram of a Neuron. Copied here for convenience to the reader.

There are two major types of axons in organisms that have neurons: unmyelinated and myelinated. Myelinated axons have insulated regions where myelin wraps around the axonal body like a roll of tape. These myelinated regions are separated by unmyelinated regions called the Nodes of Ranvier. Unmyelinated axons do not have the myelin insulation. Invertebrates use unmyelinated axons to send signals throughout their bodies. The giant squid, for example, has axons as large as $500\ \mu m$ in diameter, but the maximum conduction speed is only $25\ m/s$ [32]. Myelinated axons, on the other hand, have much smaller diameters ($< 20\ \mu m$). However, they are able to conduct signals at higher velocities by taking advantage of the insulating properties of myelin [2, 32].

Consider the diagram of the unmyelinated axon shown in Figure 3-6. Along the entire length of the axon, there are voltage-gated sodium (Na^+) ion channels that are used to propagate an action potential. When an action potential is initiated at one end of the axon, the Na^+ channels in that region open, allowing the Na^+ ions in the extracellular environment to flood into the cell and down the length of the axon. As the signal moves down the axon, Na^+ channels are continuously being opened along the length of the axon as the action potential travels. For example, consider the unmylinated axon as a series of connected pieces that combine to form the entire axon (bottom right of Figure 3-6). When the signal reaches one of these pieces, the capacitor (due to the lipid bilayer membrane surrounding the piece)

must be charged and then the Na^+ channels in the piece must open to allow for an influx of Na^+ ions. This process takes time, which slows the overall conduction velocity [55].

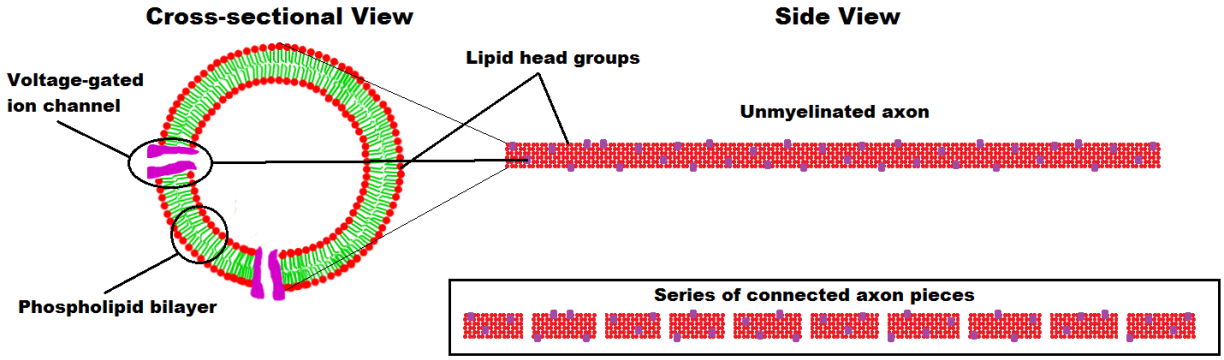

Figure 3-6: **Diagram of an unmyelinated axon and corresponding cross-sectional view.**

To increase the conduction velocity, vertebrates developed a way to insulate their axons using myelin (refer to Figure 3-7). The myelin sheaths are analogous to a roll of tape (consisting primarily of lipids) wrapped around the axon which insulates that section of the axon from the extracellular fluid. In the regions of the axon that are myelinated, there is very little capacitance (due to the thickness of the myelin sheath), so the signal does not need to charge the membrane in the myelinated regions. In addition, there is no need to wait for the Na^+ channels to open and allow for Na^+ ions to flood into the axon, because the myelin insulates the cell from the extracellular fluid. In other words, it would be difficult for Na^+ ions to reach any Na^+ channels because the ions would have to pass through the myelin sheath. By insulating the axon, the conduction speed is increased [2, 32, 54, 55].

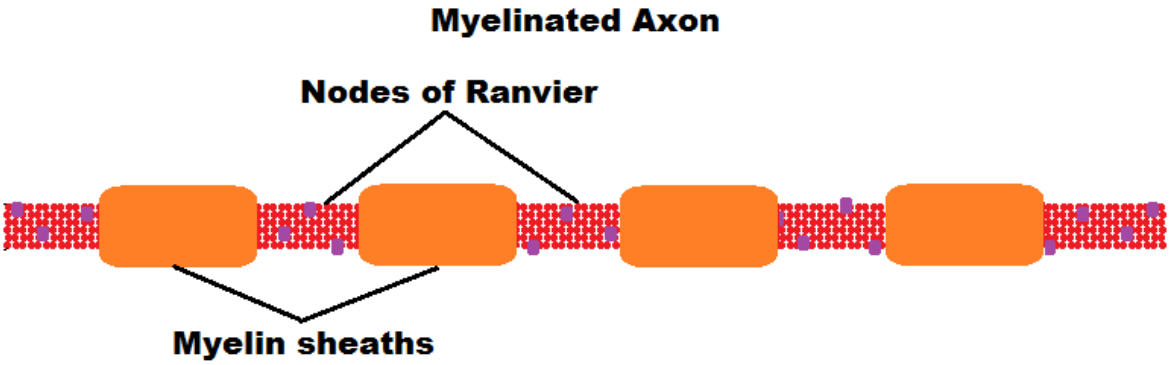

Figure 3-7: **Diagram of myelinated axon. Note that the aspect ratio of the length of the myelin sheath compared to the length of each node of Ranvier is exaggerated. The nodes of Ranvier are typically 100-1000x shorter in length than a myelinated region.**

The reason axons are not entirely myelinated is that current can still leak out of the axon even in the myelinated areas (leakage current). In other words, the signal would decay to nothing as it moved down the length of the entirely mylinated axon because the current is continuously leaking out of the system (even through the myelin insulation). To deal with this issue, nodes of Ranvier (unmyelinated regions) occur in myelinated axons approximately every 200-2000 µm along the length of the axon. Each Node of Ranvier is only about 1-2 µm in length [32, 34]. When the signal reaches the nodes of Ranvier, the Na^+ channels open and allow Na^+ ions to rush into the cell, which "boosts" the signal back to its original strength. Keep in mind that although the signal decays in the myelinated region, the amplitude is still large enough to cause the Na^+ channels to open in the successive node of Ranvier. The signal is then prepared to travel through the successive myelinated region. This process results in a finite conduction velocity, which is the speed an action potential travels down an axon.

3.3 Measuring the Conduction Velocity Experimentally

In order to show that a signal could be propagated down the artificial axon system, the measurement system had to be capable of measuring the signal conduction velocity. If the signal was traveling too fast, the measurement system would not be able to differentiate between the time when the signal reached each point. The data acquisition system (Digidata 1440A) has a maximum sampling rate of $250\ kHz$, therefore the resolution of the measurement system is $4\ \mu s$. Suppose there are two points, A and B, connected by an electrolyte. A signal is input at point A and point B is simultaneously measured. If the signal that was generated at point A reaches point B in less than $4\ \mu s$, then the measurement system would either indicate that the signal instantaneously arrived (no time delay) at point B or that it took $4\ \mu s$ for the signal to reach point B. In both cases, the measurement is incorrect. Therefore, In order to accurately measure the signal conduction velocity, the time it took the signal to travel from point A to point B would have to be increased to greater than $4\ \mu s$ [16]. This could, for example, be accomplished by increasing the length of the electrolyte line between the two points.

Assuming that the signal travels at the biological speed of $150\ m/s$, then in $4\ \mu s$ (resolution of the data acquisition system), the signal would travel $6\ \mu m$. In other words, the distance between the droplet on hydrogel bilayers (DHBs) (Figure 3-4) would need to be greater than $6\ \mu m$ in order for the data acquisition system to differentiate the time when the signal reached the first bilayer and the time when

[16] In reality, the time delay between the two points would have to be much greater than $4\ \mu s$ in order to confidently measure the signal conduction velocity due to issues with signal noise.

the signal reached the second bilayer. From a manufacturing standpoint, the smallest distance between two DHBs would be about $1 - 2\ cm$, which would correspond to a time delay of $1.5 - 3\ s$, so the data acquisition system would easily be able to measure the conduction velocity.

In order to measure the signal conduction velocity, a wave would be input at the beginning of the artificial axon system and a simultaneous measurement would be made at some point further along the system. By comparing the phase of the input signal to the measured signal, the time delay could be determined as shown in

$$\Delta t = \frac{\Delta\varphi}{360 \cdot f} \tag{3-1}$$

Where $\Delta\varphi$ is the difference in phase between the two signals in degrees, f is the frequency of the signals in Hz, and Δt is the time delay between the two signals in seconds. Note that the two signals must be operating at the same frequency for Equation (3-1) to be true.

Figure 3-8 shows two sine wave signals operating at $1\ Hz$ that have a $30\ °$ phase difference. The input signal leads the output signal by a small amount of time $(\sim 0.83\ ms)$. In other words, the signal needed about $83\ ms$ to travel from Input to Point X. The distance between Input to Point X could be measured, so the conduction velocity could easily be approximated.

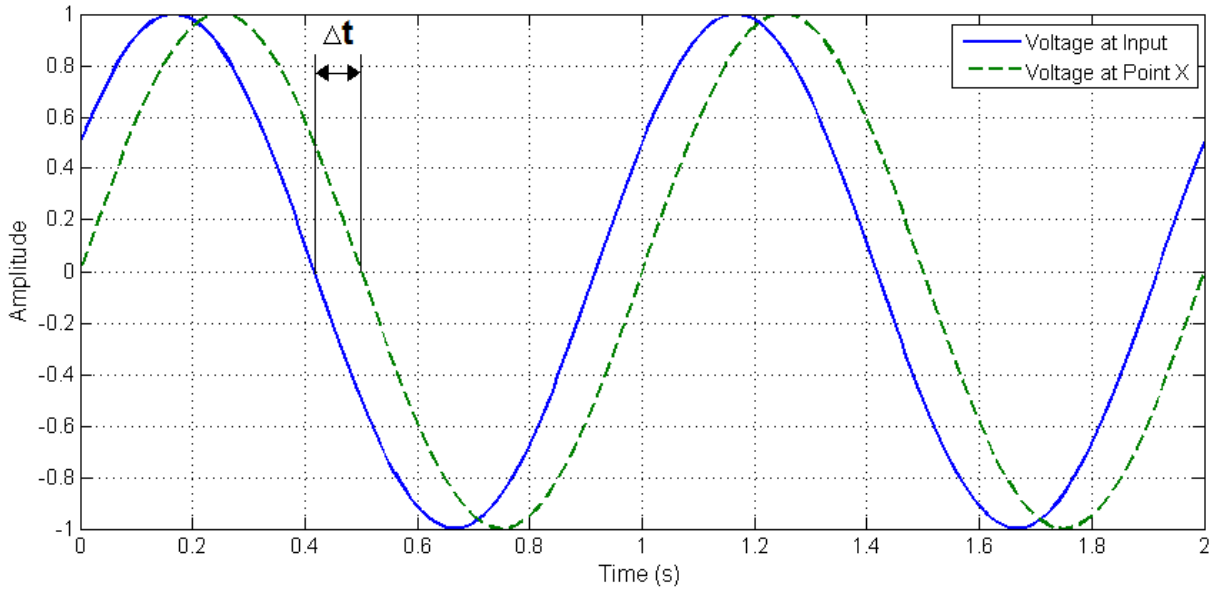

Figure 3-8: **Example of time delay between two signals. The two sine waves shown are operating at 1 Hz with a 30° phase shift (~83 ms time delay) between them.**

The expectation was that by varying the distance between the input signal and the bilayer (analogous to varying the length between successive nodes of Ranvier in an axon), that the time delay between the input signal and the signal measured at the bilayer can be controlled. For example, one would expect that a signal would take longer to travel a $5\ cm$ length compared to a $1\ cm$ length of the same diameter.

3.4 Description of Conduction Velocity Experiment and Assumptions

The purpose of the following tests was to verify that the signal conduction velocity in the artificial axon system could be measured with the data acquisition system. A $525\ mm$ length piece of $0.04"$ $(1.02\ mm)$ inner diameter $(0.07"$ $(1.78\ mm)$ outer diameter) capillary tubing was filled with a $10\ mM$ KCl solution[17] as shown in Figure 3-9. The capillary tubing had been pierced with silver-silver chloride (Ag/AgCl) electrodes at various points along its length. An input electrode was inserted into one end of the tubing and then the tubing was sealed with glue. Similarly, a ground electrode was inserted at the other end and the tubing was sealed there as well. Note that the experimental system purposely does not include a lipid bilayer in order to eliminate variations in the time delay due to the bilayer's capacitance.

[17] It was assumed that a low concentration electrolyte solution would help reduce the signal conduction speed because less ions were available to conduct the signal than in a higher concentration electrolyte solution.

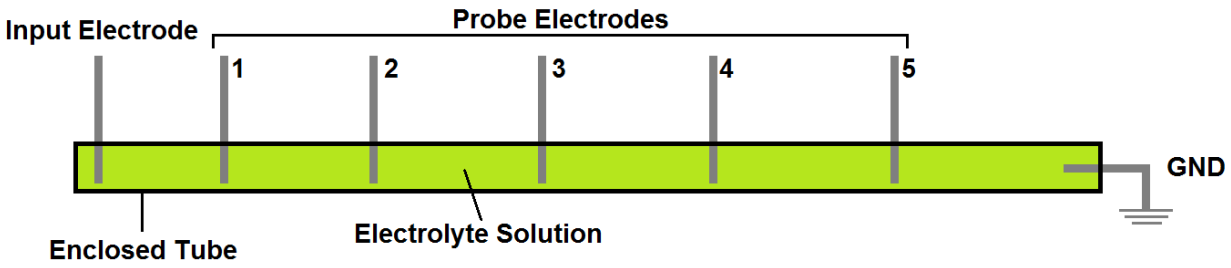

Figure 3-9: **Diagram of capillary tube filled with an electrolyte solution that has been pierced with several electrodes.**

A sinusoidal signal could be input to the system via the input electrode and it would travel towards the ground electrode. One would expect to see a phase shift in the signal at the probe electrodes compared to the input signal. This phase shift would be due to the finite signal conduction velocity. For example, the time delay (phase shift of the sine wave) between the input electrode and the probe electrode at point 2 would be less than that between the input electrode and the probe electrode at point 5 because the signal has to travel a further distance to reach point 5. If the phase shift was measureable, then the signal conduction velocity could be measured using the data acquisition system.

3.5 Experimental Results: Conduction Velocity in Artificial System

A function generator was attached to the input/GND electrodes and was used to apply a sinusoidal signal as shown in Figure 3-10. The Axopatch 200B was operated in current clamp mode (I = 0)[18] and was used to measure the voltage at various points in the system by attaching to the probe electrodes. The signal conduction velocity could be therefore determined by comparing the phase shift between the input signal and the measured signal. Recall that this phase shift is related to the time delay as described in Equation (3-1).

[18] Recall that when the Axopatch 200B is operated in current clamp mode, it is measuring the potential (voltage) at the electrode relative to its ground.

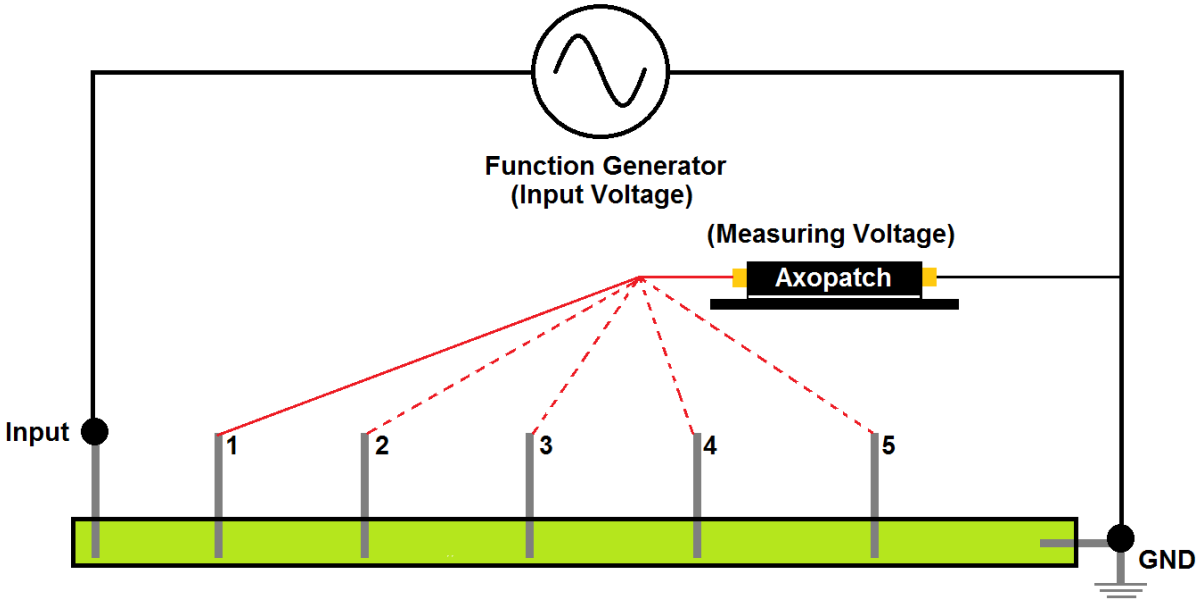

Figure 3-10: **Diagram of system used to measure the signal delay between the input voltage and the voltage measured at various points in the circuit. Note that the Axopatch 200B headstage connection (red) was moved to measure the voltage at different points in the circuit.**

Figure 3-11 shows the time delay (calculated by Equation (3-1)) between the input voltage signal and the measured voltage signal as a function of the distance from the input electrode. Note that the input signal was a $300\ mV_{pp}$ sine wave operating at $10\ Hz$. Figure 3-12 shows the amplitude of the sine wave measured as a function of the distance from the input electrode. Each data point shown in Figure 3-11 and Figure 3-12 is based on an average $30\ s$ of data sampled at $250\ kHz$. To calculate the average time delay between the input signal and the signal at the various points, the data was divided into single sine wave periods $(0.1\ s)$. The Fast Fourier Transform (FFT) of ten periods $(1\ s)$ was taken and the phase shift between the input and output was calculated at the $10\ Hz$ spectral line. For example, the FFT of periods $1-10$ was taken and the corresponding phase shift was recorded (repeated for periods $2-11, 3-12$, etc). This moving average method was used for the entire $30\ s$ of data (~ 300 averages). The average phase shift and amplitude for the entire data set could then be determined as well the corresponding standard deviations. Refer to Section A.2 in Appendix A for a copy of the MATLAB code.

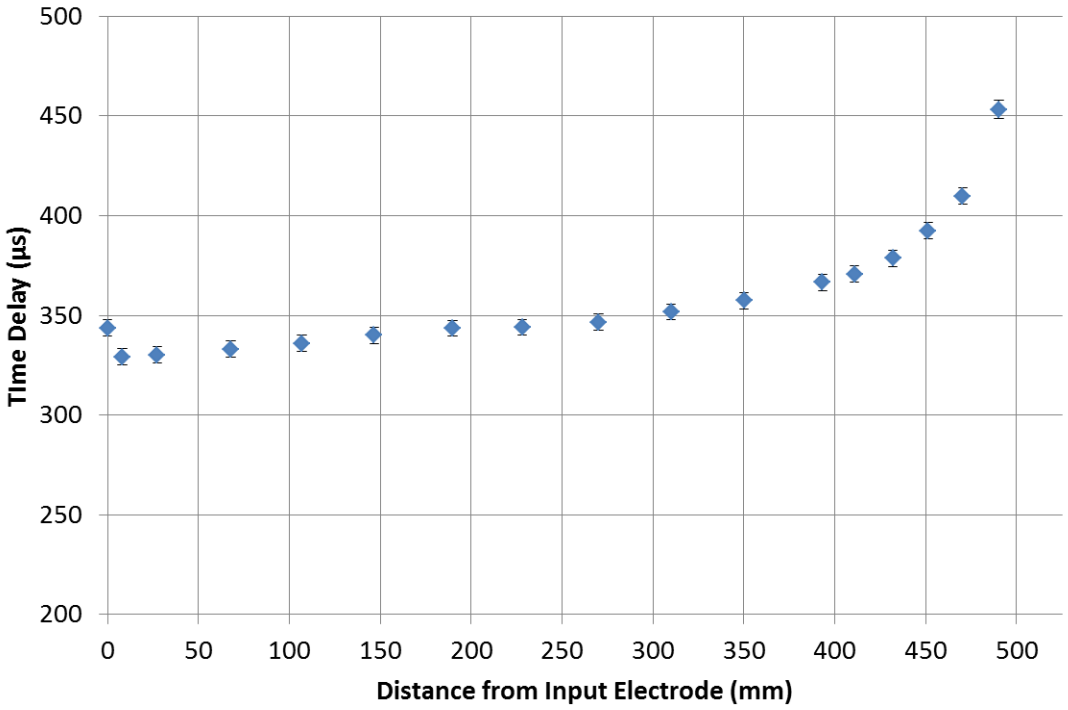

Figure 3-11: **Time delay between input signal and measured signal as a function of the distance from the input electrode. Note that the input signal is $300\ mV_{pp}$ operating at$10\ Hz$. The error bars show the 95% confidence interval using the standard deviation of the measurement as well as the resolution of the data acquisition system.**

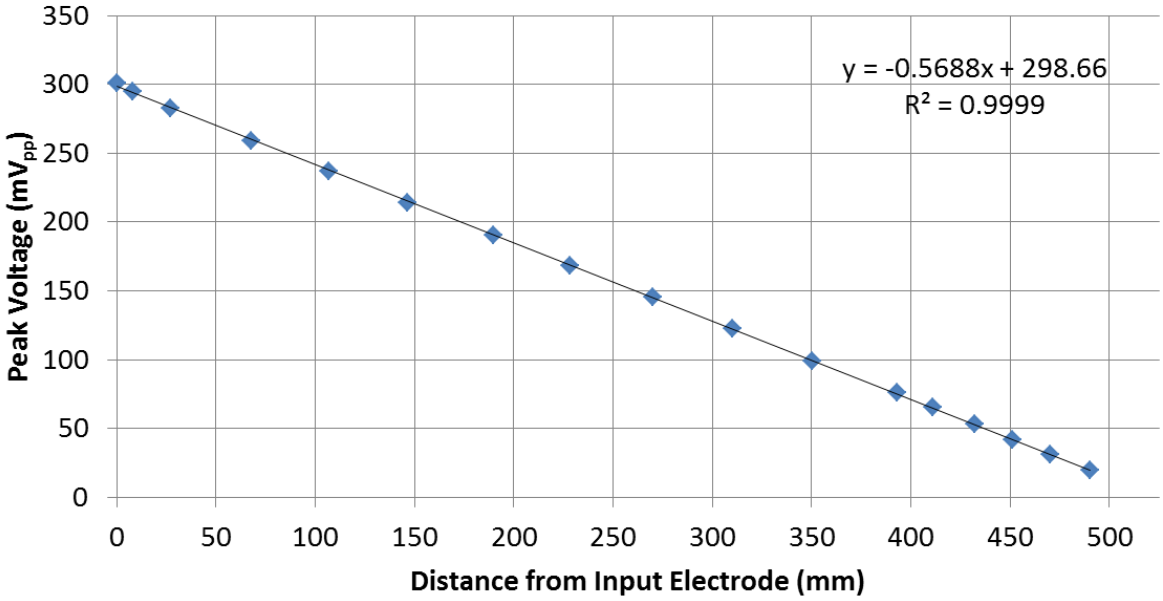

Figure 3-12: **Peak-to-peak voltage as a function of the distance from the input electrode. The input signal is $300\ mV_{pp}$ operating at $10\ Hz$.**

Note that the time delay in Figure 3-11 does not approach $0\ s$ as the distance from the input electrode approaches $0\ mm$. There is an offset greater than $300\ \mu s$. One would expect the time delay to decrease to $0\ s$ as the measurement got closer and closer to the input electrode, however, this is clearly not the case. The time delay between the input and the measured signals seems to increase linearly up to a point ($\sim 400 - 450\ mm$ from the input electrode) at which it becomes nonlinear. The nonlinearity could be due to the proximity of the measurement electrodes to the ground electrode (located $525\ mm$ from the input electrode).

Using biological signal conduction speeds (on the order of $150\ m/s$), the expected time delay between an action potential signal being generated at the axon hillock and being measured at a point located $400\ mm$ down the axon is about $2.7\ ms$. Based on the data in Figure 3-11, the corresponding time delay in the artificial axon system was only about $360\ \mu s$ (about 7 times faster) to cover that same $400\ mm$ distance. In fact, the time delay in the artificial axon system is likely even smaller because there is an offset common to all measurements of greater than $300\ \mu s$.

It was noted in Figure 3-11 that there is an offset of the time delay as the measurement electrode approaches in the input electrode. One would expect this value to approach $0\ s$, however, there is a speed associated with the Axopatch 200B's ability to clamp the current in the current clamp mode. While the Axopatch 200B is operating in current clamp mode, it is attempting to keep the current at a set value (in this case $i = 0$) by controlling the command voltage. This process is similar to a controls problem in that the Axopatch is continually adjusting the command voltage in order to get the desired current (Refer back to Section 2.8: Axopatch Theory and Operation for more information). The implication is that the signal is traveling faster than the prediction shown in Figure 3-11. In other words, the time it takes the signal to move from the input electrode to an electrode at some distance away is exaggerated by the Axopatch 200B due to the current clamp speed.

The speed of the Axopatch 200B's current clamp is dependent on the time constant of the "cell" that it is attempting to clamp the current through [52]. In other words, the speed of the current clamp is not constant if the time constant of the system is changing. For the experimental system described, as the Axopatch 200B is connected to different electrodes (refer to Figure 3-10), the time constant of the system is changing because the resistance between the measurement electrode and ground is changing. This raises the question as to whether the data shown in Figure 3-11 is actually a function of the

distance between the input and measurement electrode or if it is simply a function of the current clamp speed changing.

To get an idea of how the current clamp speed changes as a function of the distance between the measurement electrode and the ground electrode, the Axopatch 200B was changed to I-Clamp NORMAL mode and a $30\ nA_{pp}\ (10\ Hz)$ square wave current was sent into the input electrode[19]. In I-Clamp NORMAL mode, the Axopatch 200B attempts to clamp the current in the system to match that of the input current[20]. The voltage as a function of time and distance between the input electrode and ground could then be recorded. The current clamp speed is related to how fast the measured voltage transitioned from the low value to the high value of the square wave (controls problem).

Figure 3-13 shows the $30\ nA_{pp}\ (10\ Hz)$ square wave input current (top) and the corresponding voltage measurement using the Axopatch 200B (bottom). Note that the function generator not used to directly input the square wave signal to the system. Instead, the function generator was connected to the Axopatch 200B, which was used to both apply the square wave and measure the corresponding voltage (refer back to Figure 2-10).

[19] It should be noted that the current flowing through system for Figure 3-11 and Figure 3-12 was approximately $60\ nA_{pp}\ (10\ Hz, sine\ wave)$. Ideally, the clamp current input magnitude for the data shown in Figure 3-13 would match this, however, the maximum input current due to the scaling factor between the function generator and the Axopatch $(2\ nA/V)$ was less than $60\ nA_{pp}$.

[20] This is the same idea of how the voltage clamp works. When a triangle wave is input via the Ext. Command, the voltage-clamp attempts to clamp the voltage across the bilayer to match the triangle wave. The Axopatch allows you to read the current during this process. The current clamp works the same way except it attempts to clamp the current to match the input signal and allows you to measure the voltage.

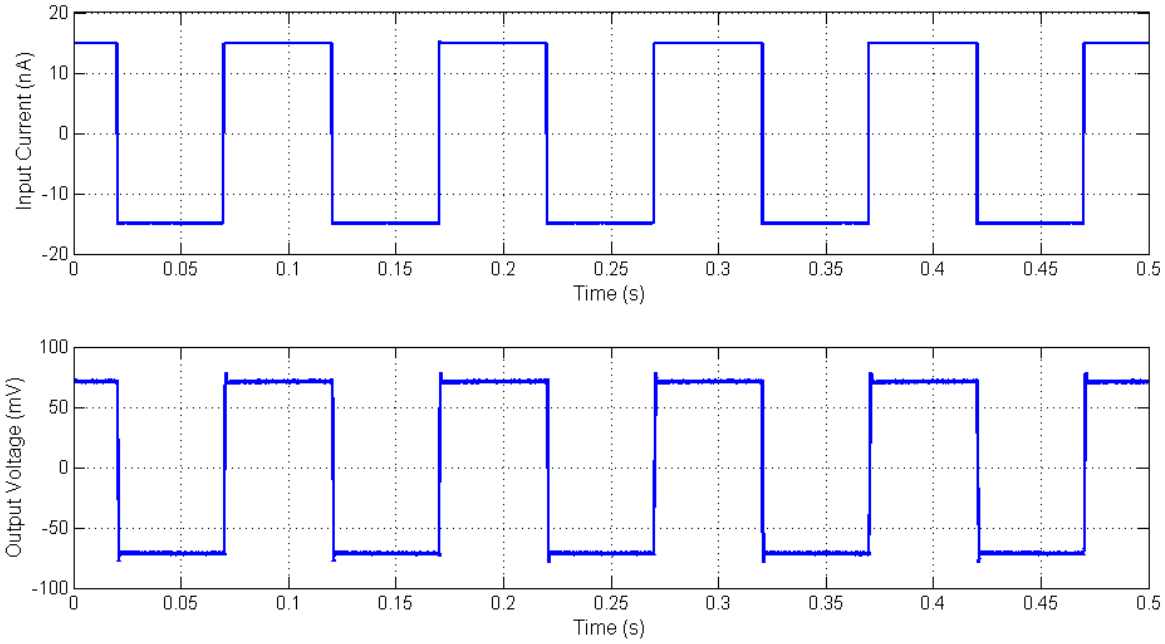

Figure 3-13: **The Axopatch was connected from the input electrode to the ground electrode of the capillary tubing system (refer to Figure 3-10). Top)** $30\ nA_{pp}\ (10\ Hz, 50\%\ duty\ cycle)$ **current input. Bottom) Corresponding voltage measurement using Axopatch operating in I-Clamp NORMAL mode.**

Figure 3-14 shows a single square wave of the current and corresponding measured voltage from the data shown in Figure 3-13. Note that the transition from the low value to the high value of the current square wave (blue line) is nearly instantaneous compared to the transition of the measured voltage (green line). The lag associated with this transition is due to the current clamp speed of the Axopatch 200B. In an effort to compare the transition time as the input electrode connection was moved, the $10-90\%$ rise time was calculated. The $10-90\%$ rise time is the time it takes the signal to move from 10% to 90% of the final value as shown in Figure 3-14.

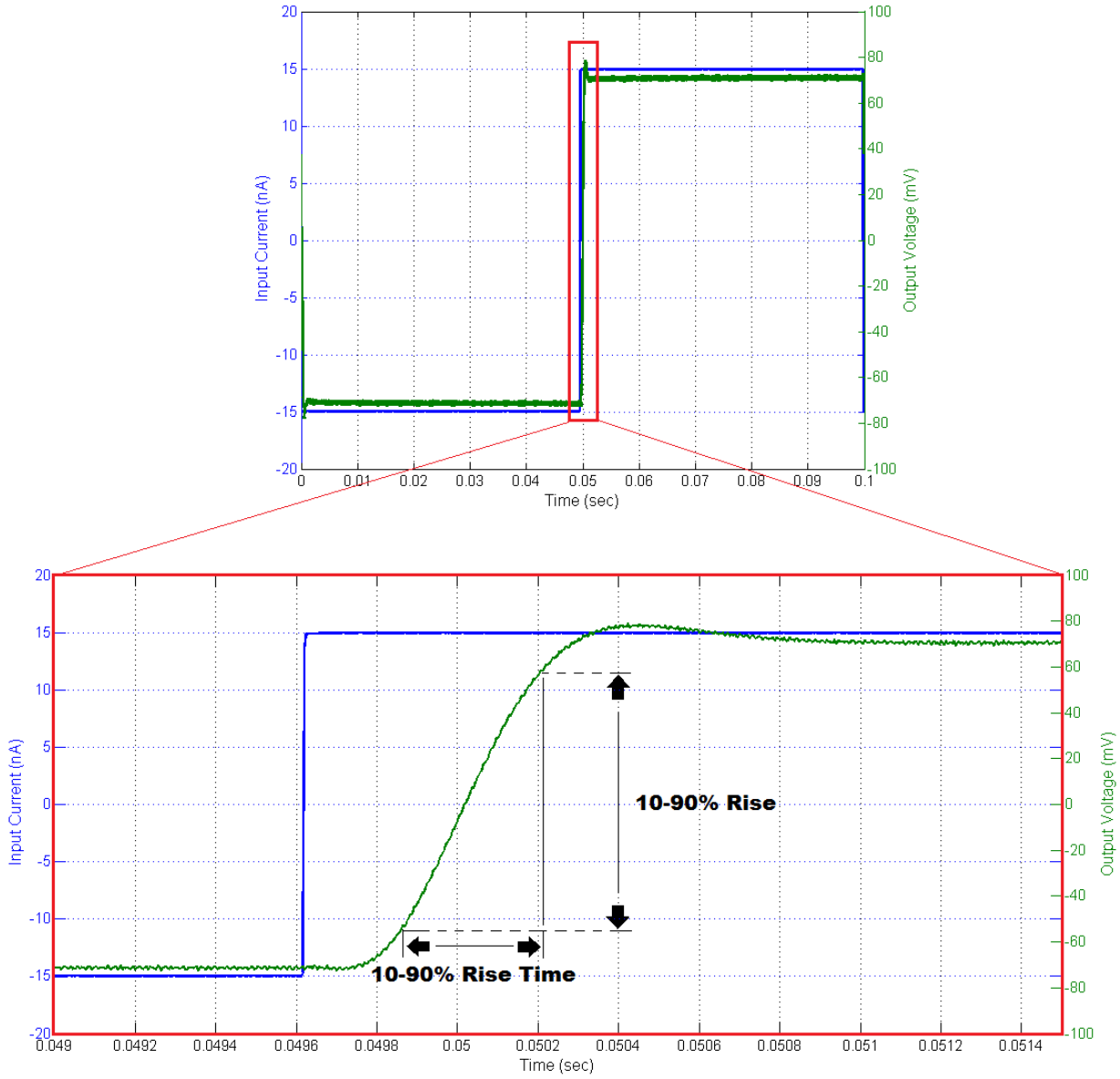

Figure 3-14: **Plot of a single square wave** $(30\ nA_{pp}, 10\ Hz, 50\%\ duty\ cycle)$ **and the corresponding voltage. The Axopatch was connected from the input electrode to the ground electrode of the capillary tubing system (refer to Figure 3-10).**

Figure 3-15 shows the measured time delay (Figure 3-11) and the corresponding $10-90\%$ rise time due to the current clamp speed. Note that the measured time delay is either less than or falls within the confidence bounds of the current clamp speed with the exception of the last few points[21]. Also keep in mind that the $10-90\%$ rise time underestimates the true time $(0-100\%)$ that the Axopatch needs to clamp the current. Based on the information presented in Figure 3-15, it would be very difficult (if

[21] The results near the ground electrode (located at approximately $525\ mm$ from the input electrode) should be questioned due to a much smaller signal to noise ratio than those points near the input electrode. The change in signal to noise ratio is due to voltage decaying over the length of the capillary tube.

not impossible) to confidently distinguish between the time delay due to the signal conduction velocity and the time delay due to the current clamp speed. This means that signal conduction velocity in the artificial axon system is orders of magnitude larger than in a real axon.

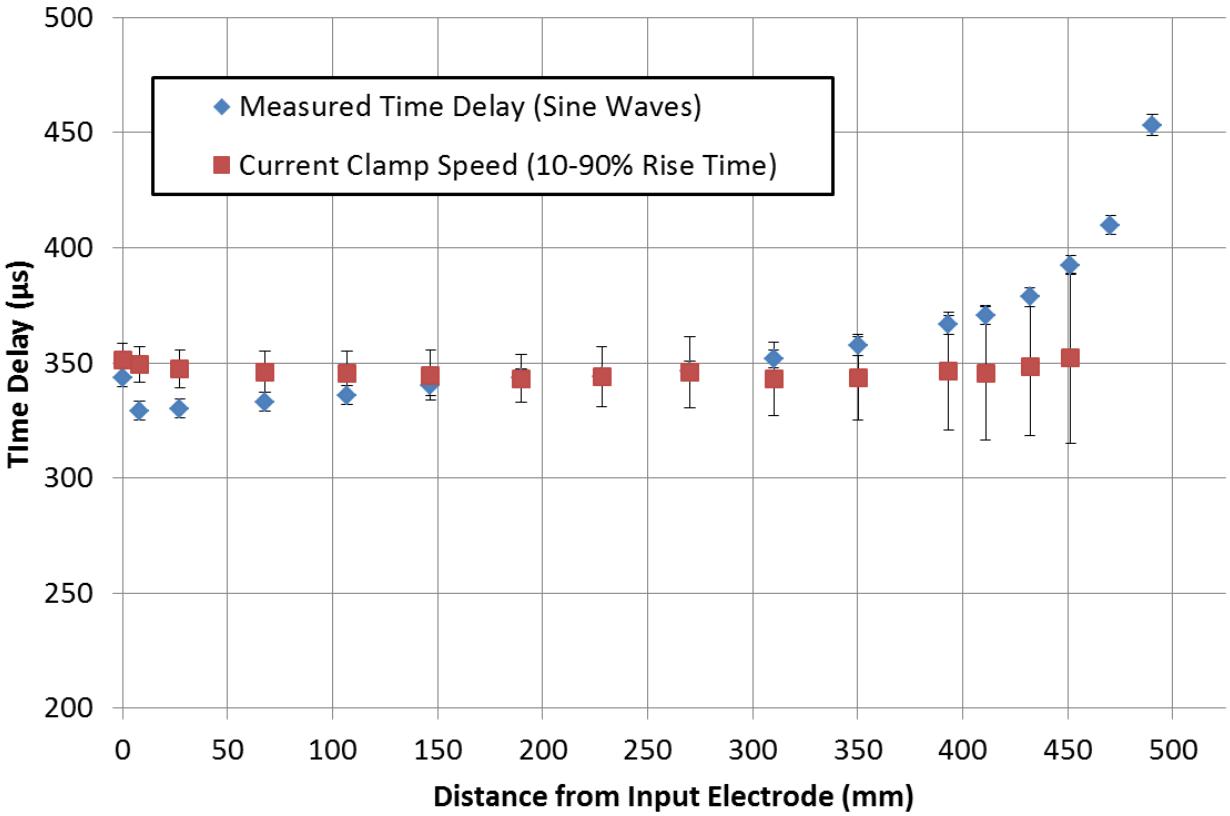

Figure 3-15: **10-90% rise time of the measured voltage as a function of the distance from the original input electrode (refer to Figure 3-10). The (+) side of the Axopatch was moved to each of the probe electrodes. Note that the input current, $30\ nA_{pp}\ (10\ Hz)$, was constant. The error bars show the 95% confidence interval using the standard deviation of the measurement as well as the resolution of the data acquisition system. The last two points of the 10-90% rise time were excluded from the plot due to issues with the signal to noise ratio.**

3.6 Important Factors Related to Signal Conduction Velocity

This section investigates why the signal conduction velocity in the artificial axon system is significantly faster than that in a real neuron. The four main reasons that the biological signal conduction velocity is much slower than that in the artificial axon system are:

1. The cell membrane must be charged as the signal travels down the axon.
2. The channel gating behavior involved in propagating the action potential is a time-consuming process.

3. The axon diameters in real myelinated nerve cells are on the order of a few micrometers whereas the capillary tubing in the artificial axon system is about $1\ mm$.
4. Electrolyte concentration has nearly negligible effects on conduction velocity.

In a real neuron, the speed (conduction velocity) of an action potential is related to the time constant (τ) of the axon, which can be calculated as:

$$\tau = r_M c_M \tag{3-2}$$

Where r_M is the resistance[22] of the cell membrane and c_M is the capacitance of the cell membrane. An ideal neuron would have an infinitely small time constant, which would mean that signals would travel instantaneously from one end of the axon to another [32]. For this ideal neuron, either r_M or c_M would have to approach 0. In the context of the electrolyte filled tubing test (Figure 3-9), the resistance, r_M, of the capillary tubing (polyvinyl material) is very large, however, the capacitance of the tubing, c_M, is very small due to the thickness of the wall. Estimating the time constant of the electrolyte filled capillary tubing is therefore not a straightforward task.

In a biological axon, the action potential is slowed down because the cell membrane (lipid bilayer) has to be charged along the length of the axon. In addition, there is a significant delay related to the opening of the sodium (Na^+) channels which play a key role propagating the action potential down the axon. The speed of a signal through the electrolyte in the capillary tube, however, is not slowed down by the presence of a significant capacitance or voltage-gated ion channels as is the case in a biological axon. Based on this, the signal propagation speed in the artificial axon system would be much larger than that in real axons and is very likely too fast to be measureable using the current data acquisition system (refer back to Figure 3-15). Even if the conduction velocity in the capillary tubing was hindered by voltage-gated ion channels and a capacitance, based on the inner diameter alone, the conduction velocity would be on the order of $6000\ m/s$ for a $1\ mm$ inner diameter axon[23] [54].

[22] Note that this is not the cross-sectional resistance of the intracellular fluid (electrolyte). r_m refers to the resistance of the cell membrane (lipid bilayer) that surrounds the axon.
[23] This is, of course, assuming that the linear relationship between myelinated axon diameter and conduction speed is true for axon diameters greater than $20\ \mu m$.

One assumption was that the concentration of the potassium chloride (KCl) electrode had an effect on signal conduction velocity. In other words, as the electrolyte concentration was reduced, so would the signal conduction velocity. The lowest KCl concentration that silver-silver chloride (Ag/AgCl) electrodes can effectively be used in is $5 - 10\ mM$ [56, 57]. Therefore, the capillary tubing was filled with a $10\ mM$ KCl solution in an effort to decrease the signal conduction velocity in the artificial axon system as much as possible. However, water actually has a similar conduction speed to that of copper wiring ($0.6 - 0.8$ times the speed of light) [58]. In other words, a $10\ mM$ KCl solution will conduct a signal just as fast as a $1\ M$ KCl solution. The difference between the two cases is that the saline concentration does affect the ease at which a signal travels. For example, suppose there are two large bodies of electrolyte solution. One contains $10\ mM$ KCl while the other contains $1\ M$ KCl. If lightning were to strike in the center of both bodies of electrolyte, the signal (electrical current) would travel much further in the $1\ M$ KCl solution compared to the $10\ mM$ KCl solution because the electrical resistance is lower in the $1\ M$ KCl solution (less losses). The signal is traveling at the same speed in both cases, but the signal strength at some distance from the lightning strike point is different.

3.7 Chapter Summary and Conclusions

This chapter introduced the artificial axon system that was used to show properties of a real myelinated nerve cell. The goal was to show that a system consisting of multiple lipid bilayers connected perpendicularly to an electrolyte line could be used to demonstrate how an action potential travels down a nerve cells axon. In order to do this, the signal conduction velocity in the artificial axon system had to be on the order of its biological equivalent. Based on experimental results, however, the speed of a signal traveling through the artificial axon system cannot be confidently determined using the measurement system. This is due to the fact that the signal moves through the artificial system at significantly higher speeds than those in a real axon. The signal conduction velocity in a real axon is much slower than in the artificial axon system because due to the charging process of the cell membrane and the opening of sodium channels as the action potential propagates down the axon.

The results presented in this chapter indicate that the signal conduction velocity in the artificial axon system is orders of magnitude larger than in a real axon. Therefore, one would not see a time delay (phase shift) between the input signal and the signal measured at some point along the artificial axon system. The signal would travel instantaneously down the axon according to the measurement system. In the future, one might use a different data acquisition system to measure the voltage. However, the

data acquisition system would have to have a large input impedance ($> 100\ M\Omega$) in order to avoid affecting the system[24].

[24] The reason for this is the same reason that one wants a high input impedance for a voltmeter. The goal is to use as little current as possible to make the measurement, otherwise, the measurement is affect the system's response.

Chapter 4: Signal Boosting Behavior

Based on the results and discussion presented in the previous chapter, the artificial axon system has limitations in that the signal conduction velocity is orders of magnitude faster than in a real neuron. The propagation of a signal from one electrode to the next along an artificial axon can be considered almost instantaneous in the described artificial axon system relative to the biological axon. However, there are other signal propagation properties related to the action potential in a biological system that can be reproduced using the artificial axon system. The signal boosting mechanism that occurs in the nodes of Ranvier is of particular interest.

This chapter discusses how the artificial axon system can be utilized to show signal boosting properties similarly to that of an biological axon. It begins with a review of the signal boosting behavior that occurs in the nodes of Ranvier of myelinated nerve cells. The electrical circuit model for the artificial axon system is introduced which is used to predict the response to various input configurations. Experimental results are presented to support the circuit model, which include plots that show the signal boosting behavior.

4.1 Brief Review of the Node of Ranviers' Signal Boosting Behavior

Recall that an action potential begins in the axon hillock and travels down towards the axon terminals as shown in Figure 1-7. In a myelinated axon, the axon is covered with the insulating material myelin. Along the myelinated axon, there are small regions where the axonal membrane is not myelinated called the nodes of Ranvier. In these regions, the neuron membrane is directly exposed to the extracellular fluid. When an action potential is initiated, it travels down the axon, but the strength of the signal diminishes with the distance traveled (even in the myelinated regions) because current leaks out of the axon. The nodes of Ranvier act to "boost" the signal back to its original strength. In other words, as the signal travels through the myelinated regions, the signal strength drops, but each time the signal reaches a node of Ranvier, the signal is boosted back to its original amplitude by gating properties of both sodium (Na^+)and potassium (K^+) ion channels [2, 32, 43]. A diagram of this process is shown in Figure 4-1.

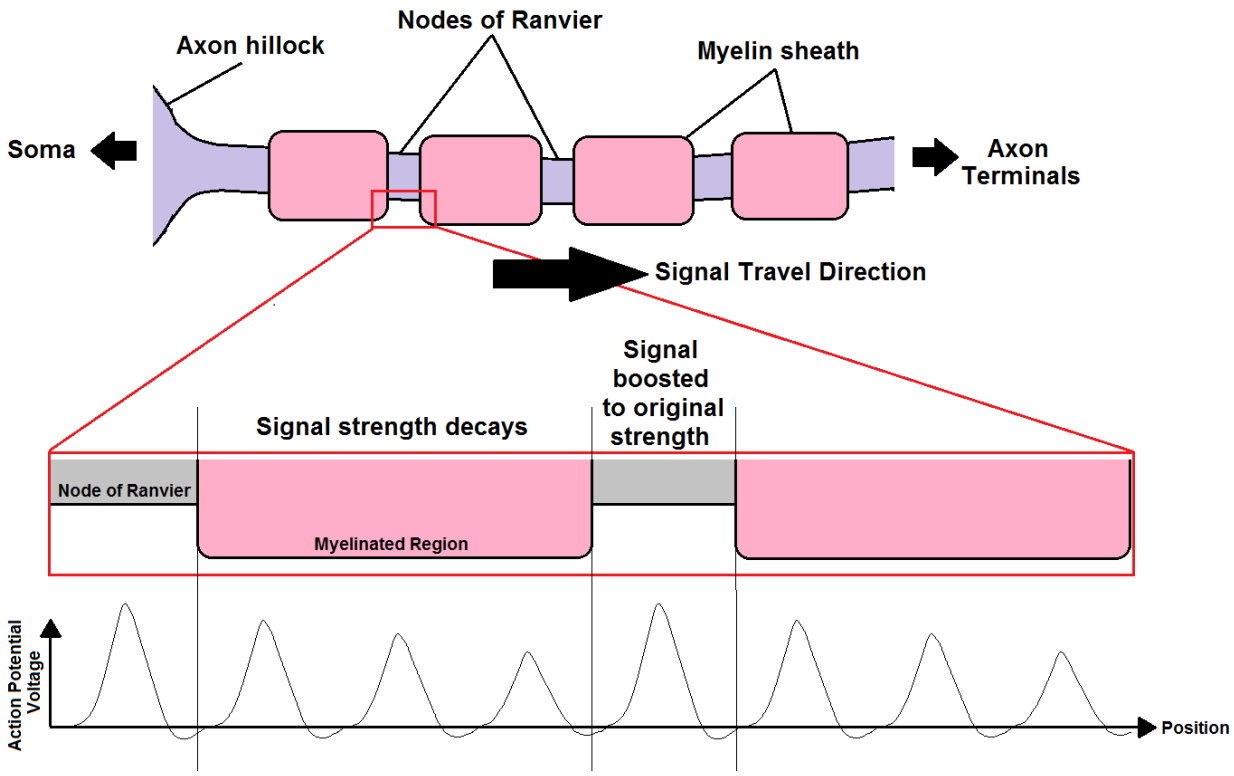

Figure 4-1: **Diagram of myelinated axon that depicts how the action potential strength decreases in the myelinated regions and then is boosted back to the original strength in the nodes of Ranvier as it travels down the axon.**

4.2 Circuit Model for Artificial Axon System

Figure 4-2 shows the equivalent circuit diagram for the artificial axon system shown in Figure 3-1. In Figure 4-2, R_1 corresponds to the resistance between the input electrode and the bilayer, R_2 is the resistance between the bilayer and the measurement electrode, and R_3 is the resistance between the measurement electrode and the ground electrode. Recall from Section 2-5 that when alamethicin is present in the electrolyte/lipid solution, the resistance of the bilayer is a function of the voltage across the bilayer. The bilayer is therefore modeled simply as a two-state resistor, R_M, which is dependent on the voltage across the bilayer $V_{M2} - V_{M1}$. When the magnitude of voltage across the bilayer is greater than the alamethicin gating potential (assumed to be $70\ mV$ for many of the following figures), R_M switches to the low resistance state. For all other potentials, R_M is in the high resistance state. The current through the capillary tubing from the input electrode to the bilayer is modeled as i_1 and the current flowing through the bilayer is modeled as i_2. By summing i_1 and i_2, the current flowing from the bilayer to the ground electrode can be determined.

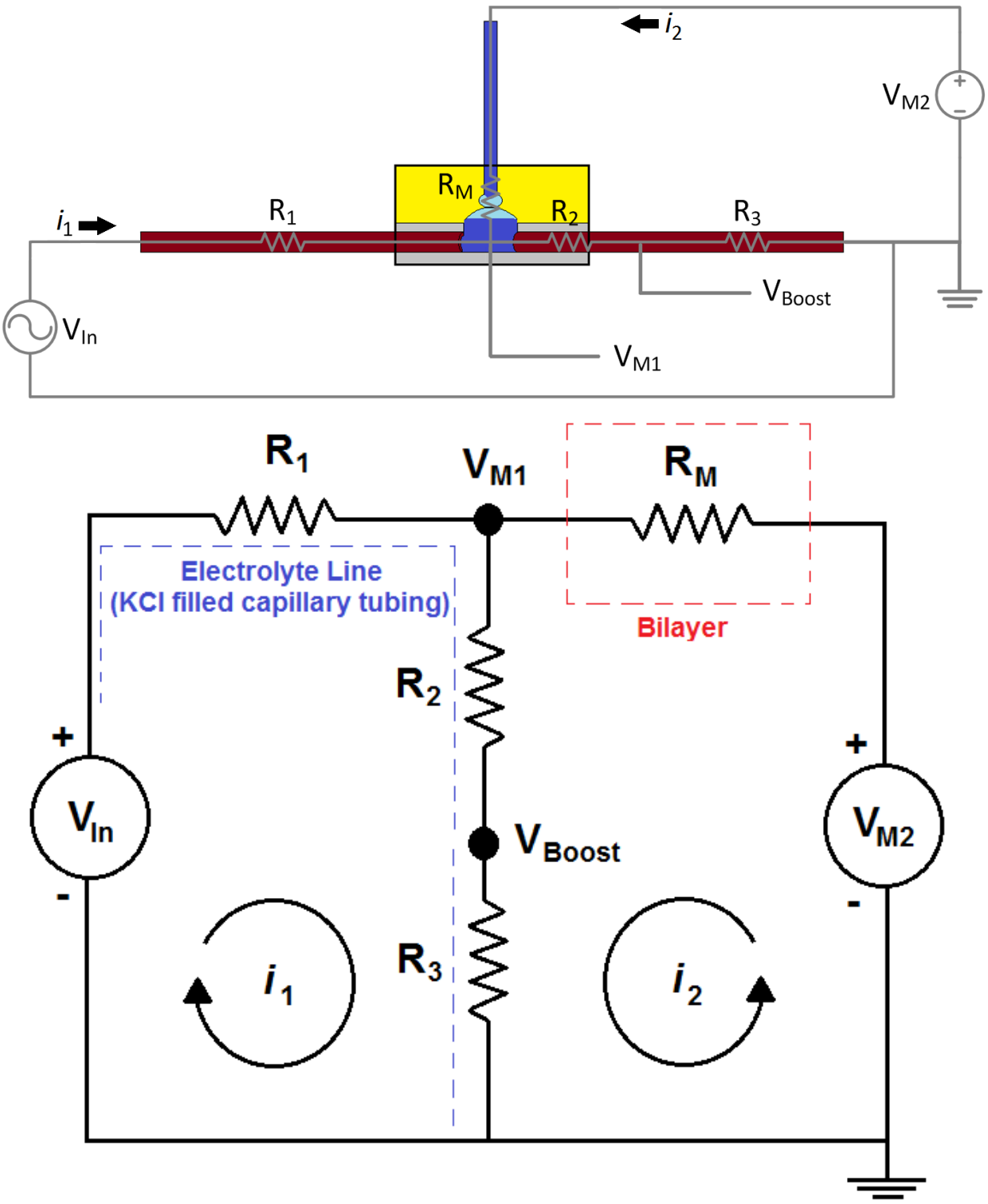

Figure 4-2: **Equivalent circuit diagram for the artificial axon system (Figure 3-1).**

The current flowing through the electrolyte line can be calculated using Ohm's Law as:

$$i_1 = \frac{V_{In} - V_{M1}}{R_1} \tag{4-1}$$

The current flowing through the bilayer can be calculated similarly as:

$$i_2 = \frac{V_{M2} - V_{M1}}{R_M} \tag{4-2}$$

The voltage at the measurement electrode can be calculated as:

$$V_{Boost} = R_3(i_1 + i_2) \tag{4-3}$$

By substituting Equation (4-1) and Equation (4-2) into Equation (4-3), it can be shown that:

$$V_{Boost} = R_3\left(\frac{V_{In} - V_{M1}}{R_1} + \frac{V_{M2} - V_{M1}}{R_M}\right) \tag{4-4}$$

The idea behind the signal boosting is that when the voltage across the bilayer $(V_{M2} - V_{M1})$ is approximately $\pm 70\ mV$, the alamethicin channels will start to gate, which will decrease the resistance of the bilayer, R_M, allowing for current to easily flow through it. In order to boost the voltage at V_{Boost}, the current through the bilayer, i_2, needs to add to the current flowing through the electrolyte solution, i_1.

When the voltage across the bilayer is less than the gating potential of the alamethicin, then $i_1 \gg i_2$. Therefore, the voltage along the electrolyte line linearly decays towards zero (as shown previously in Figure 3-12). However, by varying the magnitude of the input voltage, V_{In}, the voltage on the electrolyte side of the bilayer, V_{M1}, can be controlled as shown in Figure 4-3. In other words, the user indirectly controls the voltage across the bilayer by the magnitude of the input signal. In addition, the user can control the voltage across the bilayer by controlling the position of the bilayer relative to both the input and ground electrodes. For example, suppose the entire length of the artificial axon system is $500\ mm$, the bilayer is located $150\ mm$ from the input electrode, and that $V_{M2} = 0$ (grounded). For the case described, the alamethicin channels in the bilayer would only be gating if the input voltage was approximately $100\ mV$ or greater as shown in Figure 4-3. If the bilayer was moved to $275\ mm$ from the

input electrode, the alamethicin channels in the bilayer would only gate if the input voltage was greater than $150\ mV$.

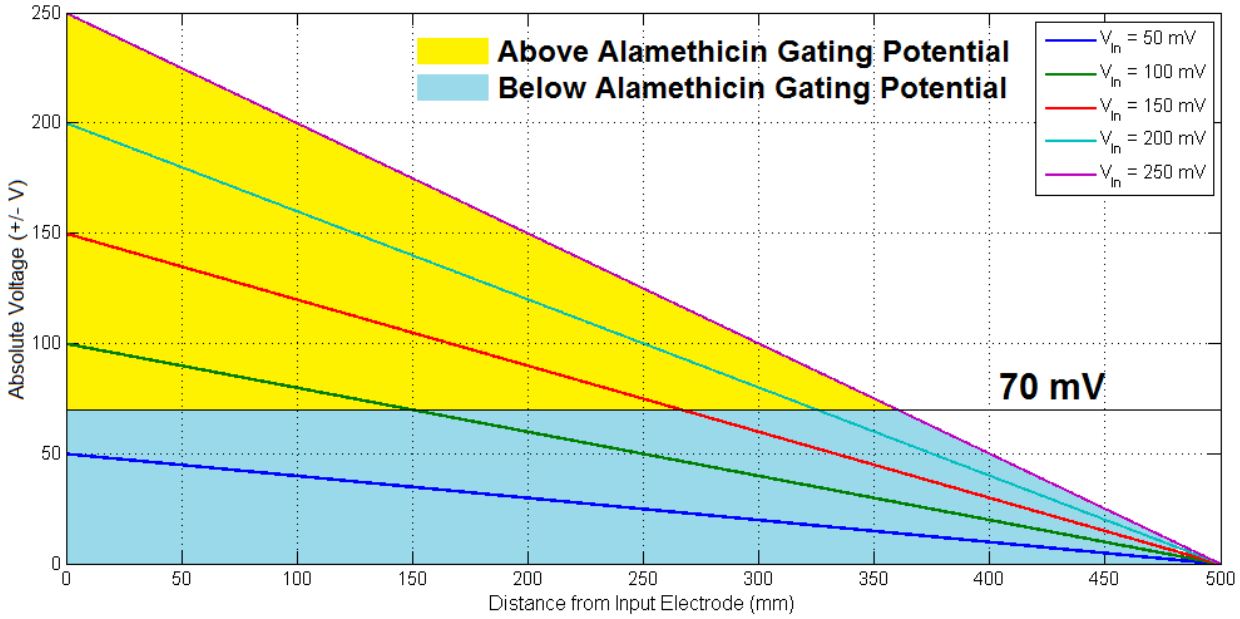

Figure 4-3: **Absolute voltage as a function of the distance from the input electrode and input voltage magnitude. The distance between the input electrode and ground electrode is $0.5\ m$. The yellow and blue regions of above/below the alamethicin gating potential assumes that $V_{M2} = 0$ (grounded).**

4.3 Investigating the Circuit Model: V_{M2} is constant

A neuron typically has a constant resting potential between -70 and $-60\ mV$ [2, 32, 35, 59]. The intracellular fluid potential is less than that of the extracellular fluid. Based on this, V_{M2} (Figure 4-2) should be a constant value that is larger than V_{M1} (analogous to the intracellular fluid) in order to be most similar to the biological system. This section investigates the circuit shown in Figure 4-2 for the case where V_{M2} is a constant value (most relevant in the biological sense). The goal is to show, theoretically, that a voltage signal can be boosted in amplitude as it travels down the electrolyte line due to the alamethicin channels in the bilayer.

In the biological case, the signal is boosted with V_{M2} set as a constant value. Figure 4-4 shows the voltages V_{M1} and V_{M2} as a function of time for a sine wave signal generated at the input electrode and V_{M2} set as a constant value. Note that the voltage on the micropipette side of the bilayer, V_{M2}, is held at a constant DC potential (red). The voltage on the electrolyte line side of the bilayer, V_{M1}, varies with time (blue). Recall that the voltage across the bilayer is simply $V_{M2} - V_{M1}$. If the bilayer contains gating

ion channels such as alamethicin, the system can be set up such that the channels gate at certain points in the sine wave (yellow section in Figure 4-4). For the case shown in the diagram, the alamethicin channels will only be gating at the trough of the sine wave because this is where the voltage across the membrane is greater than the gating potential of the channels (V_{Alm}). When the channels gate, the signal amplitude at the trough of the sine wave will be boosted as shown in Figure 4-5. The boosting only occurs at the trough of the sine wave because the alamethicin channels would only open at the trough.

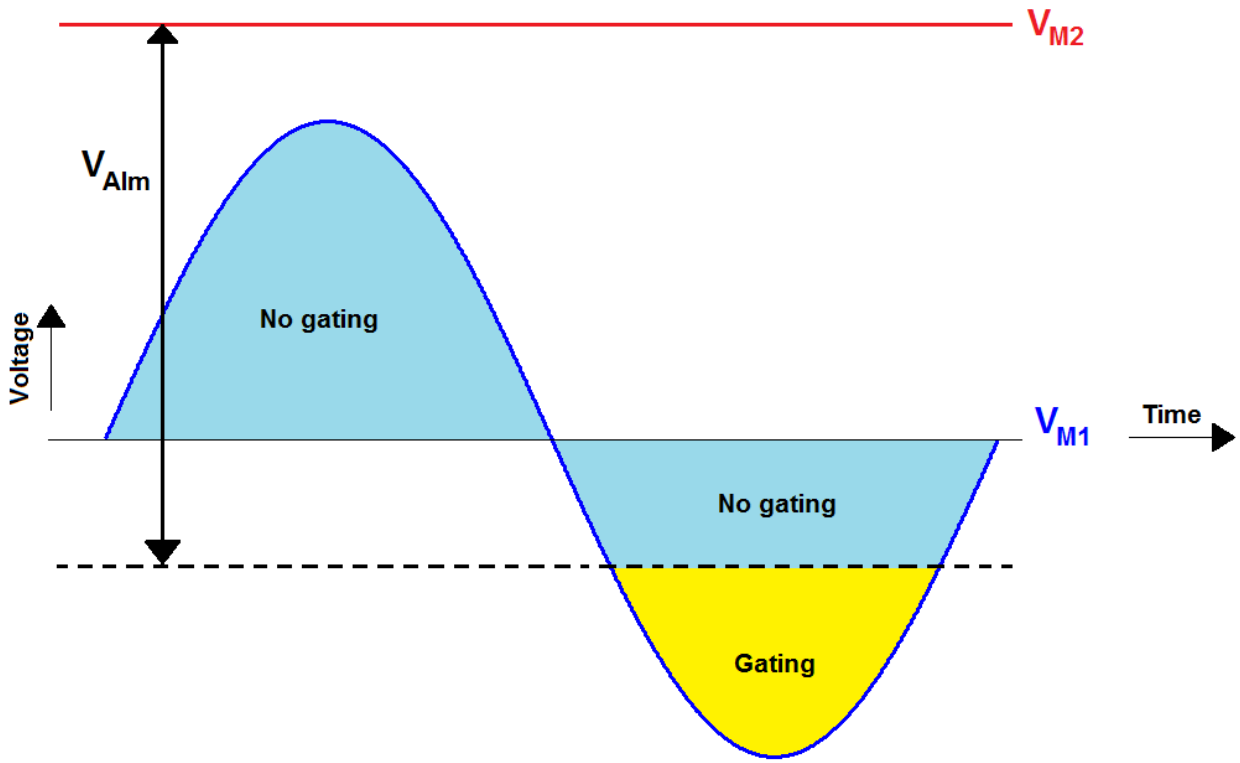

Figure 4-4: **Red) Constant DC voltage applied on the micropipette side of the bilayer (V_{M2}). Blue) Sinusoidal voltage on the electrolyte line side of the bilayer (V_{M1}) as a function of time. The light blue region shows where the voltage across the bilayer ($V_{M2} - V_{M1}$) is less than the gating potential of alamethicin and the yellow region shows where the voltage across the bilayer is greater than the gating potential of alamethicin.**

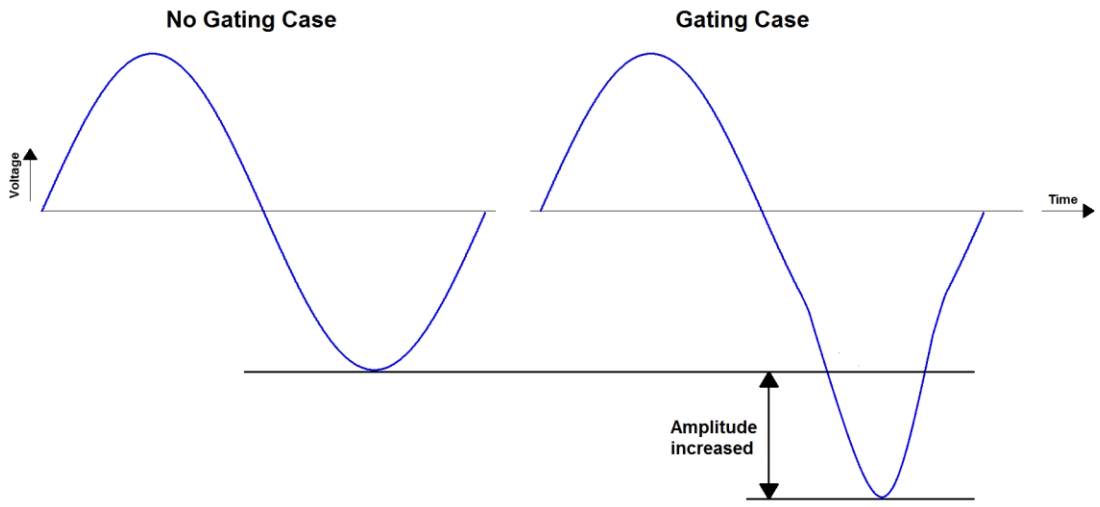

Figure 4-5: **Ideal signal boosting example corresponding to the example in Figure 4-4.**

To better document this, consider the case where V_{In} (Figure 4-2) is operating at $60\ mV_{pp}$ $(10\ Hz)$ sine wave and V_{M2} is held constant at $60\ mV$ (Figure 4-6). The voltage across the bilayer as a function of time (black) is also shown. Assuming that the alamethicin channels only open when the voltage across the bilayer is $70\ mV$, then the green region shows where the alamethicin channels open.

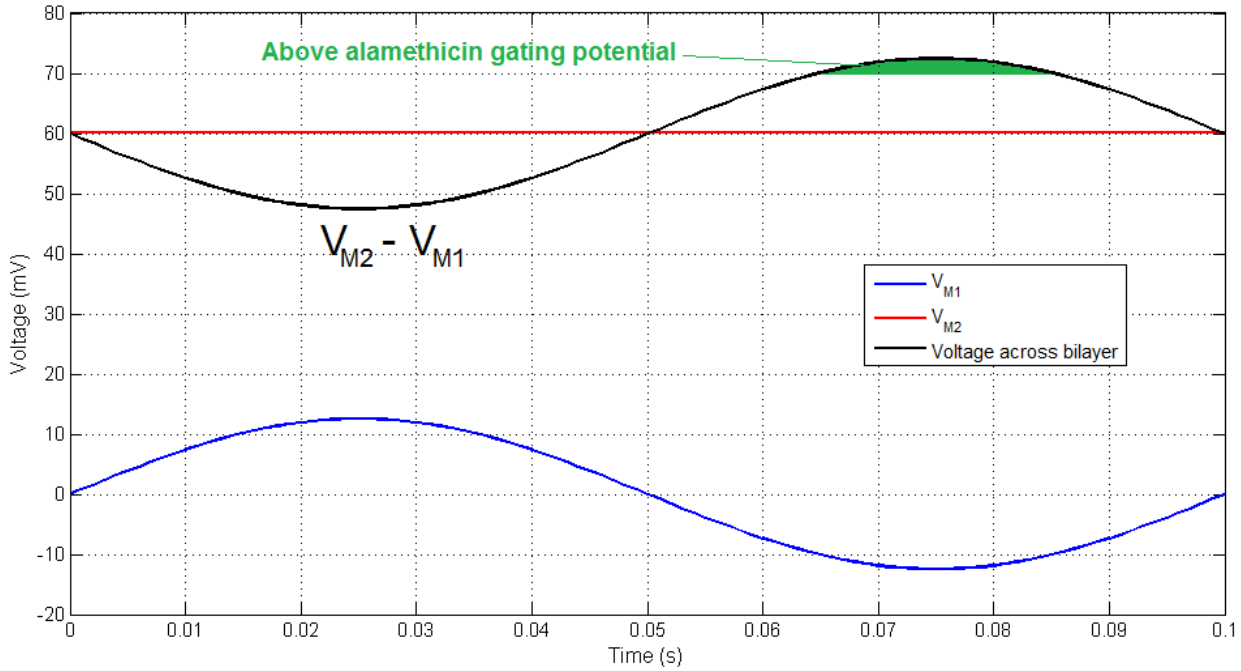

Figure 4-6: **Red) Constant $60\ mV$ voltage applied on the micropipette side of the bilayer (V_{M2}). Blue) Sinusoidal voltage on the electrolyte line side of the bilayer (V_{M1}) as a function of time (assuming a linear drop in voltage amplitude down the electrolyte line). Black) Voltage across the bilayer $(V_{M2} - V_{M1})$. List of system parameters: $V_{In} = 60\ mV_{pp}\ (10\ Hz), R_1 = 3\ M\Omega, R_2 = 150\ k\Omega, R_3 = 2\ M\Omega, V_{M2} = 60\ mV$.**

4.3.1 Two-state Bilayer Resistor Model

Due to the nonlinear behavior[25] of the bilayer resistor (R_M, Figure 4-2), the system cannot be solved simply by using a circuit analysis. However, in order to get an idea of how the voltage at the measurement electrode (V_{Boost}) responds to various input signals, a two-state bilayer resistor model was employed. In this model, R_M, was in one of two states: a high resistance state where the alamethicin channels are not open or a low resistance state where the alamethicin channels are open. This two-state model is advantageous because the system equations can be solved. For each point in time, the system is solved using the high resistance value (no channel gating) for R_M. Once the system is solved, if $|V_{M2} - V_{M1}| > V_{Alm}$, then the system is resolved using the lower value for R_M.

Figure 4-7 shows the cyclic voltammetry data measured for a lipid bilayer with $3\ \mu g/mL$ alamethcin in the lipid/electrolyte solution (blue) and the expected cyclic voltammetry data for a bilayer modeled as a two-state resistor (black). Note that when the magnitude of the voltage across the bilayer is less than $70\ mV$, the bilayer is in the high resistance state, and when the voltage across the bilayer is greater than $70\ mV$, the bilayer is in the low resistance state due to the alamethicin channels opening.

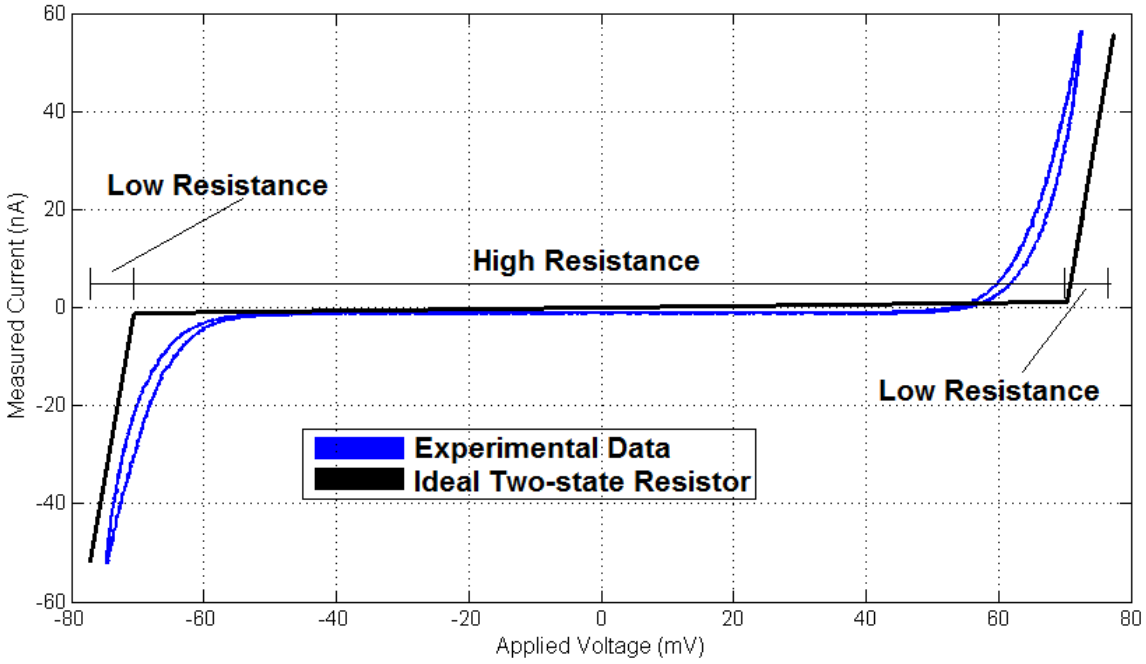

Figure 4-7: **Cyclic voltammetry data of a bilayer with the following parameters:** $R_E = 490\ k\Omega, R_M = 1.4\ G\Omega,$ and $C_M = 440\ pF$ $(\sim 300\ \mu m\ diameter)$. **The alamethicin concentration in the lipid solution was** $3\ \mu g/mL$**.** $10\ mM$ **KCl electrolyte concentration.**

[25] The nonlinear behavior is due to the presence of alamethicin channels. R_M can be thought of as a variable resistor that is dependent on the value of $V_{M2} - V_{M1}$.

Figure 4-8 shows the theoretical currents (i_1, i_2) in the system (Figure 4-2) as a function of time and for the case without alamethicin channels (red) as well as the case with alamethicin channels (blue) based on the circuit model equations. The potential on the micropipette side of the bilayer, V_{M2}, is held constant at $60\ mV$ and the input voltage, V_{In}, is a $60\ mV_{pp}$ $(10\ Hz)$ sine wave voltage. Note that the current through the bilayer (i_2) increases dramatically once the voltage across the bilayer reaches the alamethicin gating potential (assumed to be $70\ mV$ in this case). At this point, the alamethicin channels in the bilayer are open, which lowers the membrane resistance of the bilayer. The instantaneous increase is due to two-state resistor model that is being used for the bilayer resistance, R_M. If the potential across the bilayer reaches the alamethicin gating potential, then the resistance of the bilayer is decreased by a factor[26] of $1/4000$ and the system equations are resolved for that point using the new bilayer resistance.

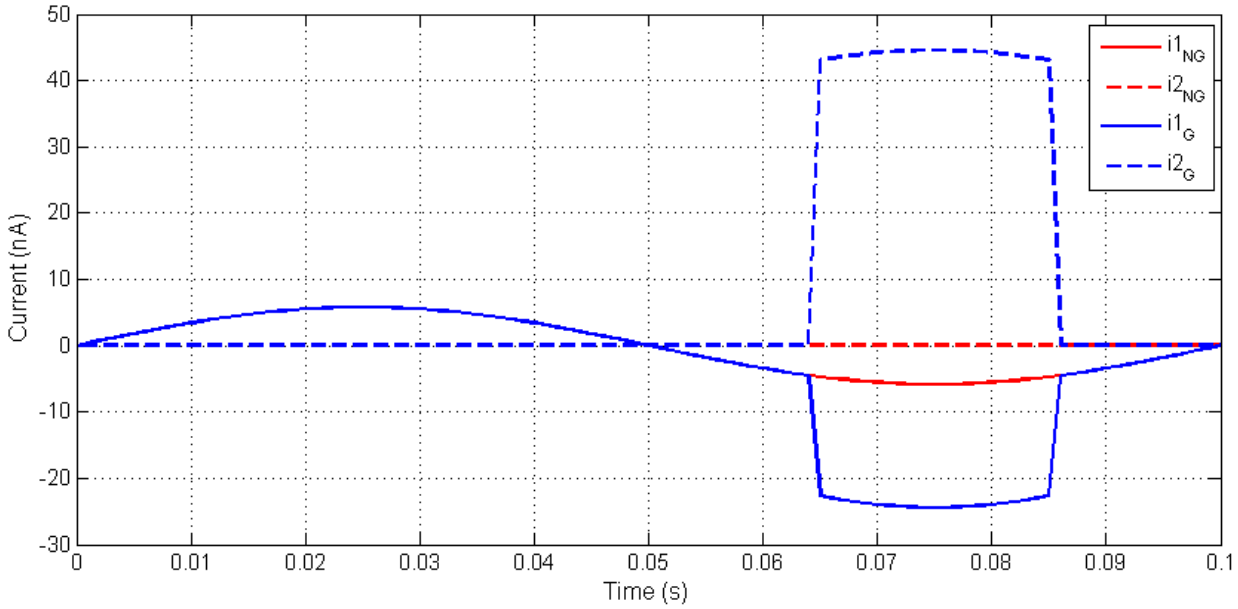

Figure 4-8: i_1 **is the current through the electrolyte line between the input electrode and the bilayer (Figure 4-2) and** i_2 **is the current through the bilayer. The sum of these two currents is the total current flowing from the bilayer to the ground electrode. Red) Case without alamethicin channels. Blue) Case with alamethicin channels. List of system parameters:** $V_{In} = 60\ mV_{pp}\ (10\ Hz), R_1 = 3\ M\Omega, R_2 = 150\ k\Omega, R_3 = 2\ M\Omega, V_{M2} = 60\ mV$. **Note that this plot was generated using the circuit equations for the two-state bilayer resistor model.**

[26] This factor is based on experimental cyclic voltammetry data measured for a bilayer with the following characteristics: $R_E = 490\ k\Omega, R_M = 1.4\ G\Omega,$ and $C_M = 440\ pF$ $(\sim 300\ \mu m\ diameter)$. The alamethicin concentration was $3\ \mu g/mL$.

Note the polarity of the currents in Figure 4-8. i_1 is negative, whereas i_2 is positive. This means that the voltage downstream of the bilayer, V_{Boost} is going to increase, rather than decrease based on Equation (4-3). In order to show a boosting behavior, V_{Boost} must decrease (larger negative number) when the alamethicin channels open, effectively boosting the amplitude of the signal as shown Figure 4-5. Based on the circuit model, as shown in Figure 4-8, when the alamethicin channels open, V_{Boost} will move towards 0, instead of towards $-\infty$ to boost the voltage amplitude. Referring back to (4-3), since i_1 is a negative value at the trough, i_2 would also need to be negative at the trough when the alamethicin channels are open in order for the signal to be boosted at the trough. However, i_2 will always be positive because V_{M2} is always greater than V_{M1} for the current case (refer back to Figure 4-6).

Figure 4-9 shows the corresponding V_{Boost} as a function of time for the case with alamethicin channels (blue) and without alamethicin channels (red). Note that the behavior is not like that of the ideal case (Figure 4-5). Instead of moving towards a larger negative value, V_{Boost} moves in the opposite direction towards a positive value. Technically, based on the plot, the signal is boosted, but in the wrong direction. Recall that this change in direction is due to the relative magnitudes of i_1 and i_2 (Figure 4-8). Since $i_2 > i_1$, the voltage at V_{Boost} must increase in the positive direction (as opposed to an increase in the negative direction).

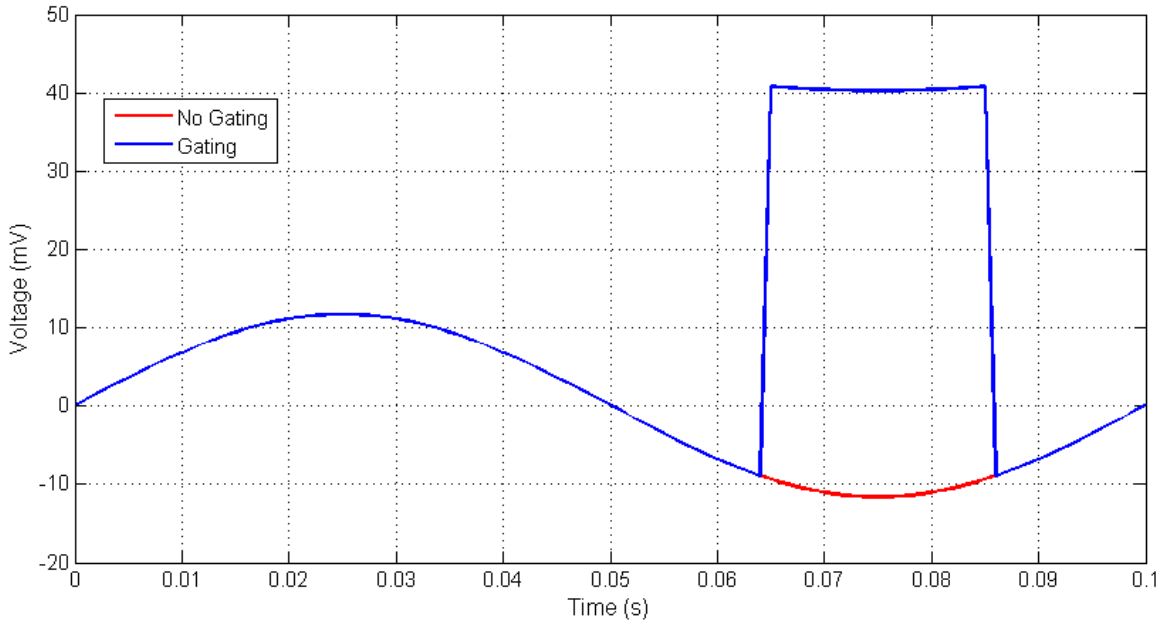

Figure 4-9: **Voltage at the measurement electrode (V_{Boost}) as a function of time for the case without alamethicin channels (red) and the case with alamethicin channels (blue). List of system parameters:** $V_{In} = 60\ mV_{pp}\ (10\ Hz), R_1 = 3\ M\Omega, R_2 = 150\ k\Omega, R_3 = 2\ M\Omega, V_{M2} = 60\ mV$. **Note that this plot was generated using the circuit equations for the two-state bilayer resistor model.**

Based on the data in Figure 4-9, one could be falsely lead to believe that the signal was boosted when a bilayer containing alamethicin channels was incorporated into the system because the amplitude of the sine wave was clearly increased. However, due to the simplistic model of the two-state bilayer resistor, the current and voltage values shown in Figure 4-8 and Figure 4-9 are unrealistically large.

One of the major issues with the two-state bilayer resistance model is that when the resistance of the bilayer drops, the voltage across the bilayer also drops, which means that alamethicin channels may not actually be gating to a sufficient degree to affect V_{Boost}. In other words, in a real system, the alamethicin channels are not simply open or closed. Based on the data in Figure 4-7, it is clear that resistance of the bilayer varies with the voltage across the bilayer. This means that the predicted voltages and currents (Figure 4-8 & Figure 4-9) are likely much larger in magnitude than they would if measured experimentally. Therefore, the two-state bilayer resistor model is only useful for showing the general trends in response to changing system parameters. Even so, based on the response shown in Figure 4-9, the signal is not boosted when V_{M2} is set to a constant value.

4.3.2 Using Cyclic Voltammetry Data To Create Theoretical Model Versus Two-State Bilayer Resistor Model

Up to this point, the functionality of the alamethicin channels has been incorporated into the circuit model (Figure 4-2) as a two-state bilayer resistor. In two-state bilayer resistor model, the alamethicin channels are either open or closed and the resistance of the bilayer can only be one of two values. The problem is that a bilayer with an aggregation of alamethicin channels cannot simply be modeled as a two-state resistor because the bilayer acts more like a variable resistor dependent on the voltage across it. In order to get more realistic estimates of the currents and voltages using the circuit model (Figure 4-2), cyclic voltammetry[27] (CV) data can be used.

Recall that Figure 4-7 shows CV data for a bilayer with $3\ \mu g/mL$ alamethicin (blue) as well as the ideal cyclic voltammetry data for a two-state resistor (black). The two-state resistor has two states, a high resistance state (between $-70\ mV$ to $70\ mV$) and a low resistance state ($< -70\ mV$ and $> 70\ mV$). Note that the transition between the two states is immediate. In other words, once the applied voltages

[27] Cyclic voltammetry data is taken by measuring the current through the bilayer as the DC potential across it is varied.

reaches $-70\ mV$ or $70\ mV$, the resistor immediately changes to a different state. The experimental data, however, does not simply have two states. As the magnitude of the applied voltage increases, the current increases exponentially. This means that in a real bilayer system, the bilayer resistance acts as a variable resistor dependent on the voltage across the bilayer.

In order to get more realistic estimates of the system currents and voltages, the experimental cyclic voltammetry data (Figure 4-7) was used in the circuit model instead of the two-state bilayer resistor. For each point in time of a simulation, the current through the bilayer (i_2, Figure 4-2) was set as one of the current points in Figure 4-7 (experimental). i_1, the voltage across the bilayer, and V_{Boost} were then calculated using the system equations for the circuit. The predicted voltage across the bilayer $(V_{M2} - V_{M1})$ was then compared to the applied voltage corresponding to the assumed current through the bilayer from the experimental CV data. Ideally, these two voltages would be very close to one another. For each point in time of the simulation, the MATLAB code would cycle through all of the experimental currents and select the one where the experimental voltage most closely matched the simulated voltage across the bilayer. A copy of the MATLAB code can be found in section A.3 in Appendix A.

Figure 4-10 shows the voltage at the measurement electrode, V_{Boost}, for the case where the potential on the micropipette side of the bilayer, V_{M2}, is held constant at $60\ mV$ and the input voltage, V_{In}, is a $60\ mV_{pp}$ $(10\ Hz)$ sine wave voltage (compare to the results in Figure 4-9). The plot was generated using the theoretical model that uses CV data. Note that the peak voltage at approximately $t = 25\ ms$ is higher for the gating case (blue) than for the non-gating case (red). One might argue that the signal is therefore being boosted. However, the voltage across the bilayer at that point is actually at a minimum in a full period because V_{M1} is at a maximum and $V_{M2} = 60\ mV$ (refer back to Figure 4-6). The reason that the voltage for the gating case is higher than the non-gating case is due to a small DC offset (note the voltage at $t = 0, 100\ ms$). The cyclic voltammetry data (Figure 4-7) predicts that the current through the bilayer, when the alamethicin channels are not gating, is higher than expected current based solely on the membrane resistance $(R_M = 1.4\ G\Omega)$. In other words, one would expect that i_2, the current flowing through the bilayer, would be negligible compared to i_1, the current flowing through the electrolyte line. However, the DC voltage offset clearly shows that i_2 is large enough, even when the alamethicin channels are not gating, to shift the voltage signal upwards by a small DC amount. It is

important to note that this phenomenon does not mean the signal is being boosted, rather, it means the entire signal is being shifted along the y-axis (voltage).

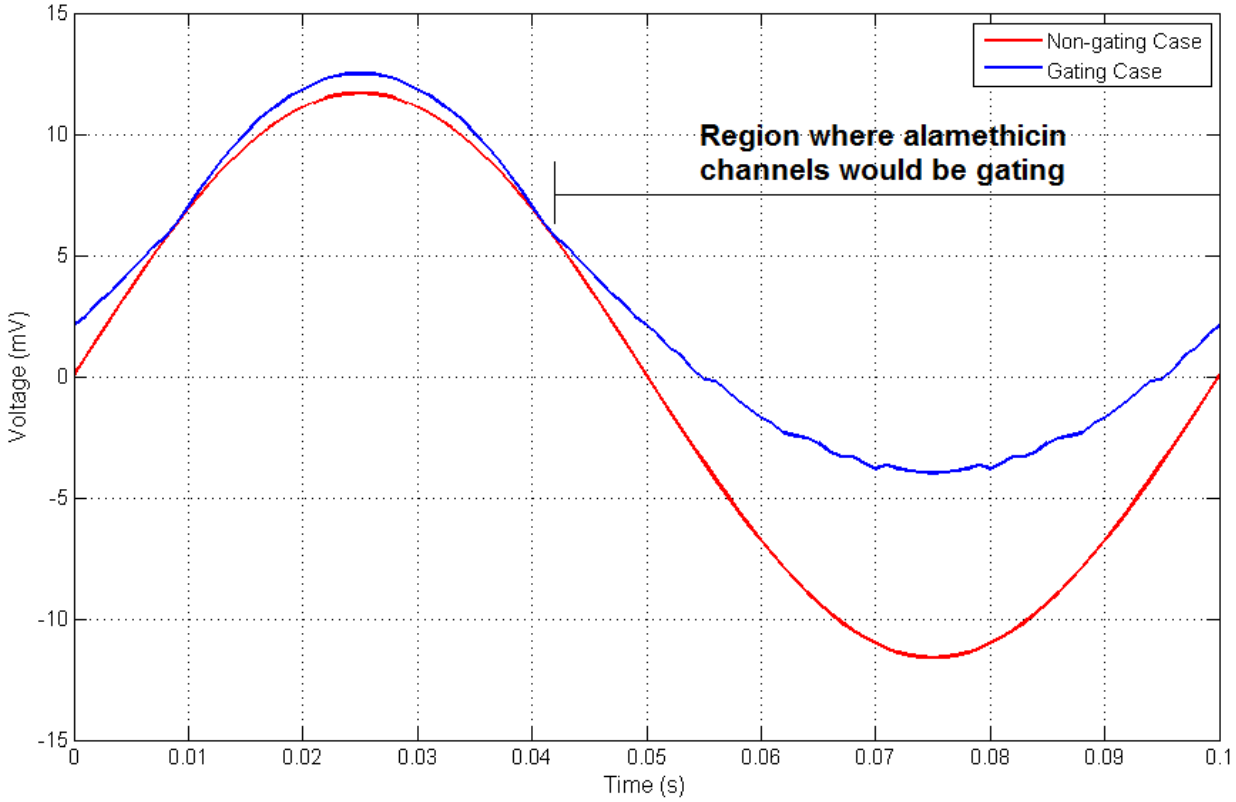

Figure 4-10: **Voltage at the measurement electrode (V_{Boost}) as a function of time for the case without alamethicin channels (red) and the case with alamethicin channels (blue) using the CV data in Figure 4-7. List of system parameters:** $V_{In} = 60\ mV_{pp}\ (10\ Hz), R_1 = 3\ M\Omega, R_2 = 150\ k\Omega, R_3 = 2\ M\Omega, V_{M2} = 60\ mV$. **Note that this plot was generated by the model that uses experimental CV data.**

Note how there is a significant difference in the amplitudes of the voltage curves near $t = 75\ ms$. The difference is due to the alamethicin channels opening in the bilayer and allowing a larger current to pass through it. This behavior is what we expected based on Figure 4-9 (two-state bilayer resistor model), but the difference in the voltage is not nearly as pronounced. The results shown in Figure 4-10 suggest that the sinusoidal signal cannot be boosted by simply using a DC potential for V_{M2} in conjunction with alamethicin channels in the bilayer.

4.4 Proof-of-Concept Experiment, $V_{M2} = 0$

A lipid bilayer was connected to a tube filled with electrolyte as shown in Figure 4-11 (refer back to Figure 3-1 for diagram of artificial axon system). The system was connected such that the input

electrode was $173\ mm$ from the bilayer and the ground electrode was $377\ mm$ from the bilayer. Based on cyclic voltammetry data for the electrolyte filled tube-only system shown in Figure 3-9, the resistance per unit length of the $0.04"$ $(1.02\ mm)$ inner diameter tubing filled with $10\ mM\ KCl$ was $9.47\ M\Omega/m$. Therefore, the total resistance between the input and ground electrode for the system shown in Figure 4-11 was $5.21\ M\Omega$.

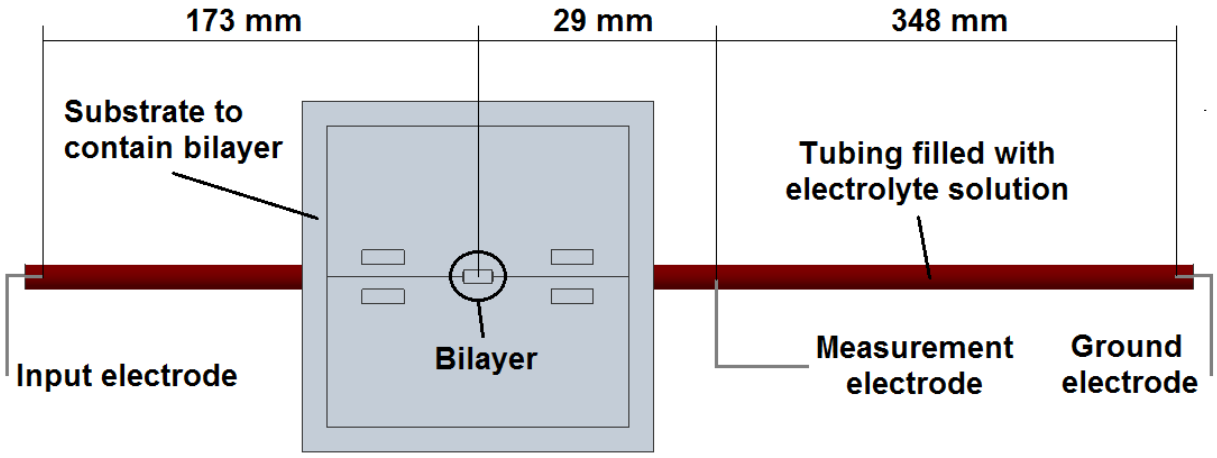

Figure 4-11: **Diagram of bilayer electrically connected to capillary tubing filled with electrolyte.**

Figure 4-12 shows the estimated current (not measured directly) through the system shown in Figure 4-11 where a bilayer is not connected in the system. The estimated current is simply calculated using Ohm's Law as the input voltage and resistance through the entire system is known. Note that the magnitude of the estimated current Figure 4-12 is on the same order as that of the cyclic voltammetry data shown in Figure 4-7 for a bilayer of similar size. This is important because it means the current flowing through electrolyte line should be on the order of the current flowing through the bilayer when the alamethicin channels are gating, which means V_{Boost} should be affected.

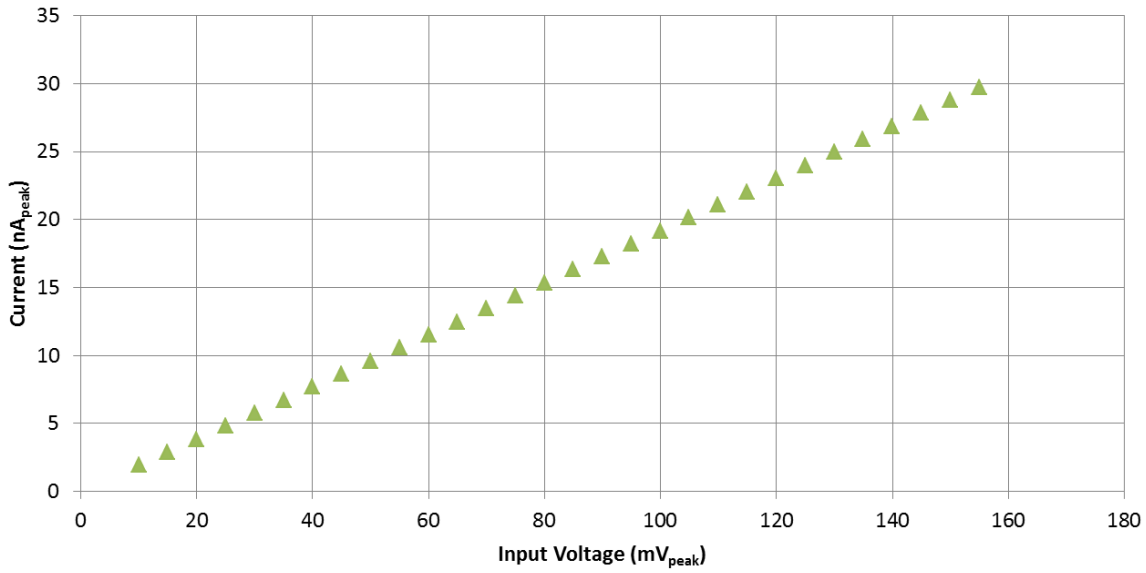

Figure 4-12: **Estimated peak current as a function of peak input voltage for the system shown in Figure 4-11 where there is no bilayer.**

Figure 4-13 shows the average voltage for a single period recorded at the measurement electrode (V_{Boost}) for the case with a bilayer (blue) and the case without a bilayer (red). The left plot shows the results for a 200 mV_{pp} (10 Hz) input signal and the right plot shows the results for a 300 mV_{pp} (10 Hz) input signal. Note that in the right plot, the amplitude of the signal for the case with a bilayer is less than that of the case without a bilayer. This decrease in amplitude is due to the alamethicin channels opening in the bilayer at the peak and trough of the sine wave, which results in a reduced V_{Boost} measurement.

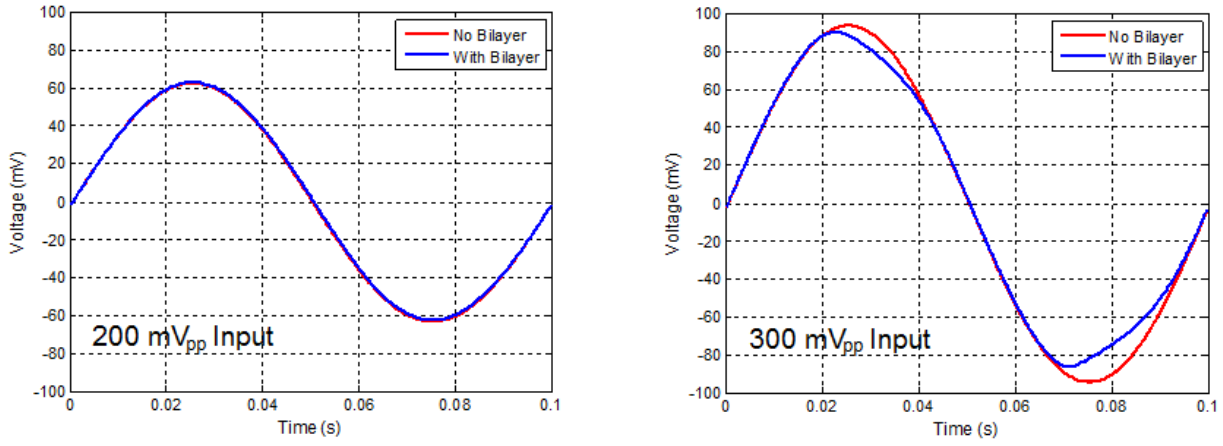

Figure 4-13: **Voltage recorded at the measurement electrode (V_{Boost}) for the artificial axon system for the case where $V_{M2} = 0$. The red plot shows the result when a bilayer is not connected to the system and the blue plot shows the case where a bilayer is connected to the system. Left) 200 mV_{pp} (10 Hz) input. Right) 300 mV_{pp} (10 Hz) input. Note that the single periods shown are based on an average ($n \approx 100$ periods).**

Figure 4-14 shows the amplitude of the voltage, V_{Boost} (Figure 4-2), at the measurement electrode (Figure 3-1 & Figure 4-11) as a function of the input voltage for two cases. The first case (red square) was where a bilayer ($480\ pF, \sim 320\ \mu m\ diameter$) was connected to the system and the second case (green triangle) was the control case (no bilayer). Note that as the input voltage approaches $120\ mV_{peak}$, the slope of the bilayer case becomes nonlinear. This is due to the alamethicin channels opening in the bilayer. When the alamethicin channels open in the bilayer, the current through the system is split in two. A portion of the current flows through the bilayer to ground and the rest flows through the electrolyte tubing to the ground. V_{Boost}, once the alamethicin channels are open, will therefore drop because less current is flowing through the line. If instead current was to flow through the bilayer in the opposite direction (towards the electrolyte line), V_{Boost} would have increased when the alamethicin channels opened instead of decreasing.

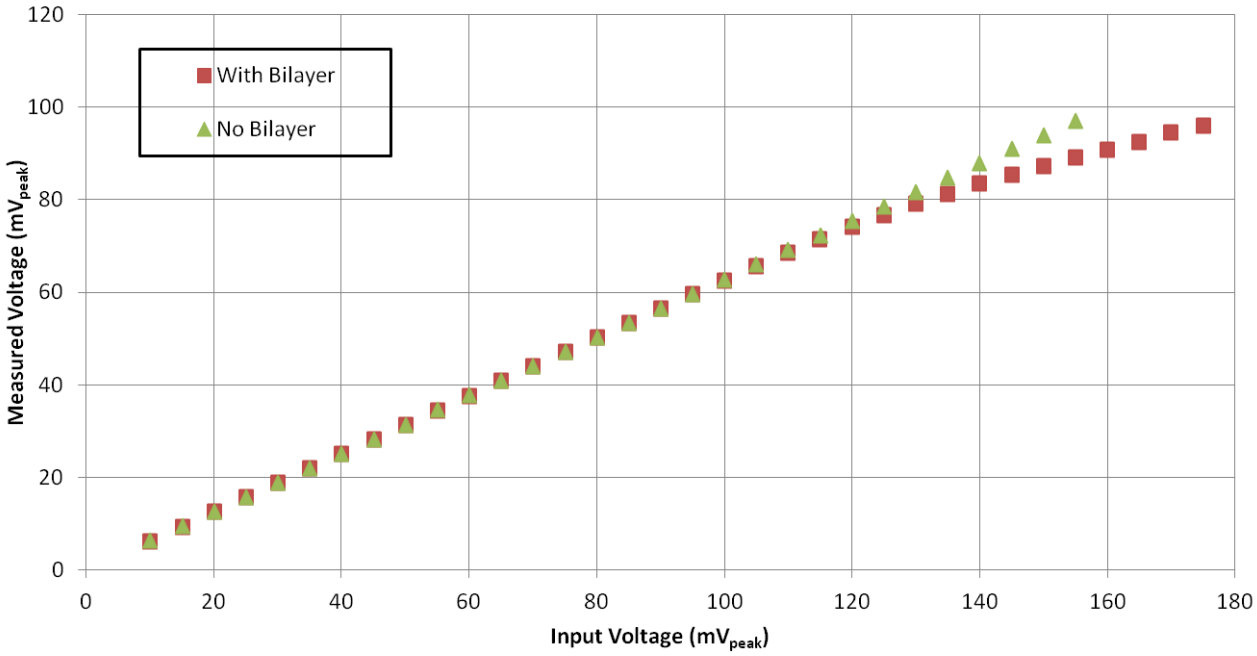

Figure 4-14: **Peak voltage measured at "Measurement Electrode" (V_{Boost}) as a function of the peak input voltage. The input voltage was sinusoidal operating at $10\ Hz$. Note that the single periods shown are based on an average ($n \approx 100$ periods).**

Figure 4-15 shows the derivative of the data shown in Figure 4-14. The derivative clearly shows the transition from a linear slope to a nonlinear slope when the input voltage approaches $100\ mV_{peak}$ due to the opening of the alamethicin channels in the bilayer.

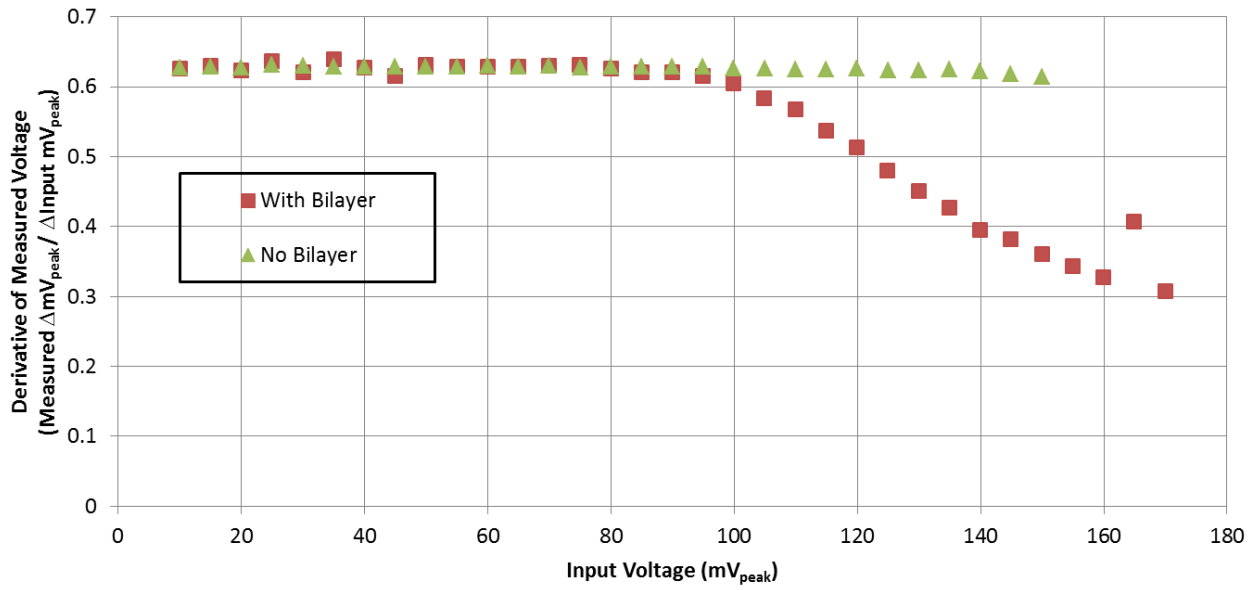

Figure 4-15: **Derivative of peak voltage measured at "Measurement Electrode" (refer to Figure 4-11) as a function of the peak input voltage. The input voltage was sinusoidal operating at $10\ Hz$. Note that the single periods shown are based on an average ($n \approx 100$ periods).**

Since the resulting wave form is not completely sinusoidal when the alamethicin channels open in the bilayer, as shown in Figure 4-13, a better way to differentiate between the case with a bilayer and the case without a bilayer would be to look at the difference in the area bounded by the two curves. Figure 4-16 shows the difference in the area bounded by the two curves as a function of the input voltage. Note that the resulting shape (purple) is very similar to that of cyclic voltammetry data (refer back to Figure 4-7). This is expected because the difference in the area bounded by the two curves is an indirect way to measure the current flowing through the bilayer when the alamethicin channels are open.

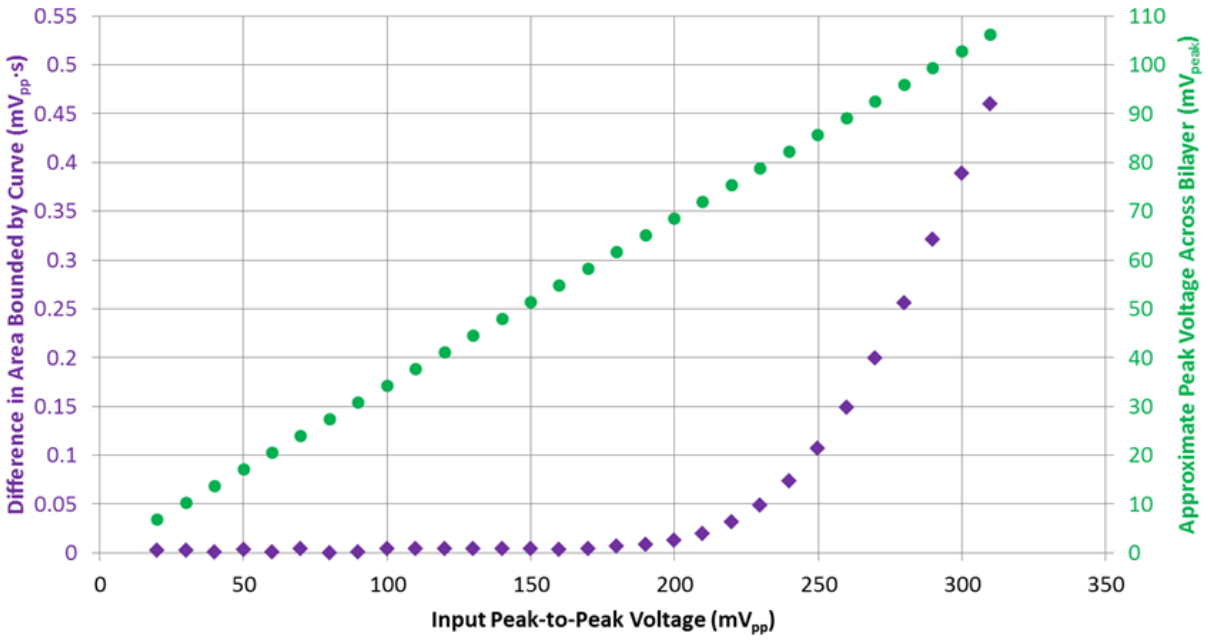

Figure 4-16: **Purple) Difference in area bounded by the curves as a function of the peak-to-peak input voltage for the case without a bilayer and the case with a bilayer (refer back to** Figure 4-13**). Green) Approximate peak voltage across the bilayer as a function of the input peak-to-peak voltage. Note that the results shown are based on an average ($n \approx 100$ periods).**

Based on the data shown in Figure 4-16, alamethicin channels in a bilayer within the artificial axon system can be used to cause a change in the voltage at the measurement electrode due to the channel gating properties. However, the signal is not being boosted, rather, the signal is being attenuated (amplitude is decreasing) due to the alamethicin channels gating.

Recall that the goal is to show that the artificial axon system can boost a signal traveling down the electrolyte line by using alamethicin channels in the lipid bilayer (connected perpendicularly to the electrolyte line). As mentioned previously, this process is similar to the regenerative boosting of the action potential in the nodes of Ranvier in myelinated nerve cells. Based on the model and data presented in the preceding sections, however, there is no way to boost the amplitude of the signal while holding V_{M2} at a constant value while using a lipid bilayer with alamethicin channels. The following section will consider the case where V_{M2} is varied in time in order to produce the desired ampltiude boosting behavior.

4.5 Investigating the Circuit Model: V_{M2} is time-dependent

It is clear that using a constant voltage on the micropipette side of the bilayer (V_{M2} = constant, Figure 4-2) will not boost the voltage in the artificial axon system based on the results shown in Figure 4-10. If, however, the voltage on the micropipette side of the bilayer were to change in time, such as a sine wave, the voltage in the system can be boosted.

Figure 4-17 shows the voltage on the electrolyte line side of the bilayer (blue) as a function in time (similar to Figure 4-4). Instead of a constant DC potential applied on the micropipette side of the bilayer, V_{M2} is a sine wave in-phase with V_{M1} but with an increased magnitude (red). The black line is the voltage across the bilayer $(V_{M2} - V_{M1})$. Note that when the magnitude of the voltage across the bilayer increases above the alamethicin gating potential, V_{Alm}, alamethicin channels in the bilayer open. In order to show the boosting behavior, this would increase the amplitude of the signal traveling through the electrolyte line as shown in Figure 4-18. This method has the advantage of boosting both the peak and the trough of the sine wave.

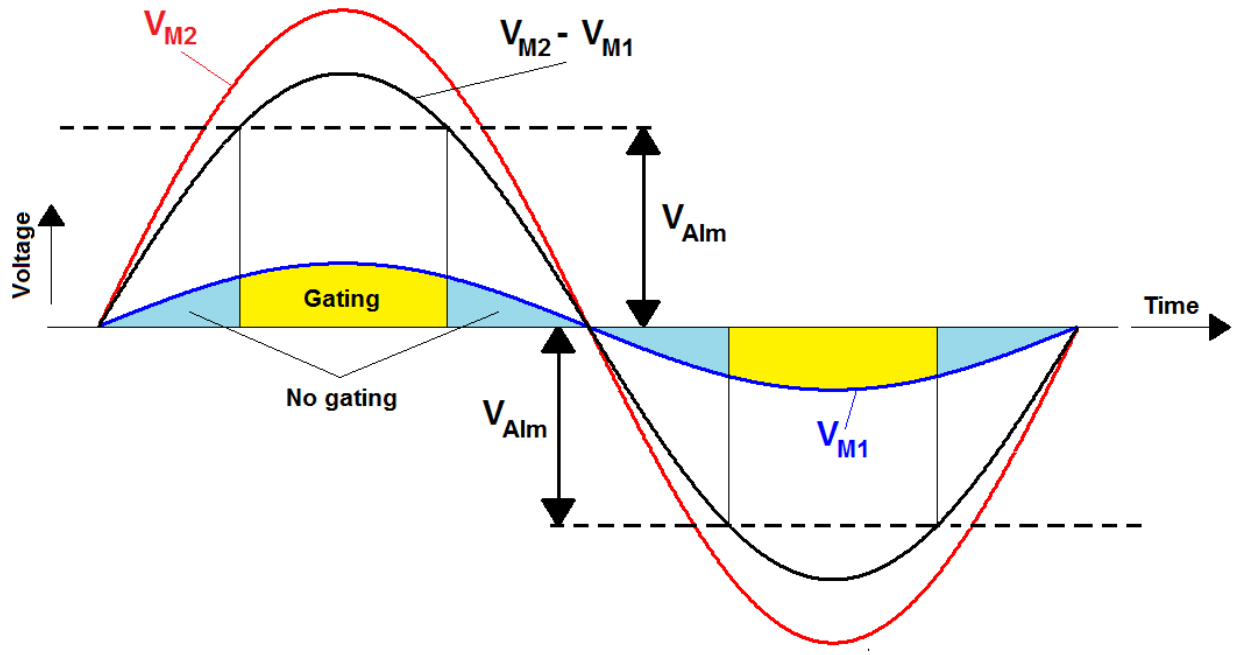

Figure 4-17: **Red) Sinusoidal voltage (in phase with V_{M1}) applied on the micropipette side of the bilayer (V_{M2}). Blue) Sinusoidal voltage on the electrolyte line side of the bilayer (V_{M1}) as a function of time. Black) Voltage across the bilayer $(V_{M2} - V_{M1})$. The light blue region shows where the voltage across the bilayer $(V_{M2} - V_{M1})$ is less than the gating potential of alamethicin and the yellow region shows where the voltage across the bilayer is greater than the gating potential of alamethicin.**

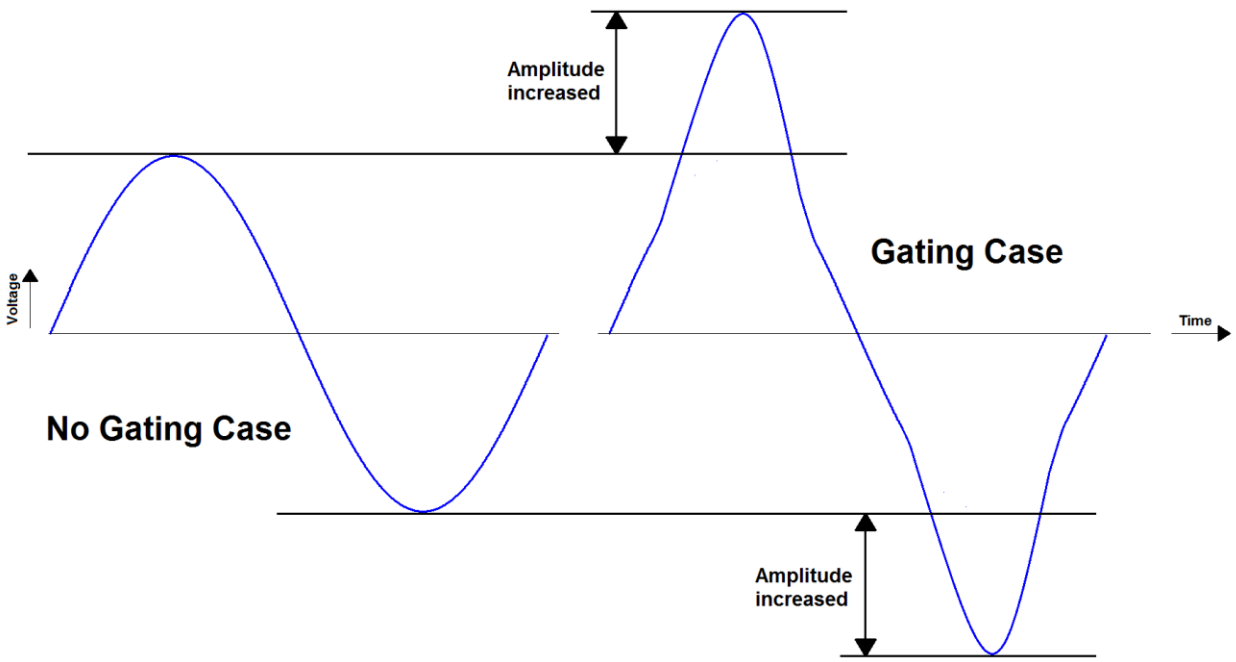

Figure 4-18: **Ideal signal boosting example corresponding to the example in Figure 4-17.**

Figure 4-19 shows the voltage on the electrolyte side of the bilayer (blue), the voltage on the micropipette side of the bilayer (red), and the voltage across the bilayer (black). Assuming the alamethicin channels open at $\pm 70\ mV$, the alamethicin channels will open at both the peak and the trough of the sine wave, which should increase the voltage at the measurement electrode.

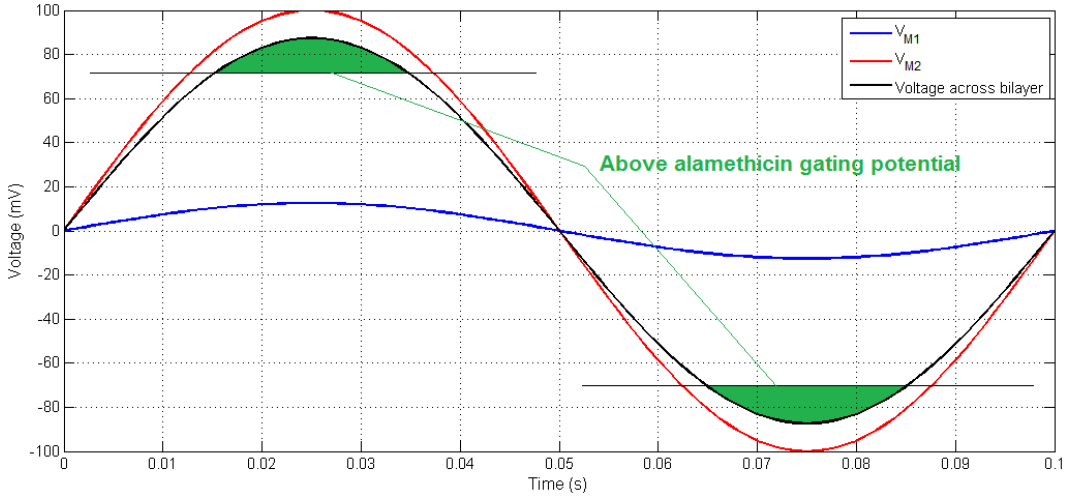

Figure 4-19: **Red)** $200\ mV_{pp}\ (10\ Hz)$ **voltage applied on the micropipette side of the bilayer (**V_{M2}**). Blue) Sinusoidal voltage on the electrolyte line side of the bilayer (**V_{M1}**) as a function of time (assuming a linear drop in voltage amplitude down the electrolyte line). Black) Voltage across the bilayer** $(V_{M2} - V_{M1})$**. List of system parameters:** $V_{In} = 60\ mV_{pp}\ (10\ Hz), R_1 = 3\ M\Omega, R_2 = 150\ k\Omega, R_3 = 2\ M\Omega, V_{M2} = 200\ mV_{pp}\ (10\ Hz)$.

Consider the peak of the sine wave in Figure 4-19. In order for the signal to be boosted, V_{Boost} needs to become a larger positive value. Using Equation (4-4), it is clear that if R_M decreases, V_{Boost} increases. At the trough of the sine wave, in order for the signal to be boosted, V_{Boost} needs to decrease towards the negative values. Since $V_{M2} < V_{M1}$ at the trough of the sine wave, based on Equation (4-4), the $\frac{V_{M2}-V_{M1}}{R_M}$ term (i_2) needs to decrease. Therefore, if R_M gets smaller, V_{Boost} decreases towards negative values, which boosts the amplitude.

Figure 4-20 shows V_{Boost} as a function of time for the non-gating (red) and gating (blue) cases using the cyclic voltammetry data shown in Figure 4-7 where V_{M2} is a $200\ mV_{pp}$ sine wave operating at $10\ Hz$ and is in phase with the sinusoidal voltage traveling through the electrolyte line (compare to the results in Figure 4-10). Note how the amplitude of the voltage is clearly increased in the gating case at both the peak and the trough. The model predicts that a voltage signal can be boosted by using alamethicin channels in the bilayer if the voltage on the micropipette side of the bilayer is sinusoidal and in-phase with V_{M1}.

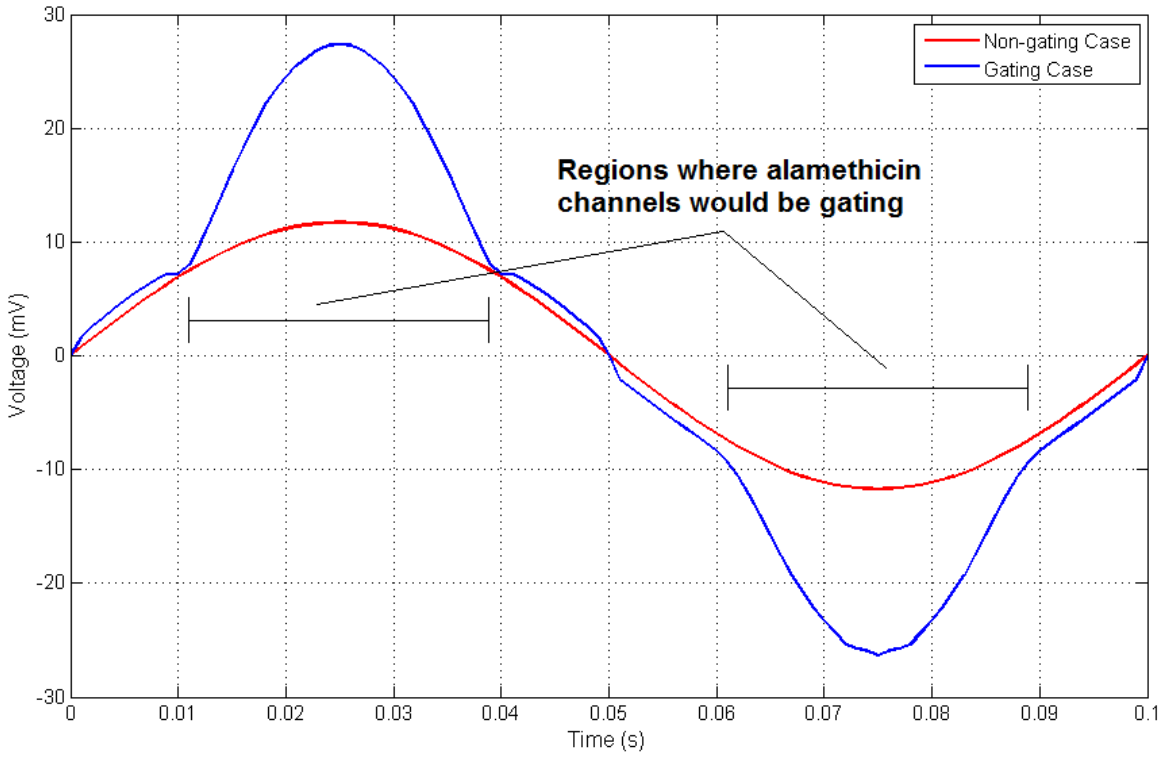

Figure 4-20: **Voltage at the measurement electrode (V_{Boost}) as a function of time for the case without alamethicin channels (red) and the case with alamethicin channels (blue) using the CV data in Figure 4-7. List of system parameters:** $V_{In} = 60\ mV_{pp}\ (10\ Hz), R_1 = 3\ M\Omega, R_2 = 150\ k\Omega, R_3 = 2\ M\Omega, V_{M2} = 200\ mV_{pp}\ (10\ Hz)$.

4.6 Experimental Results: V_{M2} is time-dependent

This section presents experimental results that show the signal boosting behavior for the case where V_{M2} is time dependent. Figure 4-21 shows the equivalent circuit diagram for the artificial axon system (Figure 3-1) where a single source[28], V_S, is used to control the input voltage, V_{In}, and the voltage on the micropipette side of the bilayer, V_{M2}. V_{M2} is simply equal to V_S (when the switch is closed), whereas V_{In} (the voltage at the input electrode) is dependent on R_X. The R_X resistor[29] acts as a voltage divider:

$$V_{In} = \frac{R_X}{1000 + R_X} V_S \qquad \textbf{(4-5)}$$

Where R_X is the resistance in Ohms. V_{In} can therefore be controlled by changing R_X. The switch controls whether or not V_{M2} is controlled. When the switch is open, V_{M2} is not controlled (floating) whereas when the switch is closed, V_{M2} is controlled directly by V_S.

[28] This is ideal because only a single function generator is needed.

[29] Note that R_X is variable resistor. The user controls its resistance by changing the resistance of the resistor in the circuit (physically replacing the resistor on the circuit board).

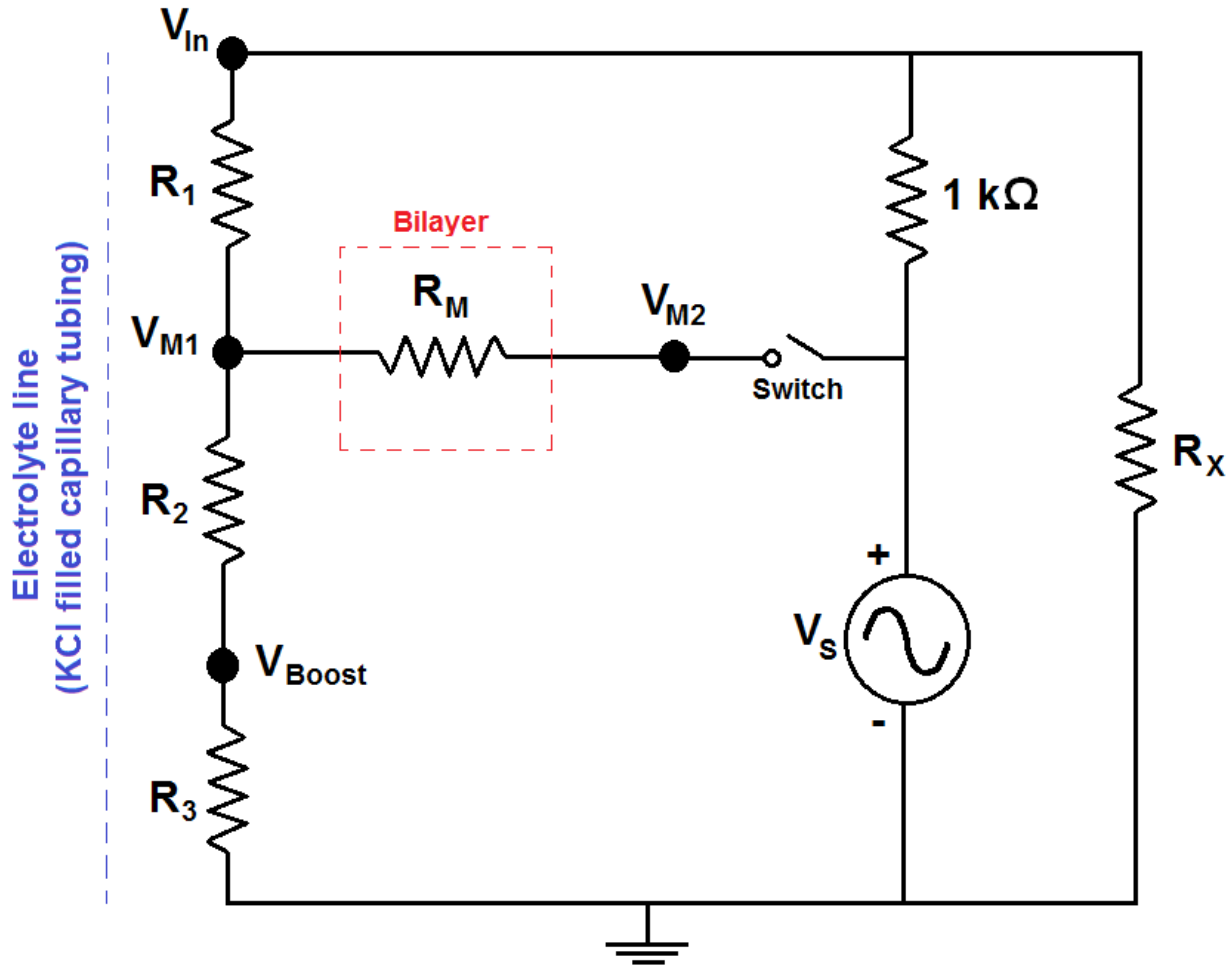

Figure 4-21: **Circuit diagram for the artificial axon system (Figure 3-1) using a single voltage source (V_S) to control both V_{In} and V_{M2}.**

Figure 4-22 shows the averaged single period[30] of V_{Boost} for the case where $V_{M2} = 200\ mV_{pp}$ and $V_{In} = 36.1\ mV_{pp}$ ($R_X = 220\ \Omega$) both operating in-phase at $10\ Hz$. Both the case where the switch is open (red) and the case where the switch is closed (blue) are plotted. Note that when the switch is closed, the amplitude of the signal is increased at the first peak ($t \approx 25\ ms$), showing the signal is boosted by alamethicin channel gating. Based on the model (Figure 4-20), one would expect a similar behavior to occur at the trough of the sine wave. The fact that the boosting behavior does not occur at the trough could be due to asymmetric voltage-dependent gating properties. In other words, the alamethicin channel conductance when the potential across the bilayer is $+70\ mV$ could be greater than that when the potential across the bilayer is $-70\ mV$, which could lead to an asymmetry in the

[30] Based on approximately 10 seconds of data (100 periods). The corresponding MATLAB code can be found in Section A.4 in Appendix A.

boosting behavior (i.e. only the peak or trough of the sine wave is boosted). Please note that the cyclic voltammetry data shown in Figure 4-23 was not recorded directly for the bilayer shown in Figure 4-22[31].

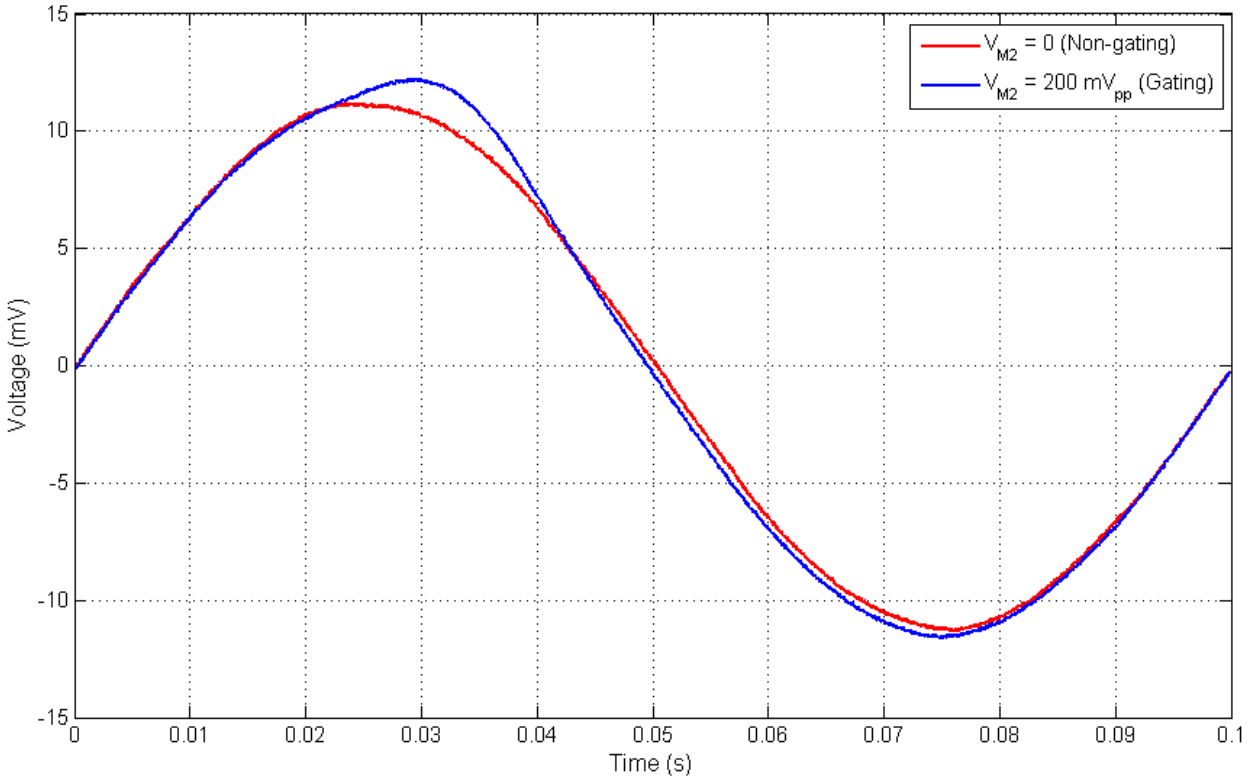

Figure 4-22: **Averaged experimentally measured voltage at the measurement electrode (V_{Boost}) as a function of time for the case where the switch is open (red) and the case where the switch is closed (blue). List of system parameters:** $V_{In} = 36.1\ mV_{pp}\ (10\ Hz), R_1 = 1.9\ M\Omega, R_2 = 315\ k\Omega, R_3 = 3.1\ M\Omega, V_{M2} = 200\ mV_{pp}\ (10\ Hz), R_X = 220\ \Omega$. **The bilayer parameters were approximated as:** $R_m = 1.7\ G\Omega, C_m = 520\ pF$ (~330 µm diameter)**. The concentration of alamethicin in the lipid solution was** $3\ \mu g/mL$**.**

[31] In order to take cyclic voltammety data, the system had to be connected to the AUTOLAB. To do this, several connections had to manually be changed, which often resulted in the bilayer rupturing due to mechanical vibrations.

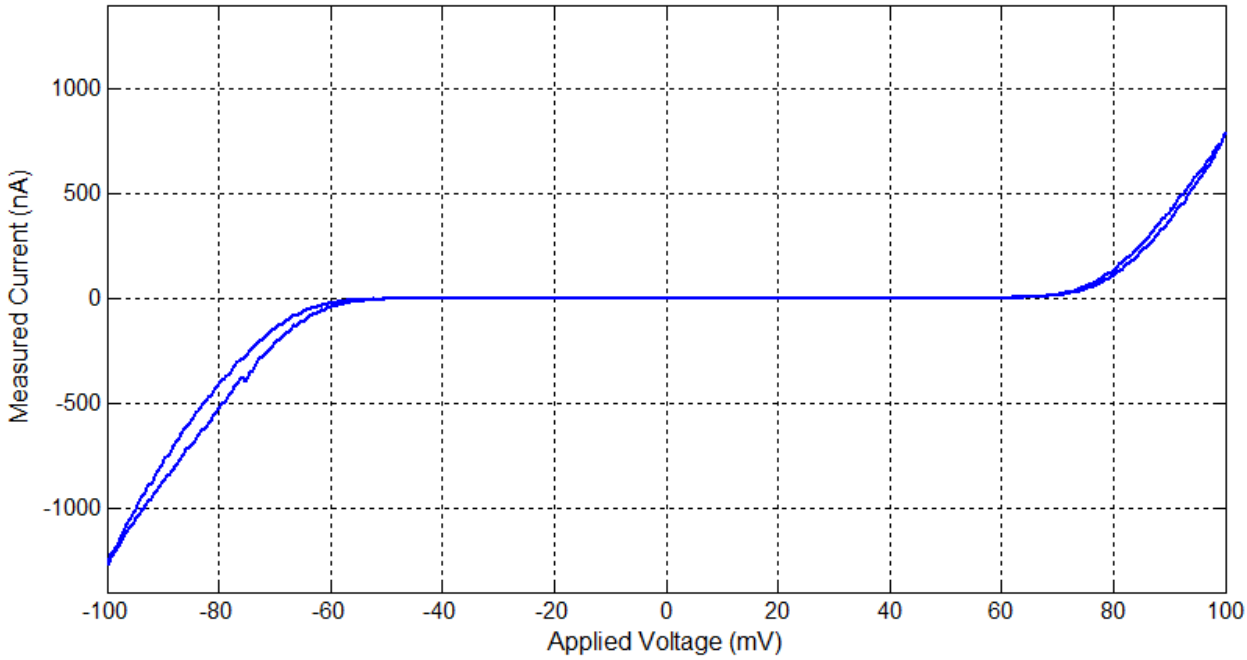

Figure 4-23: **Cyclic voltammetry data that shows asymmetry between the positive and negative potentials.**

If the input signal was decreased in amplitude (by lowering R_X), one would expect the signal to be boosted by a greater factor because the voltage across the bilayer would increase at the peaks and troughs[32]. Figure 4-24 shows the averaged single period[33] of V_{Boost} for $V_{M2} = 200\ mV_{pp}$ and $V_{In} = 18.2\ mV_{pp}$ ($R_X = 100\ \Omega$) both operating in phase at $10\ Hz$. Both the case where the switch is open (red) and the case where the switch is closed (blue) are plotted. Note that when the switch is closed, the amplitude of the signal is clearly increased at the peak ($t \approx 25\ ms$) and slightly increased at the trough ($t \approx 75\ ms$). The boosting factor at the first peak is much greater for the case where $R_X = 100\ \Omega$ (Figure 4-24) compared to the case where $R_X = 220\ \Omega$ (Figure 4-22). The greater boosting factor is due to greater potential across the bilayer, which is related to the difference in V_{In} and V_{M2}.

[32] The higher the voltage across the bilayer, the greater the current flowing through it, which means the signal should be boosted to a greater value.
[33] Based on approximately 10 seconds of data (100 periods).

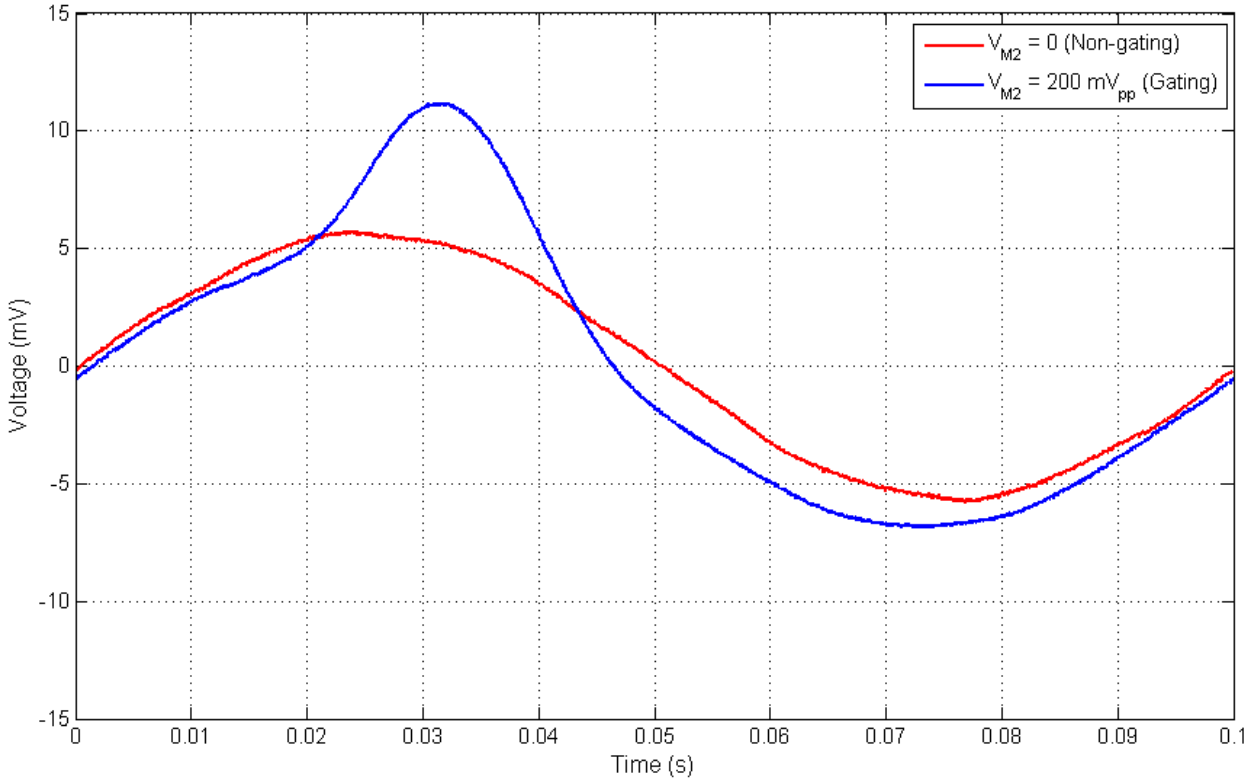

Figure 4-24: **Averaged experimentally measured voltage at the measurement electrode (V_{Boost}) as a function of time for the case where the switch is open (red) and the case where the switch is closed (blue). List of system parameters:** $V_{In} = 18.2\ mV_{pp}\ (10\ Hz), R_1 = 1.9\ M\Omega, R_2 = 315\ k\Omega, R_3 = 3.1\ M\Omega, V_{M2} = 200\ mV_{pp}\ (10\ Hz), R_X = 100\ \Omega$. **The bilayer parameters were approximated as:** $R_m = 1.7\ G\Omega, C_m = 520\ pF$ (~330 μm diameter)**. The concentration of alamethicin in the lipid solution was** $3\ \mu g/mL$**.**

Figure 4-25 shows V_{Boost} as a function of time where the state of the switch (Figure 4-21) is changed from open (off) to closed (on). It is clear that when the switch is in the on position, the signal is boosted by the greater amplitude.

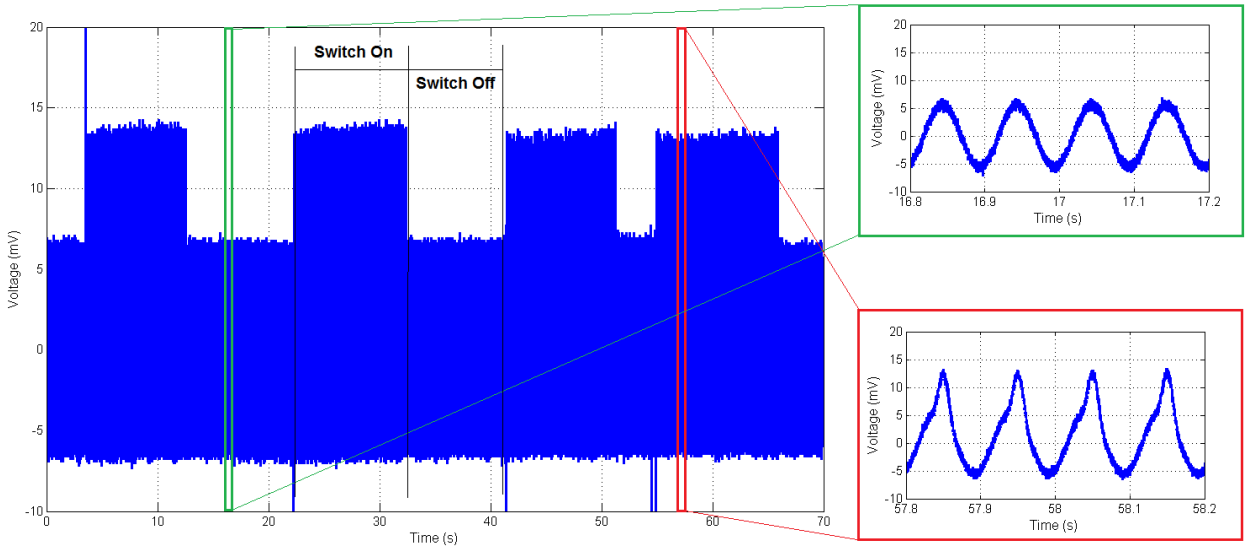

Figure 4-25: **Experimentally measured voltage at the measurement electrode (V_{Boost}) as a function of time. The state of the switch (Figure 4-21) is moved back and forth from the on (closed) to off (open) positions. List of system parameters:** $V_{In} = 36.1\ mV_{pp}\ (10\ Hz), R_1 = 1.9\ M\Omega, R_2 = 315\ k\Omega, R_3 = 3.1\ M\Omega, V_{M2} = 200\ mV_{pp}\ (10\ Hz), R_X = 100\ \Omega$. **The bilayer parameters were approximated as:** $R_m = 1.7\ G\Omega, C_m = 520\ pF$ (~330 μm diameter)**. The concentration of alamethicin in the lipid solution was** $3\ \mu g/mL$**.**

4.7 Chapter Summary and Conclusions

This chapter revisited how action potentials are propagated down a myelinated axon including how the signal is boosted at the nodes of Ranvier. The research goal was to show that a signal could similarly be boosted using the artificial axon system by taking advantage of alamethicin's voltage-gating properties. The corresponding circuit diagram for the artificial axon system was used to investigate the ideal configuration to show the signal boosting behavior. Experimental results using the artificial axon system showed the boosting behavior, but it required that the controlled voltage on the micropipette side (analogous to the extracellular fluid in a real axon) of the bilayer be time-dependent. The reason for this is because alamethicin channels operate in a fundamentally different way than voltage-gated channels in a real neuron. Alamethicin channels open above a certain potential whereas voltage-gated channels in neurons open below a threshold potential. By controlling the voltage on the micropipette side of the bilayer in a time-dependent fashion, the direction of the current flowing through the bilayer could be controlled so that the signal could be boosted rather than attenuated.

In a real axon, the potential of the extracellular fluid is a constant DC value. So while the boost behavior was reproducible using the artificial axon system, the method of doing so is not very similar to the biological case. The next chapter presents testing results using the artificial axon system that mimic parts of signal propagation in neurons.

Chapter 5: Biologically Relevant Results

Lipid bilayers can be used in conjunction with alamethicin channels in the artificial axon system to boost a signal as presented in the previous chapter. While the boosting behavior mirrors that of an action potential signal in the nodes of Ranvier in a myelinated axon, the method for replicating this behavior is not very similar to the biological case. In order to show the boosting behavior, the extracellular potential had to be time-dependent, which is not the case in a real neuron. This chapter presents results that more closely mirror not only the behavior of real neurons, but also the process that produces the behavior. In particular, the goal is to show how alamethicin channels in the artificial axon system can be used to show similar characteristics of the potassium (K^+) channels that play a key role in action potential propagation.

5.1 Potassium Channels' Role in an Action Potential

As discussed in Chapter 1, electrical signals travel through the body via action potentials in neurons [2, 32]. When an action potential is initiated, both the sodium (Na^+) and potassium (K^+) ion channels open in the membrane. However, the Na^+ channels open much more quickly than the K^+ channels, so the depolarization of the membrane is primarily due to sodium currents [36, 60]. At the peak of the action potential (refer back to Figure 1-12), the K^+ channels are fully open and the Na^+ channels close. Due the concentration gradient, K^+ ions leave the cell, which aids in the repolarization of the cell. The repolarization restores the cell to its resting potential so it is prepared for the next action potential [10, 36, 43].

In a squid axon, K^+ channel activation has a sigmoidal shape [60-63]. In other words, the K^+ channel rate of opening varies in time, which could be due to conformational changes of the channels [63]. Initially, the K^+ channels slowly open, they then transition to a rapidly opening phase, and finally return to a slow opening rate. This is important because if the K^+ channels opened at a fast rate, the efflux of potassium ions would negate the influx of sodium ions, so the action potential would not be propagated.

5.2 Experimental System Review & Corresponding Circuit Model Simplification

Figure 5-1 shows the dimensions of the artificial axon system that was used to conduct the experiments presented in this chapter. Recall that the artificial axon system consists of a bilayer is perpendicularly

connected to the electrolyte line (Figure 3-1), which runs through the capillary tubing (maroon). The electrolyte line contains $500\ mM$ KCl[34]. A voltage signal can be applied from the input electrode to the ground electrode such that the signal travels down the electrolyte line. The signal can then be modified by taking advantage of alamethicin channels in the bilayer and the resulting wave form is recorded at the measurement electrode.

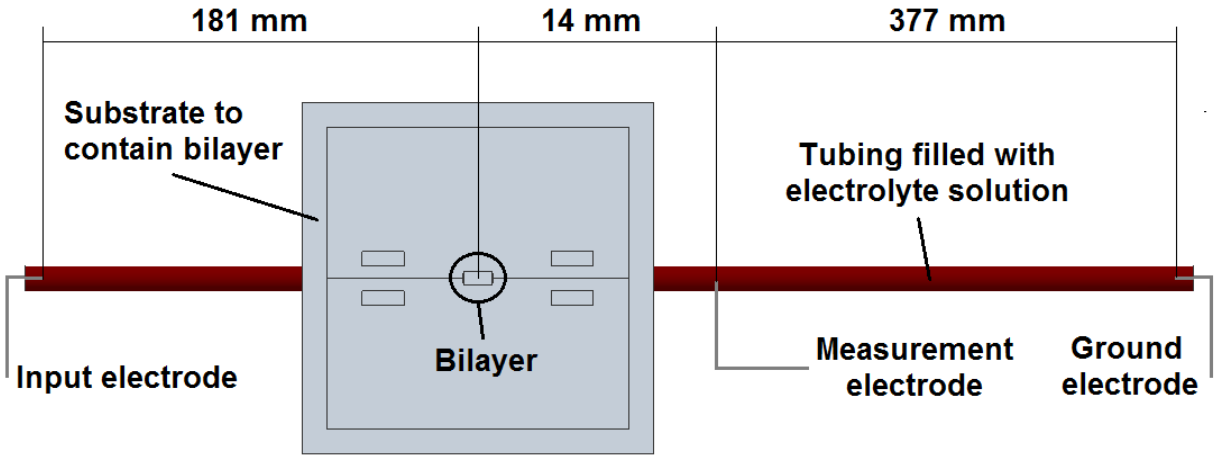

Figure 5-1: **Dimensions of experimental setup (not drawn to scale). The distances between electrodes are labeled.**

The circuit diagram for the system was original presented in Figure 4-2. However, the circuit is further simplified[35] for the experiments presented in this chapter because $V_{M2} = 0$. Figure 5-2 shows the simplified circuit diagram of a bilayer connected to an electrolyte line. V_{In} is the voltage input to the system at the input electrode, V_{M1} is the voltage on the electrolyte line side of the bilayer, and V_{Boost} is the voltage measured at the measurement electrode. Note that because the other side of the bilayer (micropipette side) is connected to ground, V_{M1} is also the voltage across the bilayer.

[34] Note that the data presented in previous chapters used a $10\ mM$ KCl solution, which was a result of the assumption that a lower electrolyte concentration would result in a lower conduction velocity. This assumption turned out to be wrong as discussed in Chapter 3. For the data presented in this chapter, a $500\ mM$ KCl solution was used.

[35] The simplification is due to the fact that the electrode on the micropipette side of the bilayer is connected to ground. Therefore, the voltage on the micropipette side of the bilayer is $0\ mV$.

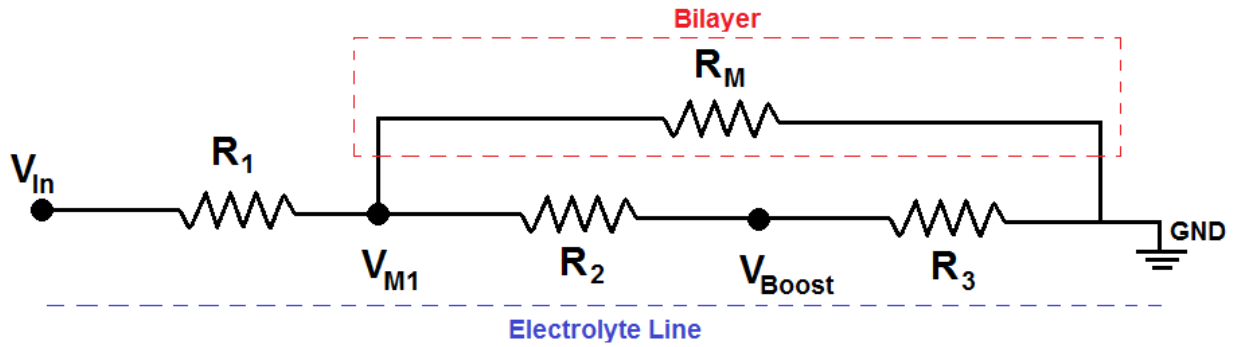

Figure 5-2: **Circuit diagram of a bilayer connected to an electrolyte line (artificial axon system). Note that this circuit diagram is a simplified version of the one previously presented in Figure 4-2).**

Using a simple circuit analysis, it can be shown that:

$$V_{M1} = V_{in}\left[\frac{(R_2 + R_3)R_M}{R_1(R_2 + R_3 + R_M) + (R_2 + R_3)R_M}\right] \quad \textbf{(5-1)}$$

Where R_1 is the resistance between the input electrode and the bilayer, R_2 is the resistance between the bilayer and measurement electrode, R_3 is the resistance between the measurement electrode the ground electrode, and R_M is the bilayer resistance. The resistance per unit length of the capillary tubing $(0.04"\ [1.02\ mm]\ ID)$ filled with $500\ mM$ KCl is $240\ \frac{\text{k}\Omega}{mm}$. Therefore, based on Figure 5-1, $R_1 = 43.4\ k\Omega$, $R_2 = 3.4\ k\Omega$, and $R_3 = 90.3\ k\Omega$. For comparison, the resistance of a bilayer, R_M, made of pure DpHPC lipids is typically greater than $1\ G\Omega$. However, when the alamethicin channels open, the bilayer resistance drops by several orders of magnitude depending on the voltage across the bilayer as shown previously in the CV data in Figure 4-7.

Figure 5-3 shows the cyclic voltammetry data for two different bilayers: one with $3\ \mu g/mL$ alamethicin mixed with the lipid solution (blue) and one without alamethicin (red). It is clear that when alamethicin is included in the lipid solution, the current increases substantially once the voltage across the bilayer increases beyond a certain value $(\sim 60\ mV)$. This increase in current is due to the bilayer resistance decreasing because the alamethicin peptides are forming channels which allow ions (current) to pass through. Referring back to Equation **(5-1**, once the voltage across the bilayer (V_{M1} in Figure 5-2) reaches approximately $60\ mV$, the formation of channels results in a larger current flowing through the bilayer.

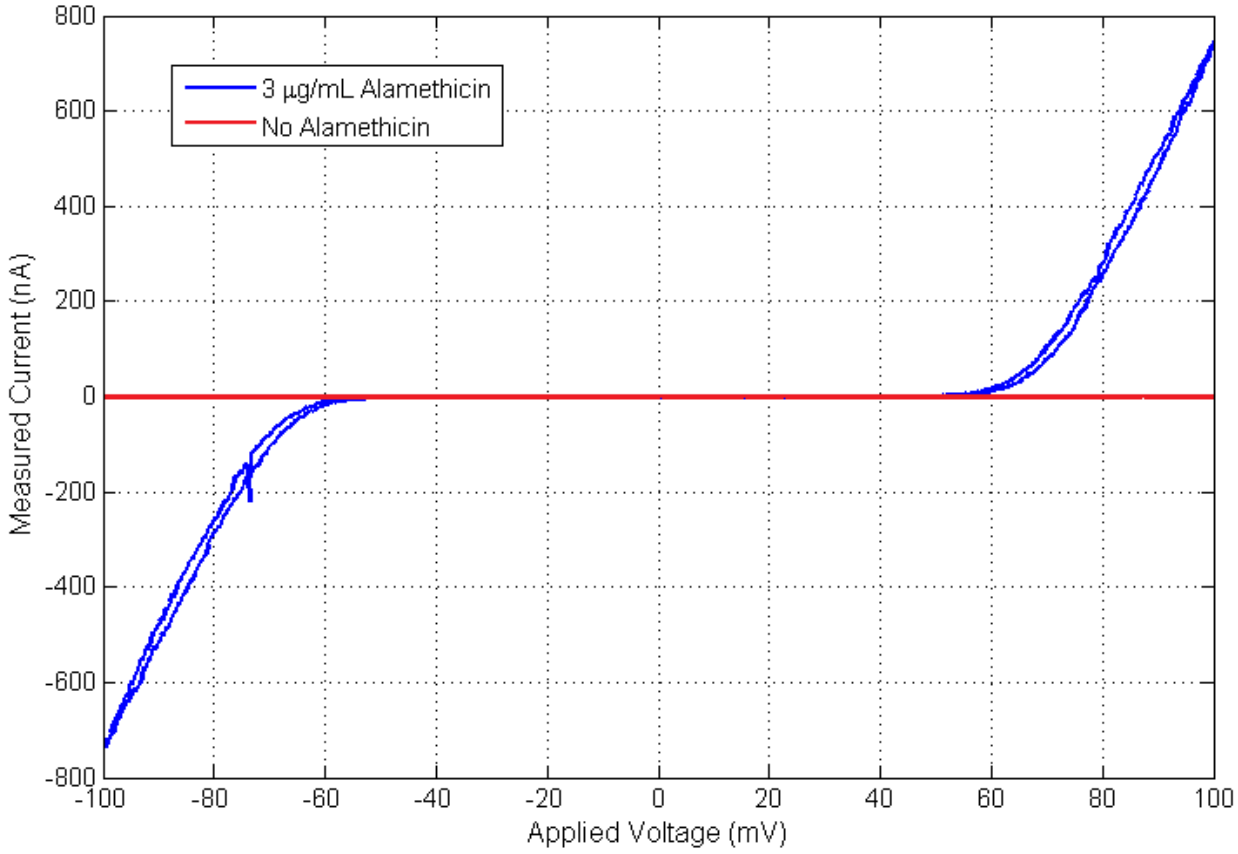

Figure 5-3: **Cyclic voltammetry data for two different bilayers: one with $3\ \mu g/mL$ alamethicin (blue) and one without alamethicin (red). Blue) $3\ \mu g/mL$ case: $1100\ pF$ $(\sim 480\ \mu m)$ Red) No alamethicin case: $360\ pF$ $(\sim 280\ \mu m)$. $500\ mM$ KCl electrolyte concentration.**

5.3 Experimental Work: Similarities to Potassium Conductance

This section presents experimental work that shows how bilayers with alamethicin channels can be used to show qualitative features of potassium channel conductance in a neuron. In particular, the sigmoidal activation curve shape of potassium channels in giant squid axons can be shown using bilayers with alamethicin channels.

Figure 5-4 shows experimental data of two $100\ mV_{pp}$ square waves operating at $10\ Hz$. One square wave does not have a DC offset (blue) whereas the other square wave (green) has a $20\ mV$ DC offset. Note that both the upper value (peak) and the lower value (trough) of the square wave for the $20\ mV$ DC offset case are $20\ mV$ greater than the case without a DC offset. Suppose that Figure 5-4 was a plot of the voltage across a bilayer that contained channels that gated at $\pm 60\ mV$ (red line). For the $100\ mV_{pp}$ square wave case without a DC offset, the potential across the bilayer would not reach the gating potential, so the channels would not open. However, for the $100\ mV_{pp}$ square wave case with a

$20\ mV$ DC offset, the potential across the bilayer would be greater than the channel gating potential, so the voltage-gated channels would open, but only at the peak of the square wave.

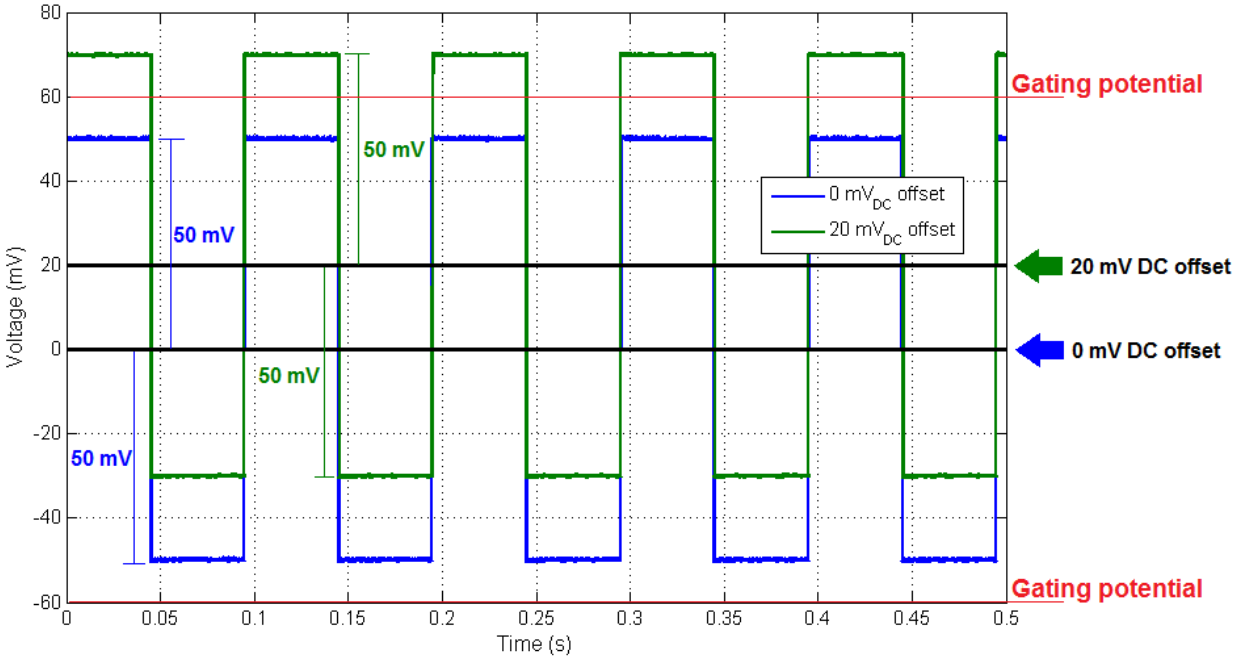

Figure 5-4: $100\ mV_{pp}$ $(10\ Hz)$ **square wave with no DC offset (blue) and a** $20\ mV$ **DC offset (green). This signal was applied from the input electrode of the electrolyte line to the ground electrode.**

Based on previous testing (refer to Figure 3-12), the voltage at points along the electrolyte line drop linearly to $0\ mV$ at the ground electrode. The major assumption is that the current through the bilayer is negligible compared to the current flowing through the electrolyte line. Since the measurement electrode is located at $195\ mm$ from the input electrode (refer back to Figure 5-1), which is at 34% of the total length $(572\ mm)$, then the amplitude of the voltage at the measurement electrode should be 66% of amplitude of the voltage at the input electrode[36]. For example, if the input voltage is $100\ mV_{pp}$, then the voltage at the measurement electrode should be $66\ mV_{pp}$. Figure 5-5 shows the average voltage measured (one period) at the measurement electrode for an input voltage of $100\ mV_{pp}$ $(10\ Hz)$ square wave. As expected, the peak-to-peak voltage is close to $66\ mV_{pp}$ at the measurement electrode.

[36] The input voltage should drop by 34%, which is the same as $66\%$of the original value.

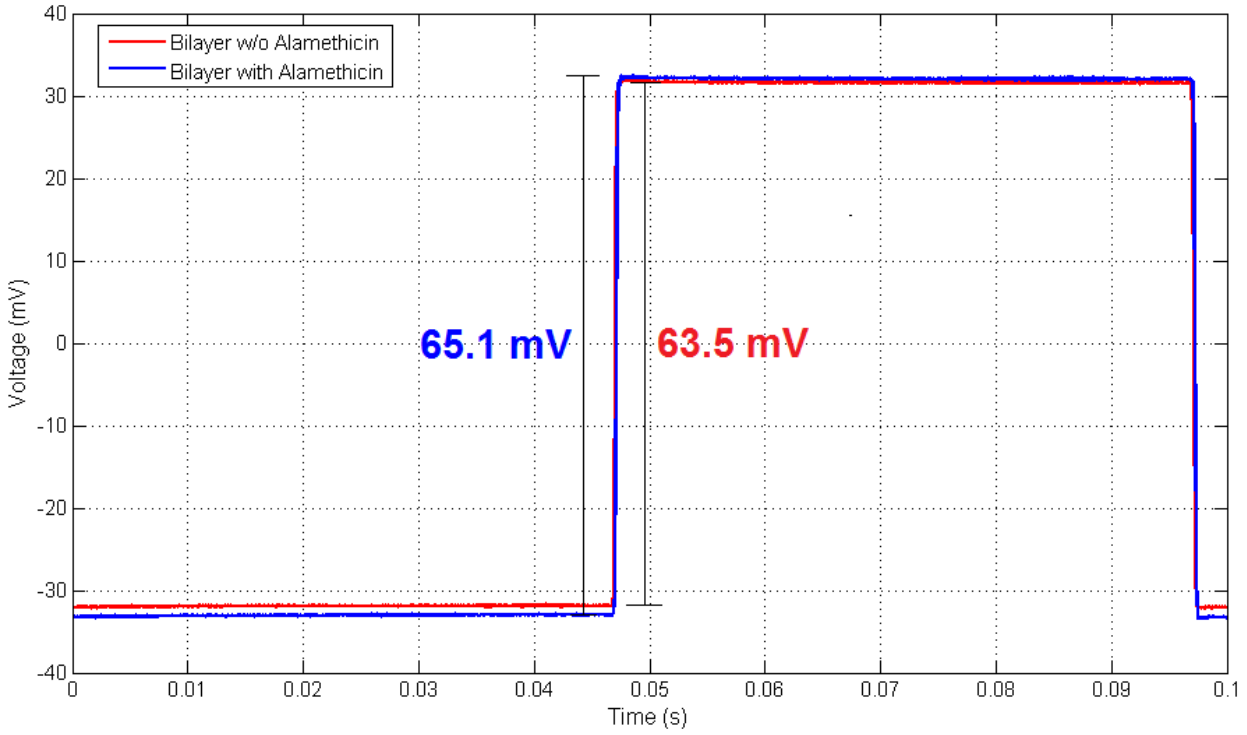

Figure 5-5: **Average voltage at measurement electrode as a function of time for a $100\ mV_{pp}$ $(10\ Hz)$ square wave with a $0\ mV$ DC offset. Note that approximately 100 square waves were used to calculate the average period shown.**

The resistance of the electrolyte in the tubing from the input electrode to the ground electrode was measured as $137\ k\Omega$, so at the peak of a $100\ mV_{pp}$ square wave $(50\ mV)$, the expected current through the electrolyte is $365\ nA$ using Ohm's Law and assuming that the current flowing the bilayer is negligible. In order to see a change in the voltage at the measurement electrode, the current through the bilayer cannot be too small relative to the current flowing through the electrolyte line.

Figure 5-6 shows the relative currents between the current flowing through the electrolyte line (red) and the currents flowing through the bilayer (blue/green). Note that the current flowing the electrolyte line is calculated for the case where no bilayer is connected to the system. For the previous case where the input signal is a $100\ mV_{pp}$ square wave, the corresponding voltage across the bilayer would be $34.2\ mV$ at the peak of the square wave (data tips shown in Figure 5-6). The current flowing the electrolyte line is approximately $365\ nA$ whereas the current flowing through the bilayer is only about $143\ pA$. Until the current through the bilayer is on the order of (or even within 2 orders of magnitude) of the current flowing through the electrolyte line, it is unlikely that the voltage measured at the measurement electrode will be affected by the presence of a bilayer.

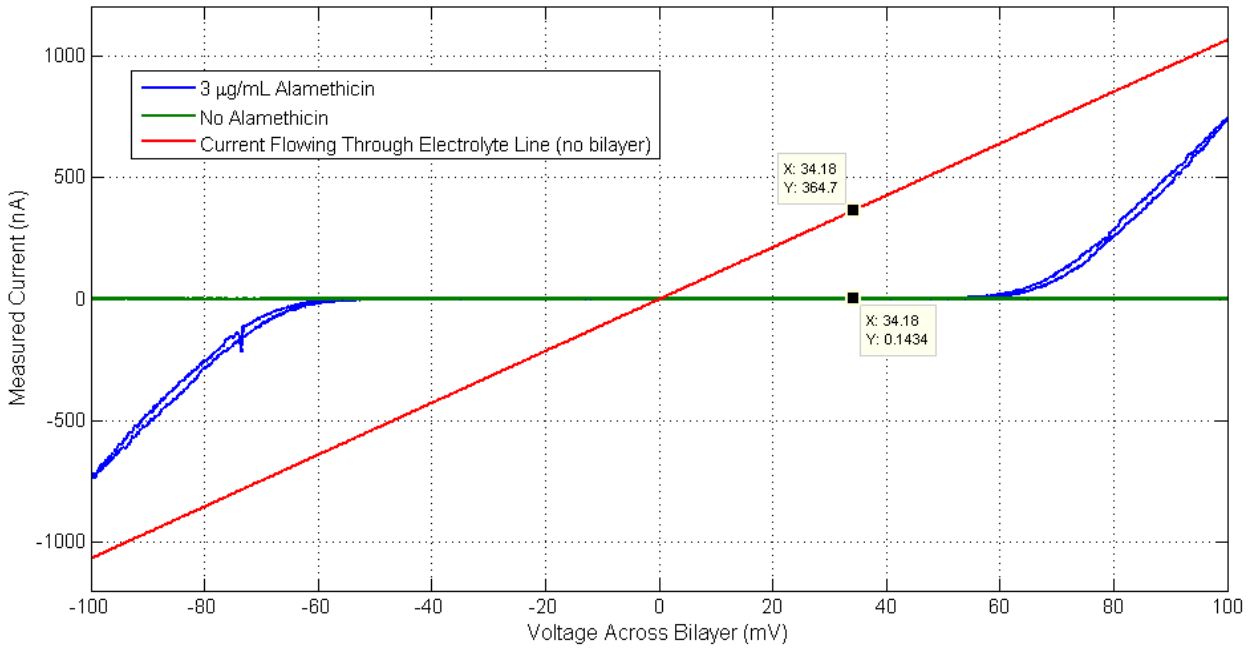

Figure 5-6: **Cyclic voltammetry data from Figure 5-3 with the calculated current flowing through the electrolyte line (assuming there is no bilayer).**

Figure 5-7 shows the averaged square wave period for a $100\ mV_{pp}$ $(10\ Hz)$ signal with a $80\ mV$ DC offset. The peak of the input square wave is therefore about $130\ mV$ and the trough of the square wave is $30\ mV$. Since the bilayer is located at 31.6% of the total electrolyte line length relative to the input electrode, the peak and trough values of the square wave at the bilayer should be $88.9\ mV$ and $20.5\ mV$, respectively. For the case with alamethicin, one would expect channel gating at the square wave peak because the voltage across the bilayer is above the gating potential (refer back to Figure 5-5 and Figure 5-6).

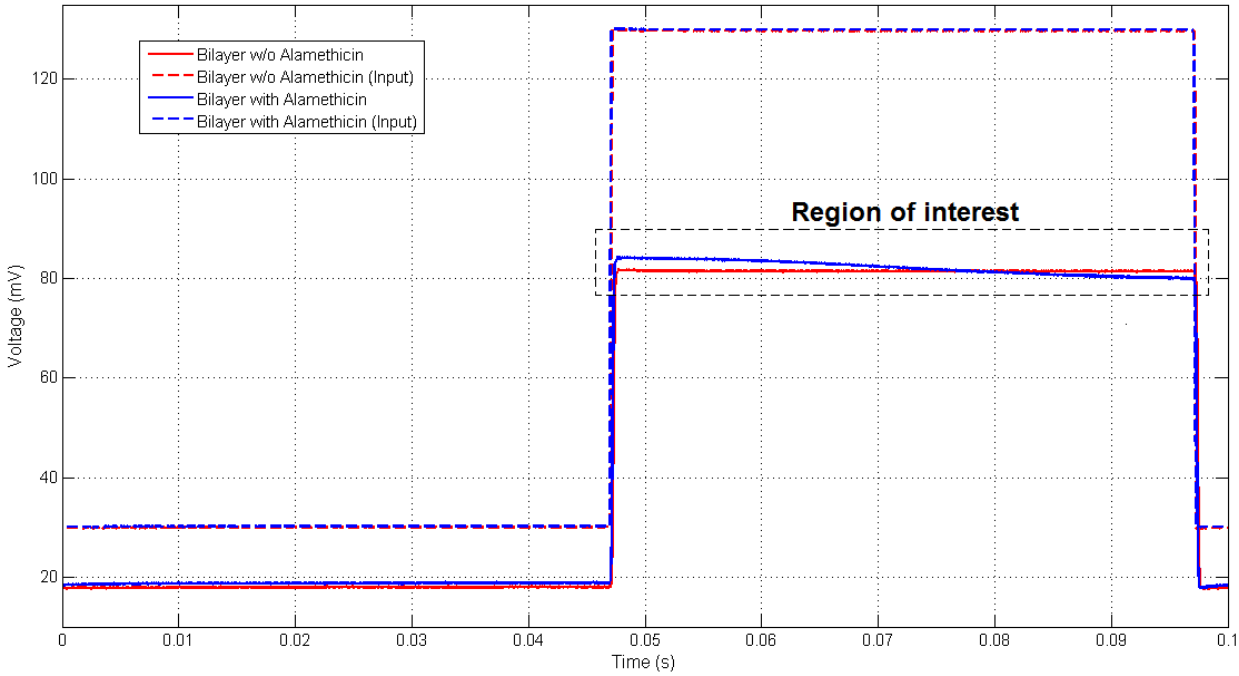

Figure 5-7: **Dotted lines)** $100\ mV_{pp}\ (10\ Hz)$ **square wave with** $+80\ mV$ **DC offset input signal. Solid lines) Voltage measured at the measurement electrode for both the case with alamethicin (blue) and the case without alamethicin (red). Note that the single average period shown is based on approximately 100 different periods.**

Notice that the peak of the square wave measured at the measurement electrode (solid blue) decays from an initial value. This suggests that the alamethicin channels in the bilayer are affecting the square wave as it travels through the system by reducing the amount of current flowing through the electrolyte past the bilayer. In other words, the current flowing through R_2 and R_3 in Figure 5-2 is reduced when the alamethicin channels are gating. When the current is reduced, so is the voltage measured at the measurement electrode because R_2 and R_3 are constants.

Figure 5-8 shows the average calculated voltage (single period) for the $100\ mV_{pp}\ (10\ Hz)$ square wave input and the corresponding voltage recorded at the measurement electrode for various input DC offsets. As the input DC offset is increased, the voltage at the peak of the square wave is also increased. Recall that the voltage decays linearly down the electrolyte line, so as the input voltage increases, so does the voltage across the bilayer (V_{M1}). At some point, the voltage across the bilayer becomes large enough that channels formed by alamethicin peptides begin to open, which means that the current flowing through R_1 is split between the two paths (R_M and R_2/R_3 in Figure 5-2). When the current flowing through the bilayer is with a few orders of magnitude of the current flowing the electrolyte line past the bilayer, the voltage at the measurement electrode should drop. For the cases shown in Figure

5-8, the voltage at the measurement electrode seems to drop when the input DC offset is $80\ mV$ and above. It should also be noted that the drop is more significant as the offset is increased.

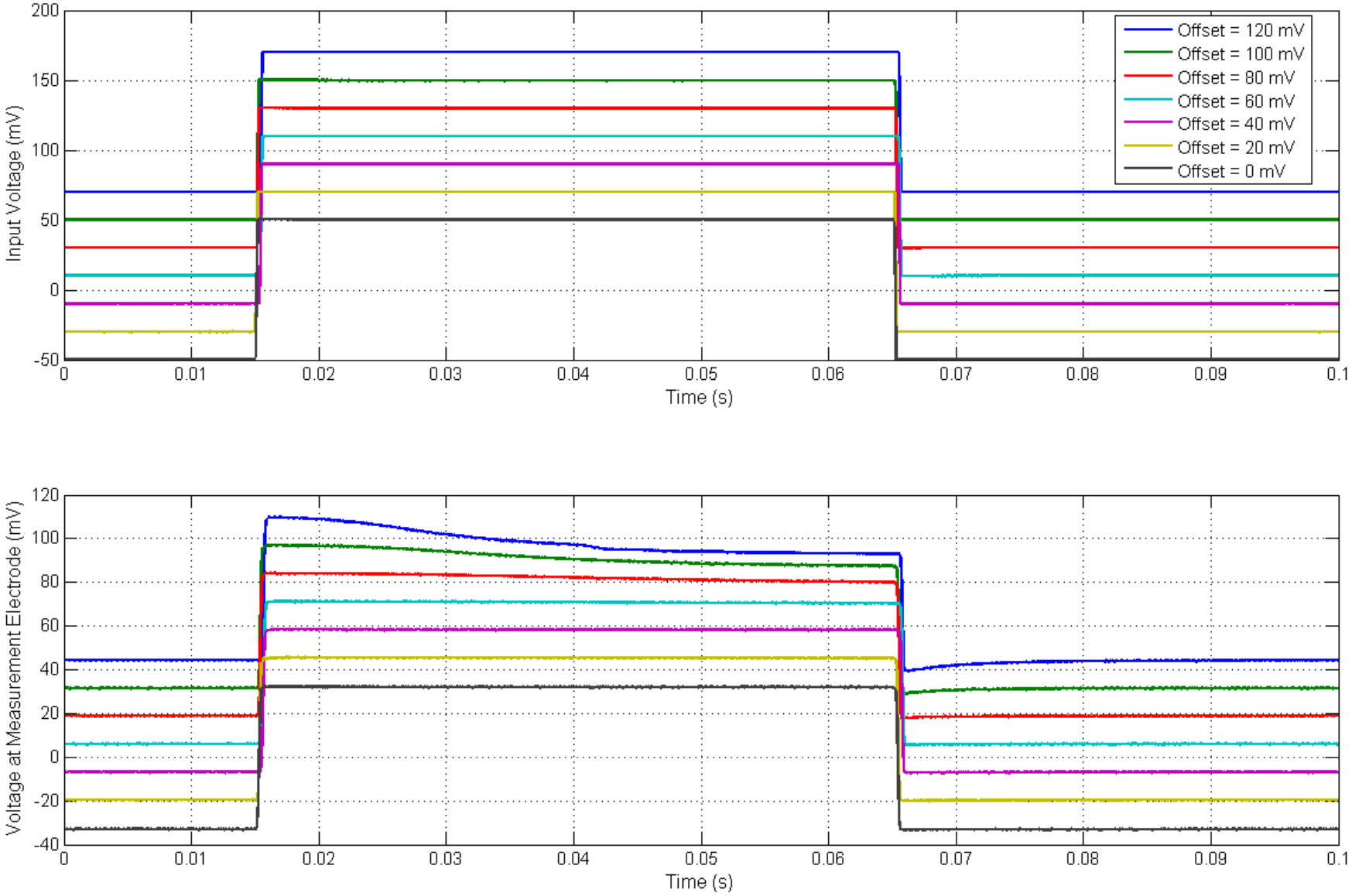

Figure 5-8: **Top) Plot of the average periods of $100\ mV_{pp}$ $(10\ Hz)$ square waves with various positive DC offsets. Bottom) Corresponding average periods recorded at the measurement electrode. Note that this data was obtained experimentally.**

The data shown in Figure 5-8 can be used to calculate the approximate values of both the voltage across the bilayer and the current through the bilayer using the circuit diagram shown in Figure 5-2. Since V_{Boost} is known, the current flowing through both R_2 and R_3 can be calculated using Ohm's Law:

$$i_{Line} = \frac{V_{Boost}}{R_3} \quad [5\text{-}2]$$

The voltage on the electrolyte side of the bilayer, V_{M1}, can be calculated as:

$$V_{M1} = V_{Boost} + i_{Line}R_2 \quad [5\text{-}3]$$

Since the other side of the bilayer is connected directly to ground and assuming that the electrolyte resistance between the bilayer and the electrode can be ignored, V_{M1} is also the voltage across the bilayer. In order to determine the current flowing through the bilayer, the current flowing through R_2 and R_3 is subtracted from the total current in the system:

$$i_M = \frac{V_{In} - V_{M1}}{R_1} - i_{Line} \quad [5\text{-}4]$$

Figure 5-9 shows the calculated voltage across $(V_{M1})$and current through (i_M) the bilayer as a function of time for a single period using the recorded data in Figure 5-8. Note the large spikes in current near the transition point for the square wave (between lower and upper values). These spikes are due to the finite current clamps speed of the Axopatch, which was previously discussed in Chapter 3. It takes the Axopatch about $300 - 500\ \mu s$ to clamp the current so the voltage can measured. Because there is such an abrupt shift in the applied voltage, there is a small delay before the Axopatch is actually able to measure the voltage.

Figure 5-10 shows the data with the current clamp speed effects minimized. As expected, as the input DC offset is increased, the total current flowing through the bilayer is also increased. Note the "S-shape" (sigmoidal) curve of the current for the $80\ mV$, $100\ mV$, and $120\ mV$ DC offset cases. This suggests that the alamethicin channels are initially slowly opening, transition to a rapidly opening rate,

and then slowly open again as the current approaches the steady-state value. This behavior is qualitatively similar to potassium channel conductance in a neuron [60-63].

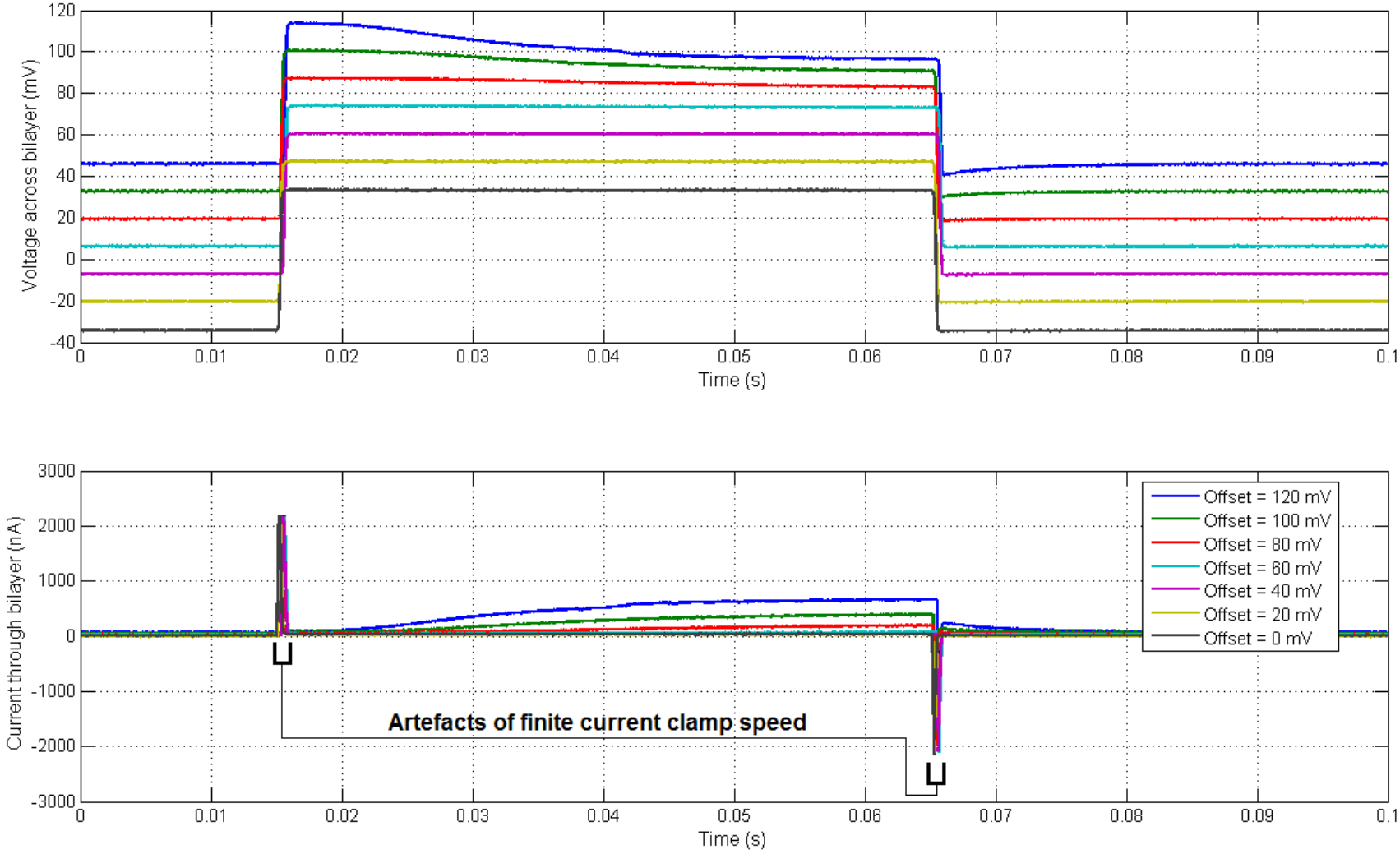

Figure 5-9: **Plots of the voltage across and the current through the bilayer as a function of time for the different input DC offsets. Note that neither the voltage across nor the current through the bilayer were measured directly. The values were calculated using the input voltage data, the voltage recorded at the measurement electrode (Figure 5-8), and the known circuit parameters.**

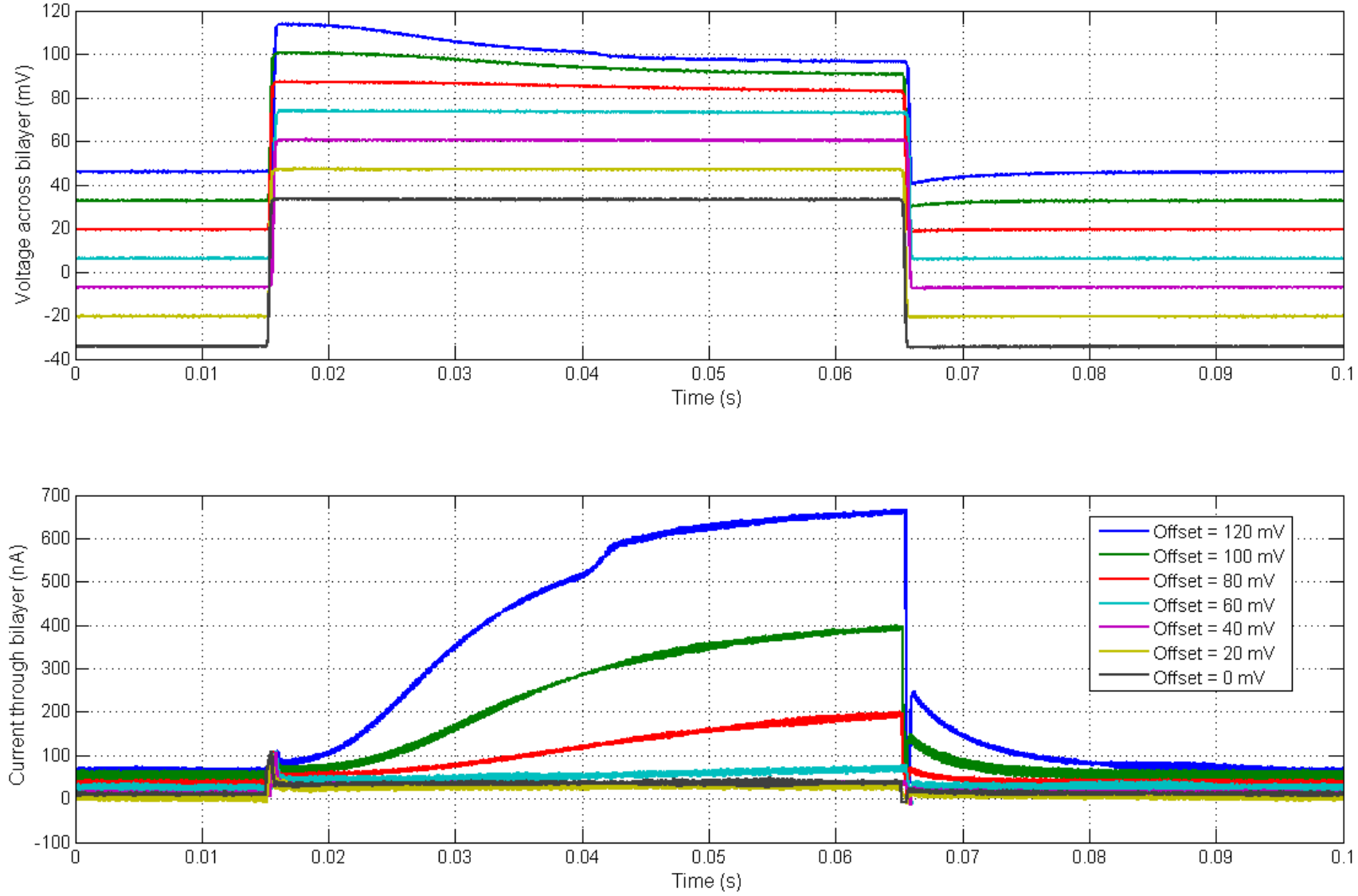

Figure 5-10: **Plots of the voltage across and the current through the bilayer as a function of time for the different input DC offsets with current clamp speed effects minimized (refer to Figure 5-9 for original plot). Note that neither the voltage across nor the current through the bilayer were measured directly. The values were calculated using the input voltage data, the voltage recorded at the measurement electrode (Figure 5-8), and the known circuit parameters.**

Figure 5-11 shows only the peaks of the average square waves for the data shown in Figure 5-8. In an effort to compare the cases more easily, the average voltage at the trough of the square wave was subtracted from the voltage at each point during the peak. Recall that at $t = 0$, the input signal has just transitioned from the trough of the square wave to the peak. This can be thought of as a step increase in the input voltage, which means that the voltage across the bilayer has also experienced a step increase. Note that regardless of the input DC offset potential, the initial voltage at the peak is very close to the expected value of $66\ mV$ [37]. The expected value is based on the assumption that the current through the bilayer can be ignored and that the voltage drops linearly down the length of the electrolyte line. Based on the data in Figure 5-11, at times close to $t = 0$, the current through the bilayer looks to be small enough to ignore because the difference in the voltage is consistent across all cases. This means that, initially, the alamethicin channels are not open. However, for the cases with input DC offsets larger than $60\ mV$, it is very clear that the current through the bilayer increases as time increases because the voltage recorded at the measurement electrode decreases.

[37] Recall that the expected value is based on where the measurement electrode is located along the length of the electrolyte line. For the cases shown, the measurement electrode was located about $1/3$ (Figure 5-1) of the way between the input and ground electrode. Since the input signal was $100\ mV_{pp}$, assuming the voltage drops linearly along the length of the electrolyte line, the voltage at the measurement electrode would be $66\ mV_{pp}$ (input voltage decreased by $1/3$).

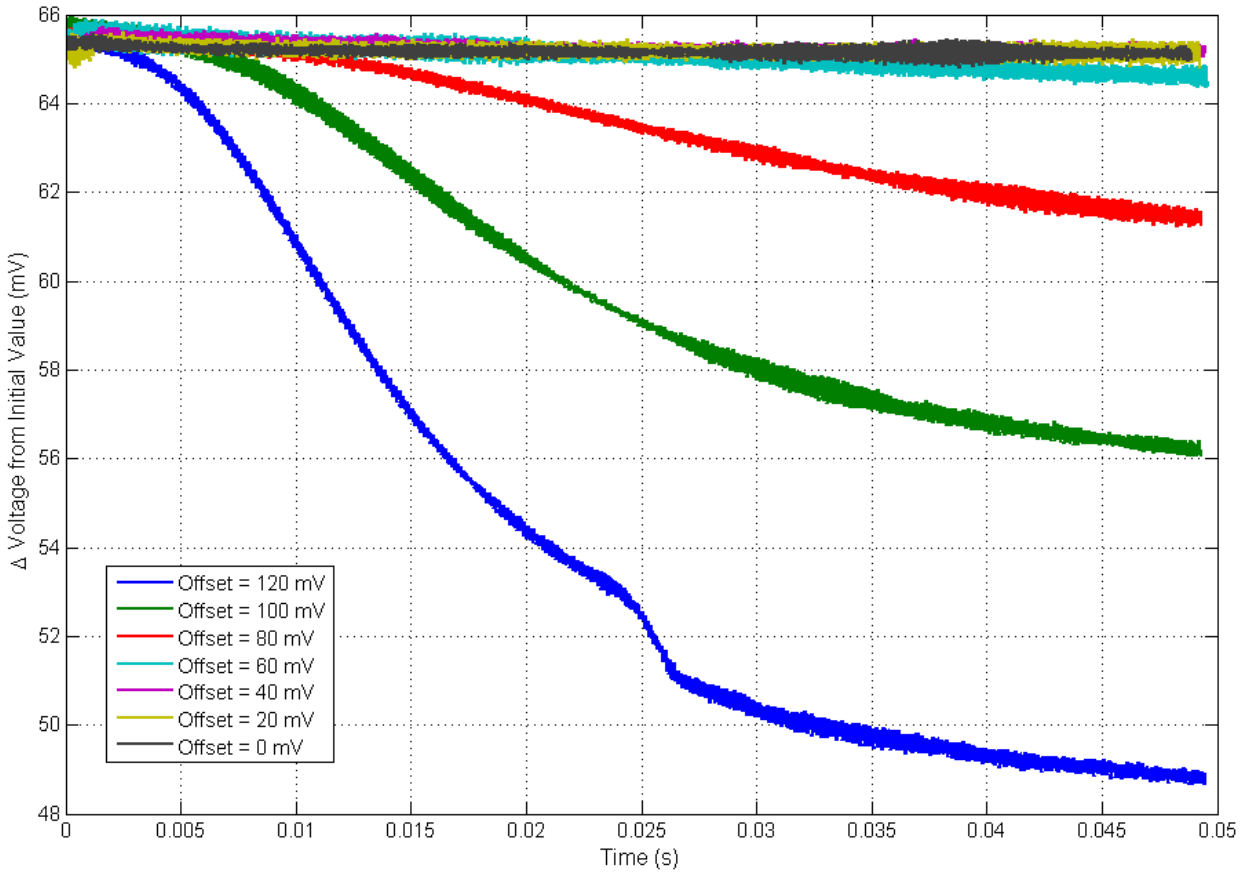

Figure 5-11: **Change in the voltage measured relative to the trough of the square wave. Data was recorded at the measurement electrode.**

As mentioned previously, one of the most interesting parts of Figure 5-11 is that for the cases where the input DC offset is greater than $60\ mV$, the voltage follows a sigmoid pattern down to a lower value. However, for all of the cases, the initial voltage starts approximately at the expected $66\ mV$ above the initial value. This suggests that the alamethicin channels are not opening instantaneously after the step increase. In other words, it takes some amount of time for the channels to open, lowering the resistance of the membrane, which leads to the decreased voltage at the measurement electrode. Figure 5-12 shows the different alamethicin channel opening rates for the case with a $100\ mV$ offset. Initially, the voltage drops slowly, which means the current through the bilayer is increasing at a slow rate (channels are slowly opening). There is then a transition where the channels are opening at a higher rate as the measured voltage drops faster than the initial speed. After this transitional period, the channels slowly open again as the potential at the measurement electrode (and thus the current through the bilayer) approaches a steady-state value.

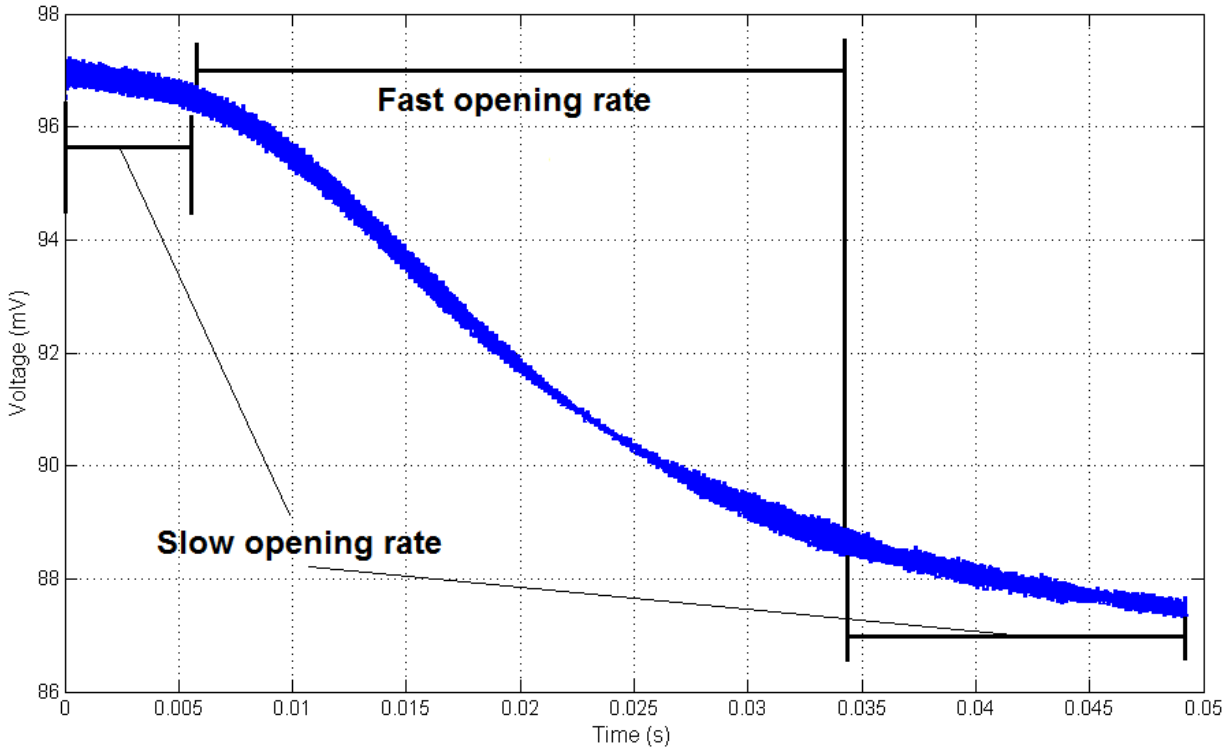

Figure 5-12: **Average voltage recorded at measurement electrode for peak of square wave for a $100\ mV_{pp}\ (10\ Hz)$ square wave with $+100\ mV$ DC offset input signal. Note that the average voltage shown is based on approximately 100 different periods.**

Refer back to the signal boosting data presented in Figure 4-24. Note how the peak of sine waves do not match for the case when the switch is open (V_{M2} is floating) and when the switch is closed (V_{M2} is controlled). The delay in the peak that occurs when the switch is closed is also due to the delayed opening of the alamethicin channels. In other words, if the alamethicin channels opened instantaneously, then the peaks for the two cases would occur at the same time. However, since the peak occurs at a later time for the case where the alamethicin channels are used to boost the signal, it is clear there is some time-dependence associated with the alamethicin gating.

5.4 High Pass Filter Application

Since alamethicin clearly has some time-dependence associated with the gating mechanism, it may be possible to use the artificial axon system in a filter application. Figure 5-13 shows the average recorded period at both the input electrode and the measurement electrode for a $100\ mV_{pp}\ (2\ Hz)$ input sine wave with a $-120\ mV$ DC offset. The two cases shown are the case where a bilayer is present and contains alamethicin channels (blue) and the other case is the recording without a bilayer (red). The purpose of this test was to show that the trough of the sine wave for the case with alamethicin is altered

due to the presence of alamethicin channels in the bilayer. The change in amplitude at the sine wave trough is a result of the alamethicin channels opening in the bilayer. Note that there is still a difference in the two cases at the peak of the sine wave. Current is flowing through the bilayer even at the peak of the sine wave, which means the voltage is smaller in magnitude for the case with alamethicin compared to the case without a bilayer. However, the magnitude of this current is much smaller at the peak of the sine wave compared to the trough, which is clearly seen by the attenuation of the trough's amplitude of the alamethicin case.

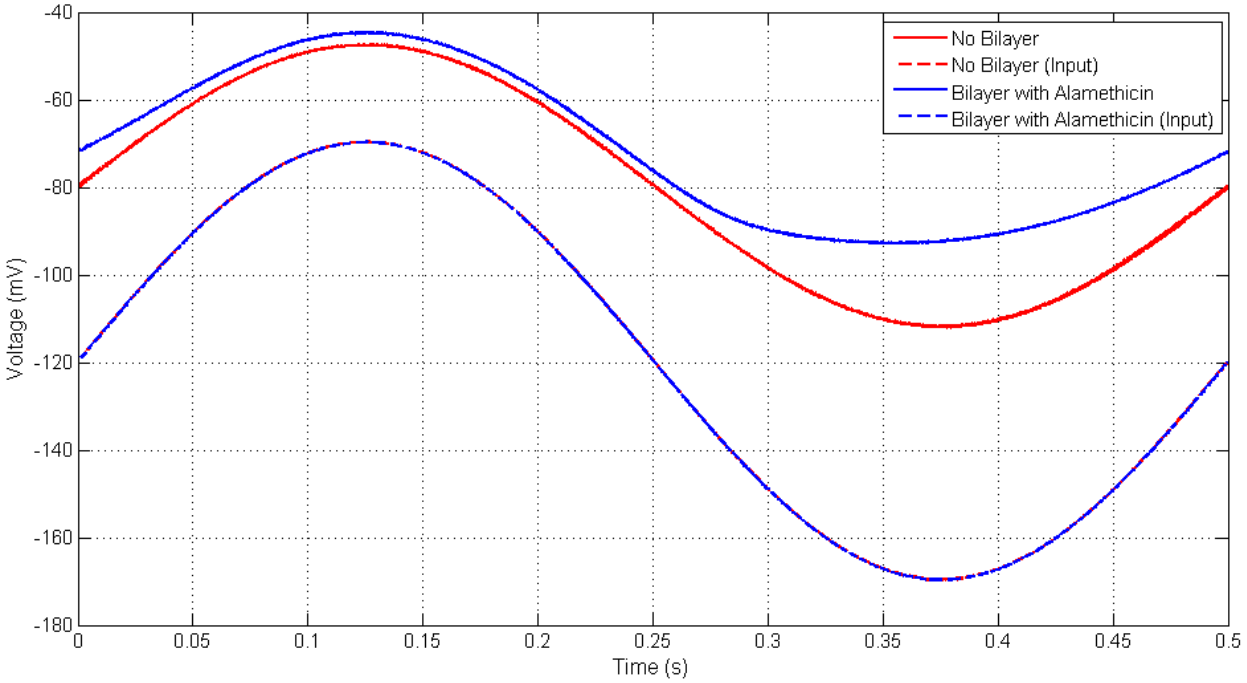

Figure 5-13: **Dotted) Average** $100\ mV_{pp}\ (2\ Hz)$ **input sine wave** $(n = 50)$**. Solid) Average sine wave recorded at measurement electrode** $(n = 50)$**.**

Based on the data shown in Figure 5-12, it is clear that the alamethicin channels take some amount of time to open. One would expect, then, that as the frequency of the signal is increased, the amplitude of the trough should be less affected by the alamethicin channels. In other words, the signal is operating at a high enough frequency that the channels do not have time to open. At low input signal frequencies, the channels would have time to open and reach the steady-state value, so the trough amplitude of the sine wave should decrease as the operating frequency is lowered.

Figure 5-14 shows the average single period recorded at the measurement electrode for different frequencies as a function of a normalized time. As expected, the trough amplitude decreases as the signal operating frequency decreases. This is because the alamethicin channels have more time to reach

their steady-state open positions. The system could therefore be used as a sort of high-pass filter. For higher frequencies, the signal would pass through the system with minimal changes whereas low frequencies signals would be attenuated.

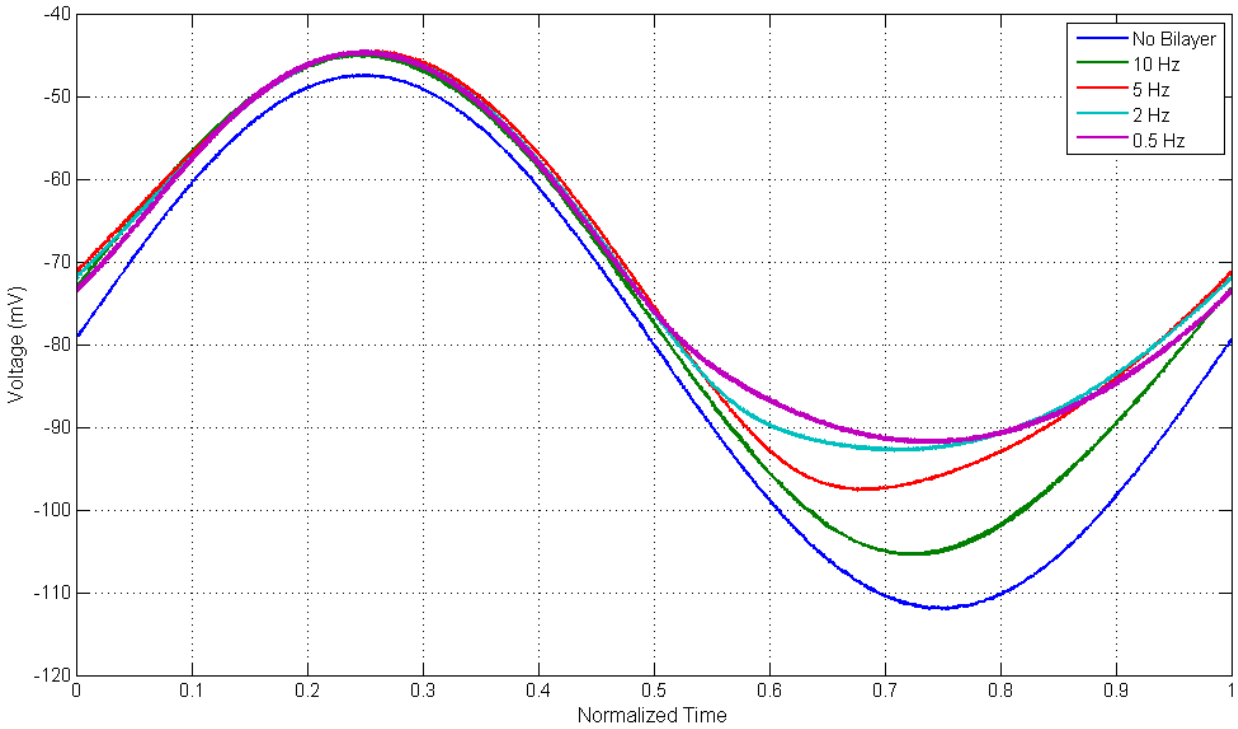

Figure 5-14: **Average sine wave for different frequencies recorded at the measurement electrode for a $100\ mV_{pp}$ sine wave input signal.**

5.5 Chapter Summary and Conclusions

When an action potential is initiated, potassium channels in the axonal membrane open much slower than the fast-acting sodium channels. Potassium channels follow a sigmoid shape of activation. In other words, initially, they are slow to open, transition to a fast opening rate, and then return a slow opening rate. Experimental data recorded using the artificial axon system showed that alamethicin channel activation also follows a sigmoidal shape. An interesting extension based on the alamethicin activation time-dependence is that the artificial axon system could be used as a filter. A signal traveling through the artificial axon system could be modified depending on the frequency of the signal. Low frequency signals would experience more attenuation than high frequency signals because the alamethicin channels have more time to open.

Chapter 6: Conclusion and Future Work

6.1 Conclusion

The work presented in this thesis consisted of two major research goals. The first was to create an artificial axon system using droplet on hydrogel bilayers (DHBs) in conjunction with alamethicin channels that is capable of showing properties of action potential signal propagation that occurs in myelinated nerve cells. The second research goal was to investigate how the artificial axon system could be used in other applications such as signal processing that do not necessarily mimic its biological equivalent. While the signal conduction velocity in the artificial axon system was orders of magnitude larger than speeds in a biological axon, it was capable of modifying signals as they traveled down the electrolyte line. Of particular interest was its capability of boosting a traveling signal's amplitude, which is similar to what occurs in the nodes of Ranvier in a myelinated axon. The method for producing the boosting behavior in the artificial axon system required that the extracellular fluid analog potential be time-dependent, which is not the case in its biological equivalent. However, by taking advantage of the gating properties of alamethicin, a signal can be boosted using the system as in a real neuron.

In addition to the signal boosting behavior, the artificial axon system was used to show that the sigmoidal activation for alamethicin is similar to that of potassium channels in a real axon. In other words, both channels slowly open, transition to a rapidly-opening rate, and then return a slow-opening pace. This behavior is very important in a neuron because it allows the action potential to be regenerated by the fast-acting sodium channels before the potassium channels help return the cell to its resting potential in preparation for the next action potential.

The artificial axon system can be used in applications other than reproducing properties of real neurons. It can be used as a filter to modify signals that meet certain amplitude or frequency criteria. It can also be used as a sensor in that if the signal reached a certain amplitude, current would start flowing through the bilayer, which could trigger a response (such as an alarm).

6.2 Future Work

It would be interesting to look at how certain parameters, such as bilayer size or alamethicin peptide concentration, affect the signal modifying properties of the artificial axon system. In other words, the

bilayer and/or channel properties may be able to be tailored in such a way that the user has more control over how a signal is modified.

One of the biggest problems that arose during testing with the artificial axon system was that air bubbles would form at the interface between the capillary tubing and the hydrogel anchored to the substrate. The air bubbles would break the electrical connection between the input and ground electrodes, so the signal could not travel through the system. Future work might focus on redesigning the artificial axon system to minimize this issue by developing a more efficient way of connecting the bilayer perpendicularly to an electrolyte line.

In order to slow the signal conduction velocity to a biological value, capacitors could be connected between the electrolyte line and extracellular fluid along the artificial axon system. These capacitors would have to be charged each time a signal attempted to travel through the electrolyte line, which would slow the signal down. This may also be achieved by connecting multiple bilayers to the electrolyte line. The bilayer capacitors would have to be charged in the same way as the signal traveled down the electrolyte line. This charging process also occurs in real neurons and is one of major reasons that the signal is slower in the biological system compared to one in the artificial axon system.

Appendix A: Supporting MATLAB Codes

A.1 EIS Data Fitting

The MATLAB codes contained within this section can be used to fit a transfer function to experimental frequency response data. The transfer function currently built into the code is for a single lipid bilayer equivalent circuit (refer back to Figure 2-2). A Metrohm/Eco Chemi Autolab PGSTAT12 was used to obtain the experimental data. The software used in conjunction with the Autolab was Frequency Response Analysis (FRA) for windows version 4.9 (developed by Eco Chemie in 2001).

A.1.1 Top Level Script

```
% This code was originially developed by Dr. Stephen A. Sarles.
% Reference: Sarles, S.A., Physical Encapsulation of Interface Bilayers,
%                2010, Virginia Polytechnic Institute and State University.

clear all;clc;close all
path = cd;
%--------------------------- Experimental Data --------------------------
%Find all files that have .dfr file type for batch processing
D=dir([path,'\*.dfr']);
%Use the size of D to determine the number of .dfr files found
size_D=size(D);num_files=size_D(1);
%Create a vector of the filenames-useful for seeing order of processing
filename_vec=char(D(:,1).name);
%Initialize plot of the electrical impedance of fitted model guesses
figure(2);clf reset
%Run through the for loop for each .dfr file found
for jj=1:num_files
%Name files:
eval(['file',num2str(jj),'=D(',num2str(jj),',1).name;']);
%-------------------------------------------------------------
%Extract data using `read_dfr.m':
eval(['data',num2str(jj),'=read_dfr(file',num2str(jj),');']);
%-------------------------------------------------------------
%Assign names to frequency, magnitude, and phase data:
eval(['freq',num2str(jj),'=data',num2str(jj),'(:,1);']);
eval(['mag',num2str(jj),'=abs(data',num2str(jj),'(:,2)-j.*data',...
num2str(jj),'(:,3));']);
eval(['phs',num2str(jj),'=atan2(-data',num2str(jj),'(:,3),data',...
num2str(jj),'(:,2))*180/pi;']);
%Complex impedance:
eval(['Z',num2str(jj),'=data',num2str(jj),'(:,2)-j.*data',...
num2str(jj),'(:,3);']); %Ohms
eval(['freq=freq',num2str(jj),';']);
eval(['mag=mag',num2str(jj),';']);
eval(['phs=phs',num2str(jj),';']);
eval(['Zexp=Z',num2str(jj),';']);
```

```
% Option to cut data points
% This can be used to remove the high frequency measurements which
% may be erroneous.
cut = 10;
freq(1:cut) = [];
mag(1:cut) = [];
phs(1:cut) = [];
Zexp(1:cut) = [];

%---------------------------- Initial Guesses -------------------------
%Bilayer Resistance (Ohms):
Rblm=max(mag); %use the maximum value of the magnitude
% as the initial guess for bilayer resistance
%Bilayer Capacitance (F):
Cblm=10e-12; %400pF is a reasonal guess for interface bilayers
% formed in this work
%Electrolyte/Test Cell (Ohms):
Re=mag(1); %pick the first data point, since frequency
% is swept from high to low during the measurement
%Frequency range (rad/s):
w=2*pi*freq; %this determines the frequency values
% used to compare the model to the data
%---------------------------------------------------------------------
%[R(RC)] Electrical equivalent model
%---------------------------------------------------------------------
%Simulated response from `model_def.m' using the initial guesses:
[Z_m0,mag_m0,phs_m0]=model_def(Rblm,Cblm,Re,w);
%Initial guess vector:
X0=[Rblm,Cblm,Re];
%Run `fminsearch.m' to minimize error in `error_def.m' by varying X
[Xf,err]=fminsearch('error_def',X0,[],w,Zexp);
%Compute the simulated impedance using optimized parameters:
[Z_fit,mag_fit,phs_fit]=model_def(Xf(1),Xf(2),Xf(3),w);
%---------------------------------------------------------------------
%Plot experimental data and fitted model
subplot 211;loglog(freq,mag,'b*-',freq,mag_fit,'ro-');
hold on
axis([10^-2 10^5.1 10^6 10^10])
legend('Experimental Data','Model');ylabel('Magnitude - \Omega');
subplot 212;semilogx(freq,phs,'b*-',freq,phs_fit,'ro-');
xlabel('Frequency - Hz');ylabel('Phase - deg');
hold on
axis([10^-2 10^5.1 -100 0])
%Compute approximate BLM area and equivalent diameter
eval(['R_BLM(',num2str(jj),')=Xf(1)/1e9;']); %GOhms
eval(['C_BLM(',num2str(jj),')=Xf(2)*1e12;']); %pF
eval(['R_H20(',num2str(jj),')=Xf(3);']); %Ohms
eval(['area_BLM(',num2str(jj),')=(C_BLM(',num2str(jj),')/1e12)/C_BLM;']); %cm^2
eval(['diam_BLM(',num2str(jj),')=sqrt(area_BLM(',num2str(jj),...
')*4/pi)*1e4;']); %microns
end
```

```
fprintf(['Electrolyte Resistance = %3.1f kOhm \n'],R_H20/1000)
fprintf(['Bilayer Resistance = %3.4f GOhm \n'],R_BLM)
fprintf(['Bilayer Capacitance = %3.1f pF \n'],C_BLM)
%---------------------------------------------------------------------
%Display results in
fit_data=vpa([R_BLM' C_BLM' area_BLM' diam_BLM'],'5')

imp = data1(:,2) + data1(:,3)*sqrt(-1);
imp = imp';
```

A.1.2 Model Definition (*model_def.m*)

```
% This code was originially developed by Dr. Stephen A. Sarles.
% Reference: Sarles, S.A., Physical Encapsulation of Interface Bilayers,
%                2010, Virginia Polytechnic Institute and State University.

function[Z,mag,phs]=model_def(R1,C1,R2,w);
%Impedance model [R(RC)]:
%
%Inputs:
%----------------------------
%1. R1 = resistance (Ohms)
%2. C1 = capacitance (Farads)
%3. R2 = resistance (Ohms)
%
%Outputs:
%----------------------------
%1. Z = complex impedance signature
%2. mag = magnitude of Z (Ohms)
%3. phs = phase angle of Z (deg)
Z=R1./(1+j.*w*R1*C1)+R2;
mag=abs(real(Z)+j.*imag(Z));

phs=atan2(imag(Z),real(Z))*180/pi;
```

A.1.3 Error Definition (*error_def.m*)

```
% This code was originially developed by Dr. Stephen A. Sarles.
% Reference: Sarles, S.A., Physical Encapsulation of Interface Bilayers,
%                2010, Virginia Polytechnic Institute and State University.

function[err]=error_def(X,w,Z_exp);
%
%Computes the norm of the square of error between experimental data
%(magnitude and phase) and the simulated response for `model_def.m':
% where, Model 1: Z(w)=R2+(R1||C1);
%
%Inputs:
%-----------------------------------------------------
%1. X = initial guesses for [R1 C1 R2];
%2. w = frequency range (rad/s)
%3. Z_exp = measured complex impedance (experimental)
```

```
%-------------------------------------------------------
%
%Outputs:
%-------------------------------------------------------
%err = norm of the square of the error in magnitude and phase
%Experiment:
real_exp=real(Z_exp); %real part of experimental impedance
imag_exp=imag(Z_exp); %imaginary part of impedance
%Model:
R1=X(1);
C1=X(2);
R2=X(3);
[Z,mag,phs]=model_def(R1,C1,R2,w);
real_mod=real(Z);
imag_mod=imag(Z);
%Error Calculation:
err_real=(real_mod-real_exp).^2;
err_imag=(imag_mod-imag_exp).^2;
%weights (same weighting as used in Autolab, developed by:
%B.A. Boukamp, Solid State Ionics, Vol. 20 (1986), 31-44)
we=1./(real_exp.^2+imag_exp.^2);
err=we'*(err_real+err_imag);
```

A.1.4 Read DRF Files (*read_dfr.m*)

```
function data=read_dfr(file_name)
%PURPOSE = read Autolab dfr file directly, without ascii conversion
%INPUT: OPENS DFR FILE -- file_name='example.dfr'
%OUTPUT 1) SAVES a MAT FILE(dfr2mat.mat)
%OUTPUT 2) Outputs Results

%READ FILE
fid22 = fopen(file_name);
line=fgetl(fid22);
line=fgetl(fid22);
num = sscanf(line, '%f');
line=fgetl(fid22);
clear matrix RESULTS
for i=1:num
   for j=1:9
      line=fgetl(fid22);
      data= sscanf(line, '%f');
      matrix(i,j)=data;
   end
end
status=fclose(fid22);

%RESULTS MATRIX in AUTOLAB FORMAT(ascii output)
%[f/Hz Z'/Ohm -Z''/Ohm time/s Edc/V Idc/A]
% RESULTS(:,1)=matrix(:,1);
% RESULTS(:,2)=matrix(:,2);
% RESULTS(:,3)=matrix(:,3);
```

```
% RESULTS(:,4)=matrix(:,6);
% RESULTS(:,5)=matrix(:,4);
% RESULTS(:,6)=matrix(:,5);
data=matrix(:,[1 2 3 6 4 5]);

% %SAVE AS MAT FILE
% save('dfr2mat', 'RESULTS')
```

A.2 Moving Average – Fast Fourier Transform

This code was used to process the data in order to produce Figure 3-11 and Figure 3-12. It cuts a full data set into smaller sets in order to take a moving average Fast Fourier Transform (FFT).

A.2.1 Top Level Script

```
% Chop and Average FFT style
% Column 1 = Time data (s)
% Column 2 = Input Voltage data (mV)
% Column 3 = Voltage data at point X (pA)
% Obviously all columns must be same length (same number of rows)

clear;clc % Clear Workspace and Command Window
close all % Closes as Figures

%% Directory Folder
FolderName = 'E:\Main Thesis Folder\TubeTest\IntegrateWithTubing\07-29-
2013\Bilayer2\PreBilayerElectrodeNoBilayer\';
% Don't forget the "\" at the end
cut = 0; % Remove last "cut" data points (used to remove erroneous data points at end of data set)

files = dir([FolderName,'*.mat']);
a = size(files,1); % Determines number of data files

h = waitbar(0,'Please wait...'); % Opens waitbar
OutputToExcel = zeros(6,a);


for b = 1:1:a
   str = strcat(FolderName,files(b).name);
   StructData = importMATfile(str);
   varname = fieldnames(StructData, '-full');
   RawData = StructData.(varname[64]);

%% User Inputs
setsize = 1000;
windowsize = 10; % Number of sets in a window
GuessDomFreq = 10; % User must guess the dominant input signal frequency [Hz]

samprate = 10000;
n = floor(size(RawData,1)/setsize); % Number of data Vin/VX_sets
numofdatasets = n;
```

```
VInavg = 0; % Used as summation variable
VXavg = 0; % Used as a summation variable
tavg = [0:1/samprate:(windowsize*setsize-1)/samprate]';
Vin_set = zeros(size(tavg,1),n); % Preallocate matrix size
VX_set = zeros(size(tavg,1),n); % Preallocate matrix size

% For loop will chop data into multiple data sets
VInfitSStot = zeros(1,n);
VInfit = zeros(4,n);
VInfitSSres = zeros(1,n);
VinfitR2 = zeros(1,n);
VXfitSStot = zeros(1,n);
VXfit = zeros(4,n);
VXfitSSres = zeros(1,n);
VXfitR2 = zeros(1,n);
TD_STDFuncOfTime = zeros(1,n);

% Find the index of the dominant frequency
[VInFMag,VInFPhase,VInfreq] = FFTandScale(RawData(1:setsize*windowsize,1),
RawData(1:setsize*windowsize,2));

% Look near the GuessDomFreq frequency to find the dominant frequency by
% checking all of the magnitudes at nearby frequencies.
VInFMagind = find(abs(VInfreq-GuessDomFreq) < 1);
VInFMagmax = 0; % Use as comparison variable in for loop
VInFMagmaxind = 0; %Use to store index of maximum magnitude
for p = 1:1:size(VInFMagind,1)
   if abs(VInFMag(VInFMagind(p))) > VInFMagmax
      VInFMagmax = abs(VInFMag(VInFMagind(p))); % VInFMag is complex, so use abs
      VInFMagmaxind = VInFMagind(p);
   end
end

Freq = VInfreq(VInFMagmaxind);
fprintf('VInFMagind corresponds to %2.2f Hz b = %1.0f \n',Freq,b)

% figure(1)
% plot(VInfreq,abs(VInFMag))
% xlabel('Frequency (Hz)')
% ylabel('Voltage (mV)')
% axis([0 1.1*GuessDomFreq 0 abs(VInFMag(VInFMagmaxind))*1.1])

for q = 1:1:n - windowsize + 1

   range = [((q-1)*setsize+1):1:(setsize*windowsize + (q-1)*setsize)]';

   [VInFMag,VInFPhase,VInfreq] = FFTandScale(tavg, RawData(range,2));
   Vin_phase(q) = VInFPhase(VInFMagmaxind);
   Vin_amp(q) = abs(VInFMag(VInFMagmaxind));

   [VXFMag,VXFphase,VXfreq] = FFTandScale(tavg, RawData(range,3));
   VX_phase(q) = VXFphase(VInFMagmaxind);
   VX_amp(q) = abs(VXFMag(VInFMagmaxind));
```

```
   maxiter = n - windowsize + 1;

   waitbar(q/maxiter,h,sprintf('Please wait...%1.0f / %1.0f completed (%1.0f / %1.0f total)', q,maxiter,b,a)) %
Update waitbar

end

Freq = VXfreq(VInFMagmaxind);
fprintf('VInFMagind corresponds to %2.2f Hz b = %1.0f \n',Freq,b)

phasediff = Vin_phase - VX_phase;
phasediff = phasediff(1,1:size(phasediff,2)-cut); % Remove points near end of data set that may be erroneous
timedelay = phasediff/(360*GuessDomFreq); % Time delay (s) for each data set
timedelaySD = std(timedelay); % Standard deviation of time delay (+/- s)
timedelayAvg = mean(timedelay); % Average time delay (s)
Vin_ampAvg = mean(Vin_amp);
Vin_ampSD = std(Vin_amp);
VX_ampAvg = mean(VX_amp);
VX_ampSD = std(VX_amp);

TD[29] = timedelay; % Store time delay as a function of time

OutputToExcel(1:6,b) = [timedelayAvg*10^6
                timedelaySD*10^6
                Vin_ampAvg
                Vin_ampSD
                VX_ampAvg
                VX_ampSD];

% Reset variables
RawData = [];
phasediff = [];
timedelay = [];
VInFMag = [];
VInFphase = [];
VInfreq = [];
Vin_amp = [];
Vin_phase = [];
VXFMag = [];
VXFphase = [];
VXfreq = [];
VX_phase = [];
VX_amp = [];

end

close(h); % Close waitbar


%% Plotting
ColorSet = varycolor(a); % Used to change colors of plots
set(gca,'ColorOrder',ColorSet);
```

```
hold all
figure(1)
for b = 1:1:a
   fprintf(files(b).name)
   fprintf('\n')

   plot(TD{b}*10^6);
   legendInfo{b} = ['X = ' files(b).name];

end
legend(legendInfo)
title('Time Delay as a function of Measurement Time')
xlabel('Time (ms)')
ylabel('Time Delay (\mu s)')
axis([0 700 340 580])
grid on
hold off

% For direct import into Excel
% Note that the data points in OutputToExcel may not be in the correct
% order.  To determine the order, look at "files" structure
%OutputToExcel = OutputToExcel';

copy = OutputToExcel;
% OutputToExcel = [copy(1,:); copy(5:12,:);copy(2:4,:)];
OutputToExcel = OutputToExcel';
pos_errbar = OutputToExcel(:,1) + OutputToExcel(:,2);
neg_errbar = OutputToExcel(:,1) - OutputToExcel(:,2);
num = 10;

figure(2)
plot([0:num-1],OutputToExcel(:,1),'o-',[0:num-1],pos_errbar,'r',[0:num-1],neg_errbar,'r')
title('Time Delay as a function of Position')
xlabel('Position')
ylabel('Time Delay (\mu s)')
legend('Data','Standard Deviation')
grid on

figure(3)
plot([0:num-1],OutputToExcel(:,5),'o-')
title('Peak Voltage as a function of Position')
xlabel('Position')
ylabel('Peak Voltage (mV_p_e_a_k')
grid on
```

A.2.2 Take Fast Fourier Transform (*FFTandScale.m*)

```
function [Fmag,Fphase,freq] = FFTandScale(time, signal)
% This function will take the Fast Fourier Transform of "signal"
% and will scale it appropriately such that the magnitudes are correct.
% It will also calculate the phase of each frequency.
```

```
% "time" array must have only 1 column (any number of rows)
n = size(time,1);
samprate = 1/(time(2)-time(1)); % Sample rate (Hz)
freq = [0:samprate/n:samprate*(1-1/n)]';

% Input Signal
signal = signal - mean(signal); % Subtract mean
HammWindow = hamming(size(signal,1)); % Generate discrete Hamming window
signal = signal.*HammWindow; % Apply Hamming window to signal
Fmag = fft(signal);
Fmag = Fmag/n; % Must divide by the number of samples
fft_Fmag01 = Fmag(1); % Stores magnitude for 0 frequency
Fmag = Fmag*2; % Should be integrating from -T/2 to T/2,
      % but we only have data from 0 to T/2.
Fmag(1) = fft_Fmag01; % Reinserts non-doubled 0 frequency term
Fphase = angle(Fmag)*180/pi(); % Calculates phase angle in degrees
```

A.3 Circuit Model Simulator – Using Cyclic Voltammetry Data

The MATLAB codes included in this section were used to simulate the response of the artificial axon system to various input signal configurations. The model uses experimentally obtained cyclic voltammetry data in order to produce a more realistic response. Both Figure 4-10 and Figure 4-20 were created using this model.

A.3.1 Top Level Script

```
% Predictor Model
% Uses cyclic voltammetry data to predict response

clear;clc

% Import Cyclic Voltammetry Data
A = importMATfile('C:\Users\zvandy\Desktop\AlmData\CVdatafor3ugmLalm.mat');

Valm = A.A(:,3);
ialm = A.A(:,2);
R1 = 1.884*10^6; % Resistance between input and bilayer [Ohms]
R2 = 315*10^3; % Resistance between bilayer and boost electrode [Ohms]
R3 = 3.083*10^6; % Resistance between boost electrode and ground [Ohms]
Rmi = 1.7*10^9; % Bilayer resistance [Ohms]

% VDC = 100*10^-3; % DC potential [V]
t = [0:0.005:0.1]';
f = 10;
w = 2*pi()*f;
A = 0.02;
VIn = A*sawtooth(w*t,0.50); % Input signal
%VIn = A*square(w*t,50) + 0.01; % Input signal
%VDC = (60*10^-3)*square(w*t - pi()/2,25) + (30*10^-3); % DC potential [V]
VDC = (60*10^-3)*ones(size(t,1),1); % DC potential [V]
```

```
Valmi = 0.07;

% % Create current as a function of voltage for alamethicin channels
% x1 = [-50:0.1:0]';
% x2 = 0*[0.1:0.1:50]';
% x3 = [0.1:0.1:50]';
% x = [x1; x2; x3];
% x = x*2*10^-3;
% y = [(x).^3]*10^-4.25;

% Valm = x;
% ialm = y + 10^-12;

h = waitbar(0,'Please wait...'); % Opens waitbar

for m = 1:1:size(VIn,1)
   X(1) = R1;
   X(2) = R2;
   X(3) = R3;
   X(4) = Rmi;
   X(5) = VDC(m);
   X(6) = VIn(m);


   for n = 1:1:size(Valm,1)

      Y = modeli2known(X,ialm(n,1));
      IsVclose(n) = abs(Y(1) - Valm(n));

      waitbar(n/size(Valm,1),h,sprintf('Please wait...%1.0f / %1.0f completed (%1.0f / %1.0f total)',
n,size(Valm,1),m,size(VIn,1))) % Update waitbar

   end

   [val ind] = min(IsVclose);
   Y = modeli2known(X,ialm(ind,1));

   indstore(m) = ind;
   VClosestore(m) = (Y(1) - Valm(ind,1))*10^3;

   i1NG = Y(2)*10^9; % i1, current through electrolyte [nA]
   i2NG = ialm(ind,1)*10^9; % i2, current through bilayer [nA]
   VM1NG = Y(3)*10^3; % VM1, voltage on tube side of bilayer [mV]
   %VBoostNG = Y(4)*10^3; % VBoost, voltage at boost electrode [mV]

   %VBoostNGCase(m,1) = VBoostNG;
   VM1NB(m,1) = VM1NG;
   I1NG(m,1) = i1NG;
   I2NG(m,1) = i2NG;

   X(4) = abs(Valm(ind,1)/ialm(ind,1));
   Rmstore(m) = X(4);
   Y = model_v2(X);
```

```
   VBoostG = Y(4)*10^3; % VBoost, voltage at boost electrode [mV]
   VBoostGCase(m,1) = VBoostG;
end

% Non-gating case
for n = 1:1:size(VIn,1)
   X(1) = R1;
   X(2) = R2;
   X(3) = R3;
   X(4) = Rmi;
   X(5) = VDC(n);
   X(6) = VIn(n);
   X(7) = Valmi;

   % Non-gating case
   Y = model(X);
   i1NG = Y(1)*10^9; % i1, current through electrolyte [nA]
   i2NG = Y(2)*10^9; % i2, current through bilayer [nA]
   VM1NG = Y(3)*10^3; % VM1, voltage on tube side of bilayer [mV]
   VBoostNG = Y(4)*10^3; % VBoost, voltage at boost electrode [mV]

   VBoostNGCase(n,1) = VBoostNG;
   VM1NB(n,1) = VM1NG;
   I1NG(n,1) = i1NG;
   I2NG(n,1) = i2NG;

end

close(h) % close waitbar
%% Plotting

%VBoost = smooth(VBoost,21);
figure(1)
plot(t,VIn*1000,t,VDC*1000)
title('Input & V_M_2')
legend('Input','V_M_2')
xlabel('Time (s)')
ylabel('Voltage (mV)')
set(findall(gcf,'Type','text'),'FontSize',12) % Change all font sizes
set(findall(gcf,'Type','line'),'LineWidth',2) % Change line width/color
set(findall(gcf,'Type','axes'),'FontSize',11) % Set axis font size

figure(2)
plot(t,VBoostNGCase,'r',t,VBoostGCase,'b')
title('Voltage at Boost Electrode')
legend('Non-gating Case','Gating Case')
xlabel('Time (s)')
ylabel('Voltage (mV)')
grid on
set(findall(gcf,'Type','text'),'FontSize',12) % Change all font sizes
set(findall(gcf,'Type','line'),'LineWidth',2) % Change line width/color
set(findall(gcf,'Type','axes'),'FontSize',11) % Set axis font size
```

```
figure(3)
plot(t,(VDC*10^3 - VM1NB),'r')
xlabel('Time (s)')
ylabel('Voltage (mV)')
title('Voltage Across Bilayer')
grid on
set(findall(gcf,'Type','text'),'FontSize',12) % Change all font sizes
set(findall(gcf,'Type','line'),'LineWidth',2) % Change line width/color
set(findall(gcf,'Type','axes'),'FontSize',11) % Set axis font size
```

A.3.2 Calculate Circuit Variables with i_2 Known (*modeli2known.m*)

```
function [Y] = modeli2known(X,i2)

R1 = X(1); % Resistance between input and bilayer [Ohms]
R2 = X(2); % Resistance between bilayer and boost electrode [Ohms]
R3 = X(3); % Resistance between boost electrode and ground [Ohms]
%Be careful here, Rm is not necessarily correct
Rm = X(4); % Bilayer resistance [Ohms]
VDC = X(5); % DC potential [V]
VIn = X(6);  % Input voltage [V]

i1 = (VIn - i2*(R2 + R3))/(R1 + R2 + R3);
VM1 = (R2 + R3)*(i1 + i2);
VaB = VDC - VM1;

Y(1) = VaB;
Y(2) = i1;
Y(3) = VM1;
```

A.4 Chop and Average Data Set into a Single Period

This function can be used to cut a data set into single periods in order to average all of the periods together. This function was used extensively in this thesis to show the average single period for a particular case.

SimpChopAndAvg.m

```
% Simple Chop and Average
% This code can be used for any type of input/output signal (not limited
% to sinusoidal signals).

% This program will cut a data set into a series of user-specified sections
% all of which will have the same length of 1 period.  If the user choses
% a length smaller or larger than the 1 period, the code will not work
% properly.  Please note that this code does not resample the data.

% User must save the data as "dat" before running this code.  "dat" must
% have the following structure:
% Column 1 = Time (s)
```

```
% Column 2 = Input Voltage (mV)
% Column 3 = Output Current (pA)

function [Y] = SimpChopAndAvg(t,V,i,samprate,inputsigfreq)

% samprate/inputsigfreq must be an integer
ptsperperiod = samprate/inputsigfreq; % Number of points per period

n = floor(size(V,1)/ptsperperiod); % Number of sets to divide dat into

tavg = [0:1/samprate:(ptsperperiod-1)/samprate]';
Vavg = 0;
iavg = 0;

for p = 1:1:n
   % Average the input voltage (1 period)
   V_set(:,p) = V((p-1)*ptsperperiod+1:1:p*ptsperperiod);
   Vavg = Vavg + V_set(:,p);

   % Average the output current (1 period)
   i_set(:,p) = i((p-1)*ptsperperiod+1:1:p*ptsperperiod);
   iavg = iavg + i_set(:,p);
end

Vavg = Vavg/n; % Take average by divide by number of data sets
iavg = iavg/n; % Take average by divide by number of data sets

% For presentation purposes, it would be useful to shift the current wave
% to a particular position (easier to compare between cases).
ind =  find(Vavg == max(Vavg)); % Index of lowest value of voltage period
Vhold = Vavg;
ihold = iavg;

Vavg = [Vhold(ind+1:end,1); Vhold(1:ind)];
iavg = [ihold(ind+1:end,1); ihold(1:ind)];

Y = [tavg Vavg iavg];
```

A.5 Current Predictor for a Single Bilayer

This MATLAB code can be used to simulate the current through a single bilayer system using the corresponding circuit model (refer back to Figure 2-2).

BilayerCurrentPredictor.m

```
% This code was originally developed by Dr. Myles Dunlap.
% This MATLAB code predicts the current response of a single bilayer to
% a user-defined voltage signal using transfer functions.
%
% The single bilayer is modeled as shown below:
%
```

```
%                 ------<Capacitor>------
%                 |                    |
%  o---<Resistor 1>---                   ---------o
%                 |                    |
%                 ------<Resistor 2>------
%
% Resistor 1 = Electrolyte Resistance
% Capacitor = Bilayer Capacitance
% Resistor 2 = Bilayer Resistance
%

function [I] = BilayerCurrentPredictor(X,t,f,A,iavg)

%% User Inputs
%Voltage stimuli inputs:
w = 2*pi*f; %[rad/s]
V = A*sawtooth(w*t,0.5); %triangle wave

%Bilayer parameters:
Rs = 1;       %[ohms] (Electrolyte resistance)
            % Note: This code effectively ignores electrolyte
            % resistance.
Rb = X(1);      %[ohms] (Bilayer resistance)
Cb = X(2);    %[Farads] (Bilayer Capacitance)

%% Program Code
%Transfer function for DIB electrical impedence:
%Z(w) = V(w)/I(w) = (Rb/(jwCbRb+1)) + Rs
%Rs = aqueous res., Rb = bilayer res., Cb = bilayer cap.

Z = tf([Rs*Rb*Cb,Rs+Rb],[Rb*Cb,1]);   %Impedance TF
Y = 1/Z; %admittance description (I=YV, Y=1/Z)
TF = Y; %I/V=Y=(1/Z);

%Applying the voltage to the bilayer and getting out current:
[I,t] = lsim(TF,V,t);
```

Appendix B: Artificial Axon System Substrate

This section includes the dimensions of the substrate and pictures of the manufacturing mold for the substrate used to contain the bilayer in the artificial axon system. It also includes a description of the manufacturing procedure.

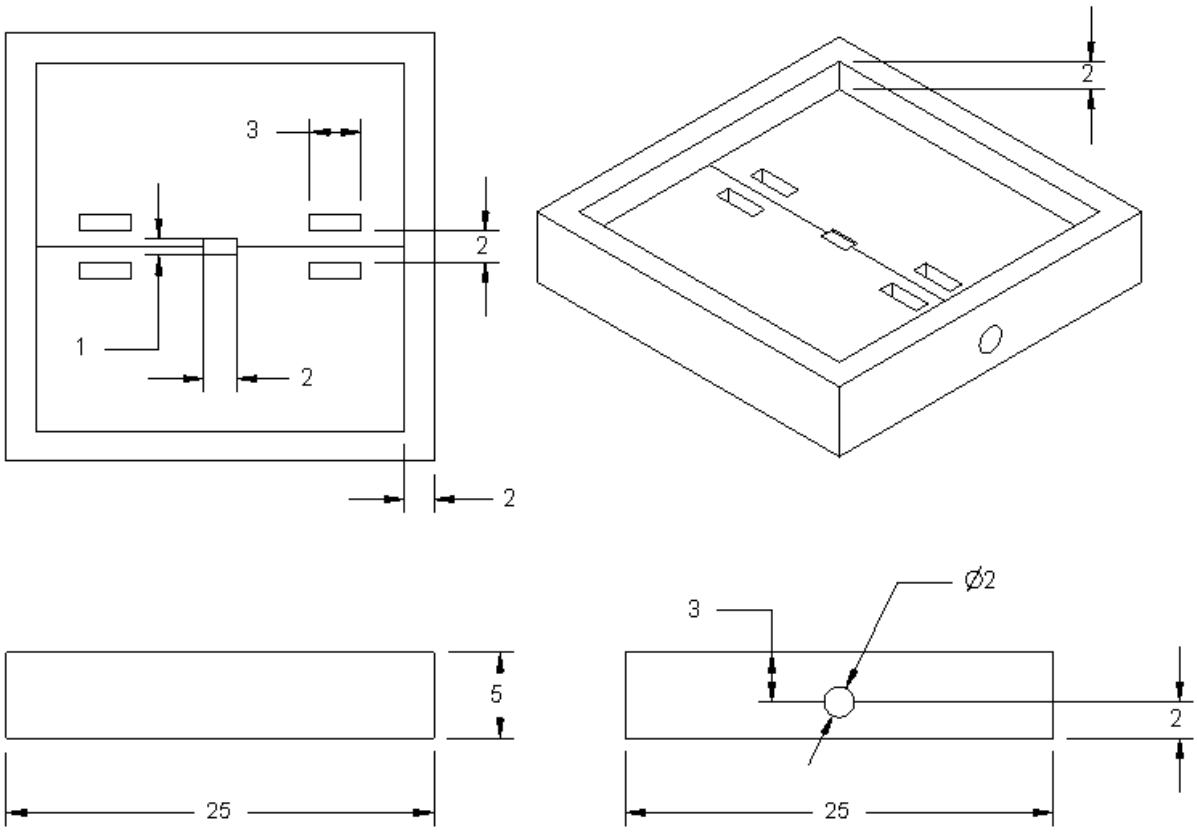

Figure B-1: **Substrate dimensions used to contain the bilayer in the artificial axon system. All dimensions are in millimeters.**

Figure B-2 is a picture of the negative acrylic mold used in conjunction with the curable polyurethane to create the experimental substrate. The capillary tubing had an outer diameter of $0.07\ in\ (1.78\ mm)$ and an inner diameter of $0.04\ in\ (1.02\ mm)$. The tubing could be placed inside the capillary tubing channels and between the capillary tubing stabilizers. Modeling clay (Mish Mish, Blacksburg, VA) was placed over the capillary tubing in the capillary tubing channels in order to prevent the liquid polyurethane from spilling over into the channels. Modeling clay was also inserted in the tubing near the hydrogel well extrusion to prevent the polyurethane from going into the tubing. Once the tubing

and clay were in place, the entire mold was sprayed with a universal mold release (Smooth-On, Easton, PA).

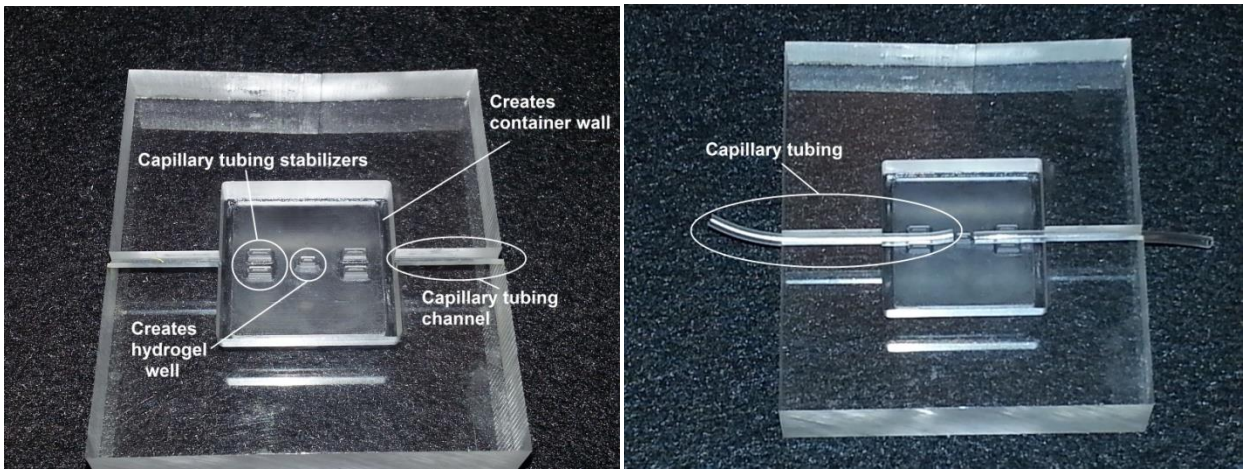

Figure B-2: **Pictures of negative acrylic mold used to create the experimental substrate. Left) Picture of mold without the capillary tubing. Right) Picture of mold with capillary tubing. Pictures taken courtesy of Joseph Najem.**

The flexible polyurethane molds were created using Smooth-On Clear Flex ® 50 Water Clear Urethane Rubber (Easton, PA). The Clear Flex ® 50 comes in two liquid parts. Part A is the liquid rubber and Part B is the liquid elastomer. Part A was mixed with Part B in a 0.9:2.0 ratio. In order to reduce the amount of air bubbles in the mixture[38], the mixture was stirred by hand on a hot plate at $50℃$ for a 2-3 minute period, then placed in a small vacuum chamber at $-25\ psi_{vac}$ $(-10.3\ psia)$.

The negative molds for the substrates were created using a CNC machine to mill out an acrylic piece. The liquid polyurethane could then be poured into the mold and cured in an oven at $80℃$ for about an hour. The polyurethane will solidify and the substrate can then be removed from the mold. The capillary tubing pieces then simply slide out of the substrate.

[38] Light must pass through the substrate to see the system under a microscope, so air bubbles should be kept at a minimum.

References

1. Bar-Cohen, Y., *Biomimetics: biologically inspired technologies*, 2006: CRC Press LLC.
2. Brodal, P., *The central nervous system: structure and function*, 2004: Oxford University Press.
3. Furber, S., *The Future of Computer Technology and its Implications for the Computer Industry.* The Computer Journal, 2008. **51**(6): p. 735-740.
4. Blows, W.T., *The Biological Basis of Mental Health Nursing*, 2011: Taylor & Francis.
5. Klipp, E., *Systems biology : a textbook*, 2009, Weinheim: Wiley-VCH.
6. Stanier, R. and G. Bazine, *Phototrophic prokaryotes: the cyanobacteria.* Annual Reviews in Microbiology, 1977. **31**(1): p. 225-274.
7. Walz, D.T.J.M.G., *Bioelectrochemistry of membranes*, 2004, Basel; Boston: Birkhäuser Verlag.
8. Aidley, D.J. and P.R. Stanfield, *Ion channels: molecules in action*, 1996: Cambridge University Press.
9. Singer, S.J. and G.L. Nicolson, *The fluid mosaic model of the structure of cell membranes.* Science, 1972. **175**(23): p. 720-731.
10. Alberts, B., A. Johnson, and J. Lewis, *Molecular Biology of the Cell*. Vol. 5th edition. 2002.
11. Sarles, S.A., *Physical Encapsulation of Interface Bilayers*, 2010, Virginia Polytechnic Institute and State University.
12. Tien, H.T. and A.L. Ottova, *The lipid bilayer concept and its experimental realization: from soap bubbles, kitchen sink, to bilayer lipid membranes.* Journal of membrane science, 2001. **189**(1): p. 83-117.
13. Winterhalter, M., *Black lipid membranes.* Current Opinion in Colloid & Interface Science, 2000. **5**(3–4): p. 250-255.
14. Overton, C.E., *Über die osmotischen Eigenschaften der lebenden Pflanzen-und Tierzelle*, 1895: Fäsi & Beer.
15. Gorter, E. and F. Grendel, *On biomolecular layers of lipids on the chromocytes of blood.* Journal of Experimental Medicine, 1925. **41**: p. 439-443.
16. Danielli, J.F. and H. Davson, *A contribution to the theory of permeability of thin films.* Journal of cellular and comparative physiology, 1935. **5**(4): p. 495-508.
17. Montal, M. and P. Mueller, *Formation of bimolecular membranes from lipid monolayers and a study of their electrical properties.* Proceedings of the National Academy of Sciences, 1972. **69**(12): p. 3561-3566.
18. Bayley, H., et al., *Droplet interface bilayers.* Molecular BioSystems, 2008. **4**(12): p. 1191-1208.
19. Hwang, W.L., et al., *Asymmetric droplet interface bilayers.* Journal of the American Chemical Society, 2008. **130**(18): p. 5878-5879.
20. Bäckström, S., et al., *Tailoring Properties of Biocompatible PEG-DMA Hydrogels with UV Light.* Materials Sciences and Applications, 2012. **3**(6): p. 425-431.
21. Jeon, T.-J., N. Malmstadt, and J.J. Schmidt, *Hydrogel-encapsulated lipid membranes.* Journal of the American Chemical Society, 2006. **128**(1): p. 42-43.
22. Ibragimova, S., et al., *Hydrogels for in situ encapsulation of biomimetic membrane arrays.* Polymers for Advanced Technologies, 2012. **23**(2): p. 182-189.
23. Young, T.T., *Lipid Bilayer Formation in Aqueous Solutions of Ionic Liquids*, 2012, Virginia Polytechnic Institute and State University.
24. Sarles, S.A., et al., *Bilayer formation between lipid-encased hydrogels contained in solid substrates.* ACS applied materials & interfaces, 2010. **2**(12): p. 3654-3663.

25. Sarles, S.A. and D.J. Leo, *Regulated attachment method for reconstituting lipid bilayers of prescribed size within flexible substrates.* Analytical chemistry, 2010. **82**(3): p. 959-966.
26. Reusser, F., *Biosynthesis of antibiotic U-22,324, a cyclic polypeptide.* Journal of Biological Chemistry, 1967. **242**(2): p. 243-247.
27. Meyer, C. and F. Reusser, *A polypeptide antibacterial agent isolated fromTrichoderma viride.* Experientia, 1967. **23**(2): p. 85-86.
28. Rippa, S., et al., *Hypersensitive-Like Response to the Pore-Former Peptaibol Alamethicin in Arabidopsis Thaliana.* ChemBioChem, 2010. **11**(14): p. 2042-2049.
29. Aidemark, M., et al., *Trichoderma viride cellulase induces resistance to the antibiotic pore-forming peptide alamethicin associated with changes in the plasma membrane lipid composition of tobacco BY-2 cells.* BMC Plant Biology, 2010. **10**(1): p. 274.
30. Mueller, P. and D.O. Rudin, *Action potentials induced in biomolecular lipid membranes.* 1968.
31. Eisenberg-Grunberg, M., *Voltage gateable ionic pores induced by alamethicin in black lipid membranes*, 1973, California Institute of Technology.
32. Nolte, J., *The Human Brain: An Introduction to its Functional Anatomy, 6th Edition.* 2008.
33. Brewer, G., et al., *Neuron network activity scales exponentially with synapse density.* Journal of neural engineering, 2009. **6**(1): p. 014001.
34. Giuliodori, M.J. and S.E. DiCarlo, *Myelinated vs. unmyelinated nerve conduction: a novel way of understanding the mechanisms.* Advances in physiology education, 2004. **28**(2): p. 80-81.
35. Pollard, T.D., W.C. Earnshaw, and J. Lippincott-Schwartz, *Cell biology*, 2007: Elsevier Health Sciences.
36. Fournier, R.L., *Basic transport phenomena in biomedical engineering*, 2011: CRC Press.
37. McKinley, M.P. and V.D. O'loughlin, *Human anatomy*, 2006: McGraw-Hill Higher Education.
38. Guyton, A.C., *Textbook of medical physiology 8th ed.* WB Saunders Company, USA, 1991.
39. Goldman, D.E., *Potential, impedance, and rectification in membranes.* The Journal of General Physiology, 1943. **27**(1): p. 37-60.
40. Malmivuo, J. and R. Plonsey, *Bioelectromagnetism: principles and applications of bioelectric and biomagnetic fields*, 1995: Oxford University Press, USA.
41. Young, J.Z., *The functioning of the giant nerve fibres of the squid.* Journal of Experimental Biology, 1938. **15**(2): p. 170-185.
42. Coon, D., *Introduction to Psychology: Exploration and Application (West, New York).* 1992.
43. Wareham, A.C., *Action potential: generation and propagation.* Anaesthesia & Intensive Care Medicine, 2005. **6**(6): p. 200-203.
44. Creasy, M.A., *Bilayer Network Modeling*, 2011, Virginia Polytechnic Institute and State University.
45. Bordi, F., C. Cametti, and A. Gliozzi, *Impedance measurements of self-assembled lipid bilayer membranes on the tip of an electrode.* Bioelectrochemistry, 2002. **57**(1): p. 39-46.
46. Baba, T., et al., *Formation and characterization of planar lipid bilayer membranes from synthetic phytanyl-chained glycolipids.* Biochimica Et Biophysica Acta-Biomembranes, 1999. **1421**(1): p. 91-102.
47. Funakoshi, K., H. Suzuki, and S. Takeuchi, *Lipid bilayer formation by contacting monolayers in a microfluidic device for membrane protein analysis.* Analytical Chemistry, 2006. **78**(24): p. 8169-8174.
48. Fujiwara, H., M. Fujihara, and T. Ishiwata, *Dynamics of the spontaneous formation of a planar phospholipid bilayer: A new approach by simultaneous electrical and optical measurements.* The Journal of chemical physics, 2003. **119**: p. 6768.
49. White, S.H., *A study of lipid bilayer membrane stability using precise measurements of specific capacitance.* Biophysical Journal, 1970. **10**(12): p. 1127-1148.

50. Hambley, A.R., *Electrical engineering: principles and applications*, 2008: Pearson Prentice Hall.
51. Gurtovenko, A.A. and J. Anwar, *Interaction of ethanol with biological membranes: the formation of non-bilayer structures within the membrane interior and their significance.* The Journal of Physical Chemistry B, 2009. **113**(7): p. 1983-1992.
52. Axon Instruments, I., *Axopatch 200B Patch Clamp: Theory and Operation.* 1999.
53. Ogden, D., *Microelectrode Techniques: The Plymouth Workshop Handbook Author: David Ogden, Publisher: Company Of Biologists Pages: 44.* 1994.
54. Waxman, S. and M. Bennett, *Relative conduction velocities of small myelinated and non-myelinated fibres in the central nervous system.* Nature, 1972. **238**(85): p. 217-219.
55. Sachs, N.A., *Electrical stimulation of the orbicularis oculi to restore eye blink*, 2007: ProQuest.
56. Purves, R.D., *Microelectrode methods for intracellular recording and ionophoresis*, 1981, London; New York: Academic Press.
57. Thomas, R.C. and R. Thomas, *Ion-sensitive intracellular microelectrodes: how to make and use them*, 1978: Academic Press London.
58. Horak, R., *Telecommunications and data communications handbook*, 2007: John Wiley & Sons.
59. Alberts, B., et al., *Molecular Biology of the Cell 4th edition*, 2002: National Center for Biotechnology InformationÕs Bookshelf.
60. Hodgkin, A.L. and A.F. Huxley, *Currents carried by sodium and potassium ions through the membrane of the giant axon of Loligo.* The Journal of physiology, 1952. **116**(4): p. 449.
61. Cole, K.S. and J.W. Moore, *Potassium ion current in the squid giant axon: dynamic characteristic.* Biophysical Journal, 1960. **1**(1): p. 1-14.
62. White, M.M. and F. Bezanilla, *Activation of squid axon K+ channels. Ionic and gating current studies.* The Journal of General Physiology, 1985. **85**(4): p. 539-554.
63. Bezanilla, F., *Gating of sodium and potassium channels.* Journal of Membrane Biology, 1985. **88**(2): p. 97-111.
64. Understanding, C.o., I.K.-E.E.i.t.U. States, and N.R. Council, *Engineering in K-12 Education: Understanding the Status and Improving the Prospects*, 2009: The National Academies Press.